A THERMAL EXPANSION STUDY OF CHEMICAL, MAGNETIC AND SUPERCONDUCTING ORDER-DISORDER TRANSFORMATIONS

THESIS SUBMITTED FOR THE DEGREE OF
DOCTOR OF PHILOSOPHY

BY
GOUTAM DEV MUKHERJEE

SCHOOL OF PHYSICS
UNIVERSITY OF HYDERABAD
HYDERABAD - 500 046
INDIA
DECEMBER 1996

DECLARATION

I hereby declare that the matter embodied in this thesis is the result of investigations carried out by me in the School of Physics, University of Hyderabad, Hyderabad, India, under the supervision of Prof C Bansal

Place: Hyderabad

Date: 7-12-96

(Goutam Dev Mukherjee)

CERTIFICATE

This is to certify that the research work described in this thesis entitled **"A Thermal Expansion Study of Chemical, Magnetic and Superconducting Order-Disorder Transformations",** has been carried out by **Mr. Goutam Dev Mukherjee** under my direct supervision and the same has not been submitted for the award of research degree of any university.

Place : Hyderabad

Date   :   7-12-96

(Thesis Supervisor)

Dean

School of Physics

to my parents

ACKNOWLEDGEMENTS

It is with great pleasure and deep sense of gratitude I thank my advisor, Professor Chandrahas Bansal, for his superb guidance, constant support and continuous encouragement throughout my Ph.D. work.

I am deeply indebted to Dr. Ashok Chatterjee for his continuous encouragement and helpful discussions throughout my research tenure. I am extremely grateful for his crucial suggestions and constructive criticisms. I also owe special thanks to Soma for her infinite patience and cooperation.

I thank the Dean, School of Physics, for providing necessary facilities.

I take this opportunity to thank the faculty, School of Physics, many of whom were my teachers in my M.Sc. for building up my personality and introducing me to this inspiring research career.

I thank Mr. Ravi Sankar for his timely help and friendly cooperation whenever I needed them most. I also thank other non-teaching staff of the School for their cooperation.

I am grateful to Dr. K.V. Reddy, Principal Scientific Officer, Central Instrumentation Laboratory and other staff for their help. The help and cooperation of the staff, Central Workshop are also gratefully acknowledged.

I must acknowledge Chandan, Ashoka, Nirmal, Sharief, Harshawardhan, Jolly and Satish for their extended support on all occasions. Interactions with them helped me to learn many things and have made my stay here pleasant and colorful. I also thank my seniors Dr. J.T.T. Kumaran, Dr. P.D. Babu, Dr. T.V.S.M. Mohan Babu, Dr. V. Siruguri and Dr. P.K.Rajan for their timely cooperation.

I should also thank my juniors, Pradip, Aparupa, Subhojit and all other friends who with their love and affection have made my stay here pleasant.

CONTENTS

List of Publications

Publications in International Journals

(1) *Thermal expansion of alkali halides : a semiclassical model,* G.D. Mukherjee, C. Bansal and Ashok Chatterjee, Mod. Phys. Lett. B 8, 425 (1994).

(2) *Anomalous thermal expansion behaviour of the YBaCuO superconductor: indirect evidence of polaron formation.* G.D. Mukherjee, C. Bansal and Ashok Chatterjee, Physica C **232,** 241 (1994).

(3) *Thermal expansion study of ordered and disordered Fe_3Al: an effective approach for the determination of vibrational entropy,* G.D. Mukherjee. C. Bansal and Ashok Chatterjee, Phys. Rev. Lett. **76**. 1876 (1996).

(4) *Vibrational and magnetic contribution to entropy of an $L1_2$ ordered and partially ordered Ni_3Mn alloy : results from thermal expansion measurements and model calculations,* G.D. Mukherjee. C. Bansal and Ashok Chatterjee, submitted for publication.

(5) *Configurational entropy and stability limit of a glass,* G.D. Mukherjee, C. Bansal and Ashok Chatterjee, submitted for publication.

Papers in Conference Proceedings

(1) *Effect of 0.18% Re impurity on the Neel transition in Chromium,* G.D. Mukerjee, C. Bansal and E. Fawcett , AIP Conferecne Proceedings **286,** (eds: V. Srivastava, A.K. Bhatnagar and D.G. Naugle), 330 (1993).

(2) *Study of magnetic and anharmonic contributions to thermal expansion of Fe_2MnSi alloy,* G.D. Mukherjee, C. Bansal and Ashok Chatterjee, Solid **State Phys.** (India) **37C**, 94 (1994).

(3) *Anomalous thermal expansion behaviour of Bipb-2223 superconductor*, G.D. Mukherjee, C. Bansal and Ashok **Chatterjee,** Solid State Phys. (india) 36C, 357 (1993).

Abstract

The effect of chemical, structural, magnetic and superconducting order-disorder transformations on the thermal expansion behaviour **in** solids is studied in this thesis. Thermal expansion measurements have been performed on a newly designed and constructed three terminal **capacitance** dilatometer. The fractional length changes with respect to a reference temperature are measured with an estimated error of 3.5×10^{-7}.

For the analysis of the thermal expansion data a new semiclassical model is developed using an anharmonic lattice potential. This new theoretical approach has been used to obtain the anharmonicity parameters and accurate values of the Debye and Einstein temperatures of different materials. For ferromagnetic materials the magnetic contributions to thermal expansion due to the conduction electron moments and the localized electron moments have been separated out using methods developed from the Stoner model of itinerant electron ferromagnetism and Bloch's theory for spin-waves respectively.

Thermal expansion measurements have been performed on chemically ordered and disordered Fe_3Al and Ni_3Mn alloys and estimates of vibrational and magnetic entropies are made using **our** models. We show that the lattice vibrations play an important role in the ordering transition of these alloys and contribute significantly to their phase stability, whereas the magnetic interactions do not have any influence on their chemical ordering. Thermal expansion data on ordered $Fe_{3-x}Mn_xSi$ and $Fe_{3-x}Mn_xAl$ alloys show that with **Mn** addition the electron-magnetic contribution to the thermal expansion **coefficient** increases whereas the **magnon** contribution decreases. Estimates of magnetic entropies show that the itinerant nature of the electron moments decreases in both the systems with increase in Mn concentration.

A simple method is proposed for the first time for the calculation of the configurational entropy of a glass from thermodynamic considerations and thermal

expansion measurements and is applied to a bulk metallic glass of composition $Zr_{65}Ni_{10}Cu_{17.5}Al_{7.5}$. We have calculated the Gibb's free energy differences between the glassy and the crystalline states which measures the thermal stability of the glassy phase.

We have studied the thermal expansion behaviour of $YBa_2Cu_3O_{7-}(\delta - 0.15)$ and $Bi_{1.6}Pb_{0.4}Sr_2Ca_2Cu_3O_y$ superconductors in both the normal and the superconducting phases using our semiclassical model. It is shown that there is an anomaly in the temperature variation of thermal expansion which begins to show up at a temperature higher than T_C. We have also found that there is a large increase in the quartic anharmonicity parameter indicating a softening of lattice **potential** below T_c. For $YBa_2Cu_3O_{7-\delta}$ superconductor we attribute this anomaly to the phenomenon of polaron formation. But in the case of $Bi_{1.6}Pb_{0.4}Sr_2Ca_2Cu_3O_y$ superconductor the data in the superconducting region also show the indication of two dimensional gaussian fluctuatioas along with a BCS electronic term.

CHAPTER 1

INTRODUCTION

The study of thermal expansion **behaviour** of materials is important from **the** point of view of applications as well as basic research. Technologically, a knowledge of the thermal expansion behaviour is essential for **the** design **of structures** right from very large ones such as bridges and railroads **to** very small ones such as integrated circuits. At the basic level also it is very important **to** understand the thermal expansion behaviour as the dimensional changes in any material take place with temperature so as to minimize the free energy, contributions to which come from static lattice, lattice vibrations, magnetic ions, itinerant electrons etc. Although extensive data exist in literature, a good understanding of the thermodynamic and microscopic aspects of the experimentally observed behaviour is lacking. In this thesis an attempt is made in this direction by a careful experimental study of systems showing different types of transformations such as chemical, structural and magnetic order-disorder and analysing the observed data using proposed theoretical models. It has been shown for the first time **how** it is possible to get quantitative estimates of configurational, vibrational and magnetic entropies, characteristic Debye and Einstein temperatures, anharmonicities in lattice potentials etc. from thermal expansion data. The importance of thermal expansion measurements for understanding the basic thermo-physical aspects of properties of materials is demonstrated.

1.1 Definitions

The change of any geometrical parameter describing the dimensions of a solid with temperature is defined as thermal expansion [1]. This takes into account a simple expansion or contraction of volume of a solid which is termed as volumetric thermal

expansion or of length which is termed as linear thermal expansion.

The volumetric thermal expansion coefficient $\beta(T)$ at constant pressure is defined by,

$$\beta(T) = \frac{1}{V}\left(\frac{\partial V}{\partial T}\right)_P, \tag{1.1}$$

where V is the volume and T is the temperature. For an isotropic solid $\beta(T)$ is three times the linear thermal expansion coefficient $\alpha(T)$ for small values of a **and** is given by

$$\beta(T) = 3\alpha(T) = 3\left(\frac{\partial lnL}{\partial T}\right)_P. \tag{1.2}$$

where L is the length of **the** material at the temperature T.

The coefficient of volumetric expansion $\beta(T)$ given in eqn.(1.1) can be expressed **as,**

$$\beta(T) = \left(\frac{\partial lnV}{\partial T}\right)_P = -\left(\frac{\partial lnV}{\partial P}\right)_T\left(\frac{\partial P}{\partial T}\right)_V = \chi_T\left(\frac{\partial P}{\partial V}\right)_T, \tag{1.3}$$

where χ_T is the isothermal compressibility :

$$\chi_T = -\left(\frac{\partial lnV}{\partial P}\right)_T. \tag{1.4}$$

Eqn.(1.3) has a simple physical interpretation . It shows that when heat is given to any material, the internal pressure is increased with increase in temperature if volume is kept fixed. Once the desired temperature is reached, the material is allowed to relax isothermally to the external pressure with a change in volume.

1.2   Thermodynamics of Thermal Expansion

Using standard thermodynamic relations [1-4] $\beta(T)$ can be related to the Gibb's free energy G(P,T) as,

(1.5)

As the experimentally observable quantities are volume (V) and temperature (T) it will be more useful to talk **interms** of the Helmholtz free energy F(T,V) which is a natural function of T and V :

$$\beta(T) = \chi_T \left(\frac{\partial P}{\partial T} \right)_V = -\chi_T \left(\frac{\partial^2 F}{\partial V \partial T} \right) = \frac{1}{B_T} \left(\frac{\partial S}{\partial V} \right)_T \; ,$$

where B_T is the isothermal bulk modulus and is the reciprocal of χ_T.

Eqn.(1.6) shows that the thermal expansion comes from the volume dependence of entropy. This can also be physically understood from the discussions of the previous section. In thermal expansion the temperature dependence of volume is measured at a fixed external pressure say P_0. The internal pressure in the solid (P = - dF/dV) first changes due to temperature and then relaxes back to the external pressure P_0. Equating the internal pressure to the external pressure we get

$$P_0 = - \left(\frac{\partial F}{\partial V} \right)_T \; , \tag{1.7}$$

$$\text{or.} \quad \frac{\partial}{\partial V}(F + P_0 V) = 0 \; . \tag{1.8}$$

The quantity $F + P_0 V$ is a constrained Gibb's free energy function $G(P_0, T)$ and eqn.(1.8) shows that this function has a minimum with respect to volume. **Fig**. 1.1 shows a schematic plot of $G(P_0, T)$ as a function of volume (V) at a fixed temperaure
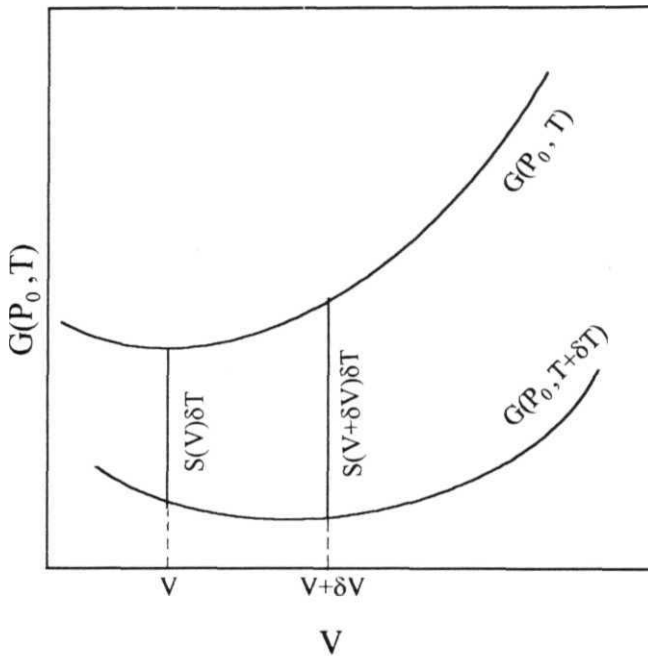
Fig. 1.1 : Schematic representation of constrained Gibb's free energy with volume at two different temperatures T and $T+\delta T$

(T). Now if the temperature is changed from T to $T+\delta T$

$$
\begin{aligned}
G(P_0. T + \delta T) &= F(V.T + \delta T) + P_0 V \\
&= F(V.T) + \frac{\partial F(V,T)}{\partial T}\delta T + P_0 V \quad\quad \textbf{(1.9)}
\end{aligned}
$$

$$
= G(P_0, T) - S(V)\delta T . \quad\quad (1.10)
$$

The value of the new constrained Gibb's free energy function G at $T+\delta T$ is less than the value of the function at T by an amount $S(V)\delta T$. $G(P_0, T+ bT)$ can **therefore** be obtained for all values of V from $G(P_0, T)$ values which is shown in Fig. **1.1** and the difference **in** the two curves depends on $S(V)$. The position of the **minimum** will therefore shift to a higher volume because S increases with volume. From eqn.(1.6) one can also see that the amount of expansion will depend upon the compressibility and highly compressible materials will have large expansion. Experimentally it is observed that for a solid at low temperatures the compressibility does not change much with temperature.

The total free energy of a solid can be expressed as a sum of different contributions, such as, electronic (F_{el}), magnetic (F_m) and vibrational (F_{ph}), if the mutual interactions between the different subsystems can be neglected. Thus we write

$$
F = F_{el} + F_m + F_{ph} . \quad\quad (1.11)
$$

From the above equation independent additive contributions can be obtained for the derivatives of F, such as, entropy 5, specific heat C_ι and for the thermal expansion coefficient $\beta(T)$, by taking a total bulk modulus B_T. Thus the total thermal expansion coefficient can be written as

$$
\beta(T) = \beta_{el} + \beta_m + \beta_{ph} = \frac{1}{B_T}\left\{\left(\frac{\partial S_{el}}{\partial V}\right)_T + \left(\frac{\partial S_m}{\partial V}\right)_T + \left(\frac{\partial S_{ph}}{\partial V}\right)_T\right\} \quad\quad (1.12)
$$

where the subscripts *el,* m and ph refer to electronic, **magnetic** and vibrational contributions.

1.3   Griineisen Parameter

In his pioneering microscopic theory of thermal expansion. Griineisen [5] had used the Einstein model for lattice vibrations with a volume dependent frequency ω of the harmonic oscillator. Using this model he calculated the specific heat at constant volume C,., the entropy S and the coefficient of volumetric expansion β. A dimensionless parameter defined by,

$$\Gamma_G = \beta B_T V / C_v \tag{1.13}$$

was calculated with the simplified model and found to be

$$\Gamma_G = -\partial ln\omega / \partial ln V \tag{1.14}$$

where the dimensionless parameter Γ_G is termed as Griineisen parameter. From the above equation one can see that Γ_G comes from the volume dependence of the frequency ω and consequently gets related to the anharmonicity in the lattice potential. Though Γ_G comes from the ratio of two strongly temperature **dependent** experimentally measurable quantities β and C_v, it itself is weakly temperature dependent. Also it has been observed experimentally that Γ_G does not vary much in a fairly wide temperature range [2,6,7] and is generally referred to as Griineisen constant. Hence it has become very useful in theoretical studies of thermal expansion and also used widely for the analysis and the presentation of the experimental thermal expansion data. There have been a host of theoretical works [6-12] which used the Griineisen constant since its first presentation by Griineisen. The Griineisen

Γ_G has become very popular as the **experimental thermal expansion** data can bo related to different thermodynamic parameters such as specific heat and entropy through eqn.(1.13).

The electronic and magnetic contributions to Griineisen parameter become very useful for the theoretical analysis of electronic and magnetic **contributions** to thermal expansion and separately they are given by

$$\Gamma_G^{el} = \beta_{el} B_T V / C_{el} \tag{1.15}$$

$$\Gamma_G^{m} = \beta_{m} B_T V / C_{m} \tag{1.16}$$

where Γ_G^{el} [13] and Γ_G^{m} [14] are electronic and magnetic contributions to Γ_G. As **the** entropy and the specific heat can be expressed as a sum of separate contributions coming from electronic, magnetic and lattice. then the total measured Γ_G defined by eqn.(1.13) is an average of different contributions to Γ_G and weighted by their respective heat capacities [1]

$$\Gamma_G = \frac{\Gamma_G^{el} C_{el} + \Gamma_G^{m} C_m + \Gamma_G^{ph} C_{ph}}{C_{el} + C_m + C_{ph}} \tag{1.17}$$

For non-magnetic metals Γ_G^{el} can be calculated using the simple free electron model and from the volume dependence of the electron density of states it has been found out to be 2/3 [1,2]. But this is not universally correct as for different materials it has been found out experimentally that Γ_G^{el} is different. The reason for this non-agreement may be attributed to the nonparabolicity of the bands and the band-overlapping [13,15,16]. For magnetic metals and alloys this discrepancy is much more because of their complicated band structure and complex magnetic behaviour. But there have been very few attempts to calculate Γ_G theoretically. Therefore

in this thesis a new semiclassical model using **the** anharmonic potential has been proposed to represent the vibrational part of the thermal expansion theoretically. The vibrational contribution to the Gruneisen parameter Γ_G^{v} has been estimated from the vibrational contributions to thermal expansion **coefficient** and specific heat using the proposed model. The help of the band structure calculations are taken to calculate the magnetic contributions to Γ_G arising due to the conduction electron moments. Also for the ferromagnetic materials the spin wave theory of **Bloch** is used to find out the magnon contribution to Γ_G. The values of different contributions to Γ_G have been calculated for different types of materials using the models developed in this thesis and are discussed in detail in the relevant chapters.

1.4 **Plan of** the Thesis

Historically, since 1930 thermal expansion measurements have been continuing, but due to the non-availability of proper techniques, good quality data could not be obtained particularly at low temperatures. But since world war II, there has been a great deal of progress in this area due to advanced cryogenic facilities and more interest in various materials. Therefore a host of sensitive methods for thermal expansion measurements have been developed (see Chapter 2). Recently a highly sensitive method of measurements using three terminal capacitance bridge technique has been developed. With this improved sensitivity in measurements very small changes in lengths can be detected making it possible for the separation of electronic, magnetic etc. contributions from the major vibrational part. Therefore a newly designed cell has been constructed based on the three terminal capacitance bridge technique for thermal expansion measurements [17,18]. The details of the

construction and testing of the cell has been described in Chapter-2.

Whenever a thermodynamic transformation occurs due to co-operative interaction between phonons, electrons or magnetic ions etc., there is a change of order **which** is reflected in thermal expansion due to the change in entropy. If one can separate out various contributions to thermal expansion the behaviour of entropy changes due to electronic, magnetic and vibrational effects can be observed. The main hurdle still has been to separate out the vibrational part properly due to unavailability of a suitable model for it. In Chapter-3 a new semiclassical model has been developed to get the vibrational contribution to thermal expansion theoretically using an anharmonic potential [19]. Then for non-magnetic solids the free electron model is used to calculate the electronic contribution to entropy and the electronic contribution to thermal expansion from its volume dependence. But for ferromagnetic solids the itinerant electron moments and localized moments contribute to the thermal expansion. A generalized Stoner-Wohlfarth model has been used with the electronic band structure calculations to give a theoretical expression for the electron-magnetic contribution to thermal expansion [18,20]. The Heisenberg interaction is used to get the expression for the magnon contribution to thermal expansion. Also the same method has been used for the calculation of the magnetic Griineisen parameters [18,20]. The theory for the vibrational contribution to thermal expansion along with the electronic and the magnetic expressions have been used to fit the experimental thermal expansion data of few metals like, Cu, Al, Ni. Fe [18] and for alkali halides like NaCl, KC1, KBr and KI [19] which returned very good estimates of the characteristic temperatures Θ_D, Θ_E and electron-magnetic **and** magnon Griineisen parameters for magnetic systems. Basically in Chapter-3 the theoretical models have been developed and the validity of the models have

been tested. These models have been applied to the more complicated systems for the analysis of their thermal expansion data which are **experimentally** studied in this thesis.

Effect of order and disorder on the thermal expansion of the binary alloys Fe_3Al [17] and Ni_3Mn[20] has been studied in Chapter-4. Our theoretical models have been used to separate the vibrational and magnetic parts from the total thermal expansion. Estimates of differences in vibrational entropies between the disordered and ordered states of these alloys have been done to see the effect of the ordering transition on lattice vibrations of these alloys and to their phase stability. The magnetic Gruneisen parameters are calculated to see the effect of magnetic entropies on the chemical ordering.

Chapter-5 deals with the chemically ordered ternary alloy systems of $Fe_{3-x}Mn_xSi$ for $0 < x < 1.8$ and $Fe_{3-x}Mn_xAl$ for $0 < x < 1.2$ [21]. In these alloys the thermal expansion has been measured and the effect of substitution of Mn for Fe on lattice vibrations has been studied. Also the magnetic parts are separated out from the total contribution to thermal expansion and the effect of itinerant and localized character of electron spins with Mn concentration are studied.

In Chapter-6 a simple method of estimating the configurational entropy of a glass has been proposed from thermodynamic considerations and thermal expansion measurements done in both the glassy and the crystalline forms and has been applied to a bulk metallic glass of composition $Zr_{65}Ni_{10}Cu_5Al_{7.5}$ which has important technological applications [22]. The Gibb's free energy difference between the glassy and the crystalline states is also calculated which measures the thermal stability of the glassy phase. The method used also predicts a new isentropic instability temperature beyond which a glass cannot be superheated.

In Chapter-7 the temperature variation of thermal **expansion** data of $YBa_2Cu_3O_{7-\ell}$ [23] and $Bi_{1.6}Pb_{1.4}Sr_2Ca_2Cu_3O_y$[24] superconductors have been studied in a wide temperature range both in **the** superconducting and normal phases. The data analysis have been done using the semiclassical model described in Chapter-3 to see the effect of superconducting transition on lattice anharmonicity.

Finally we give a summary of the important results presented in this thesis.

References

[1] T.H.K. Barren, J G. Collins and G.K. White. Adv. Phys. 29, 609 (1980).

[2] J.G. Collons and G.K. White, Prog. Low Temp. Phys. 4, 450 (1964).

[3] T.H.K. Barron, J. Appl. Phys. 41. 5044 (1970).

[4] D.C. Wallace, Thermodynamics of Crystal (John Wiley, New York. 1972).

[5] E. Griineisen, Ann. Phys. Lpz. 33, 33 (1910); Ann. Phys. 39, 257 (1912).

[6] R.S. Krishnan, Proc. Indian Acad. **Sci.** A 24. 33 (1946).

[7] J.G. Collins. **Phil.** Mag. 8. 323 (1963).

[8] E. Grüneisen, Handb. Phys. 10, 1 (1926).

[9] M. Born, Atomtheorie des festeii Zustandes (Leipzing, Teubner, 1923).

[10] E. Griineisen and E. Goens. Z. Phys. **29**, 141 (1924).

[11] R.O. Davies, Phil. Mag. 43. 472 (1952).

[12] J.K. Roberts and A.R. Miller. Heat and Thermodynamics, **Fourth** edn. (London, Blackie, 1951).

[13] J.H.O. Varley, Proc. Roy. Soc. A **237,** 413 (1956).

[14] G.K. White, J. Phys. Chem. Solids **23**, 169 (1962).

[15] G.K. White, J.G. Collins, J.A. Birch, T.F. Smith and T.R. Finlayson, Inst. Phys. Conf. Series, No.39 (London : Inst. Phys.), p.420.

[16] R.W. Munn, Phys. Lett. A **29,** 395 **(1969).**

[17] G.D. Mukherjee, C. Bansal and Ashok Chatterjee, Phys. Rev. Lett. **76.** 1876 (1996).

[18] G.D. Mukherjee, C. Bansal and Ashok Chatterjee, *Thermal expansion study of Ni and Fe : an effective method for calculation of electron-magnetic and magnon Grüneisenparameter,* to be communicated for publication.

[19] G.D. Mukherjee, C. Bansal and Ashok Chatterjee, Mod. Phys. Lett. B 8. 425 (1994).

[20] G.D. Mukherjee, C. Bansal and Ashok **Chatterjee,** *Vibrational and magnetic contribution to entropy of an $L1_2$ ordered and partially ordered Ni_3Mn alloy : results from thermal expansion measurements and model calculations,* submitted for publication.

[21] G.D. Mukherjee, C. Bansal and Ashok Chatterjee, Solid State Phys. (India) **37C,** 94 (1994).

[22] G.D. Mukherjee, C. Bansal and Ashok Chatterjee. *Configurational entropy and stability limit of a glass,* submitted for publication.

[23] G.D. Mukherjee, C. Bansal and Ashok Chatterjee. Physica C **232,** 241 (1994).

[24] G.D. Mukherjee, C. Bansal and Ashok Chatterjee, Solid State Phys. (india) **36C,** 357 (1993).

CHAPTER 2

EXPERIMENTAL

2.1 Introduction

Over the years, several **experimental** methods have been developed to measure **the** thermal expansion of solids [1]. These can be classified into four groups based on the techniques used : mechanical (push rod dilatometer [2] and scissors dilatometer [3']). optical (interferometric [4-9] and twin-telemicroscopic [10-16]), diffraction (neutron [17] and X-ray [18-21]) and electrical (three terminal capacitance bridge [22-32]. variable differential transformer [33]). In recent years the three terminal **capacitance** bridge technique has been more commonly used for the study of thermal expansion at low temperatures with a high sensitivity. This method was first developed by Professor G.K. White at the National Measurement Laboratory in Sydney. Australia [22]. The basic principle of this technique is to construct a parallel plate capacitor cell in which the sample serves as one of the plates of the cell and a reference material such as copper is used as the second plate. A change in sample dimensions changes the distance between the capacitor plates and the value of the capacitance. which can be measured accurately. Both the plates (terminals) are completely surrounded by a third terminal which is held at ground potential. The capacitance is measured using the ratio transformer bridge developed by Thompson [34]. The balance condition of the bridge is not affected by the capacitance of the parallel plates with respect to ground and by lead capacitances. Several modifications of the capacitance cell has been reported [27-32] to enable absolute measurement of thermal expansion. In all these designs the temperature of the sample is made to change and the other parts of the cell are kept at fixed temperatures.

A new cell design has been reported in the present work which is based on a suggestion by White [35]. The sample is directly placed in between the two plates

of a three terminal parallel plate capacitor, **one** of **the** plates of which is **spring** loaded so as to hold the sample in position between the two plates. A change in sample length alters **the** distance between the capacitor plates directly and changes its capacitance, which is measured. The details of the cell design are described in the next section.

2.2   Capacitance Cell

The cell design used in **the** present work is simple in construction and can be used for expansion measurements of small samples. The schematic cell design is shown in Fig.2.1. It consists of two capacitor plates (C1 and C2) made out of high purity oxygen-free copper. The plates are highly polished to get smooth and plane surfaces. Cl is rigidly fixed to the base B using **three** teflon rods (R). C2 is guided to move freely along the three teflon rods and it rests on three phosphor bronze springs (S1, S2 and S3). This end of the springs are electrically insulated and the other end of the springs are rigidly fixed to the base B. The sample which is insulated at both the ends using thin mylar foils can be inserted between the two plates Cl and C2. by slightly pushing C2 towards the base B. A copper chamber (can) C, encloses the plates and the sample. The sample is grounded so that the capacitance between the plates and the sample does not contribute to the parallel plate capacitance. The can C is also connected to the ground and it serves as the third terminal for the cell. This helps to minimize the effect of stray capacitances. The temperature is controlled by using a non-inductively wound heater H (resistance 25 ohms) around the can C and a platinum resistor sensor (PT103 from Lakeshore) attached to the bottom of the can C Another platinum resistor thermometer (PT2) is fixed on
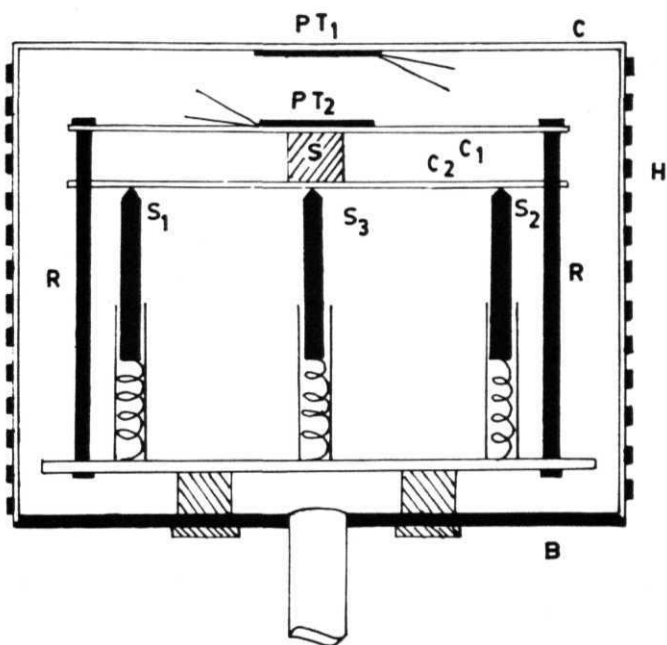
Fig.2.1 : Schematic diagram of three-terminal capacitance cell used for thermal expansion measurements.

one of the capacitor plates and is used to monitor the sample temperature. Small depressions are made on the edge of the copper capacitor plates and the capacitor leads (ultra miniature co-axial cable of type C1 from Lakeshore cryotronics) arc soldered strongly to the plates placing them inside the depressions. Special care has been taken to shield the leads to avoid noise pickups from any outside source.

2.3   Insert and Cryostat

The thermal expansion measurements in the temperature range 80-300K are carried out using a homemade experimental set up. The schematic block diagram of the cryostat and the insert are shown in Fig.2.2. The cryostat arrangement consists of a liquid nitrogen double walled glass dewar and a glass chamber with a provision for evacuating the sample space through the vacuum port P. The glass chamber is fixed vertically on a steel flange (BF) using epoxy adhesive (araldite) which has a hole in its center and the diameter of the hole is same as the inner diameter of the glass chamber. The surfaces of both the walls in the annular space of the glass dewar are silvered to minimize heat radiation. The inserr is made up of a thin walled seamless stainless steel tube (ST) with the capacitance cell (CC) attached to its one end. The other end of the tube comes out through the central hole of the top steel flange (TF) and is sealed using a teflon plug and araldite. The steel tube is fixed to the top flange vertically using araldite. The capacitance leads are taken out through the tube and through two small holes drilled in the teflon plug. Other electrical connections to the temperature controller, digital multimeter and current source are taken from the MS connector (MS 3102R-20-27P from Allied Electronics Corporation, Bombay). The MS connector is attached to the insert by holding it on
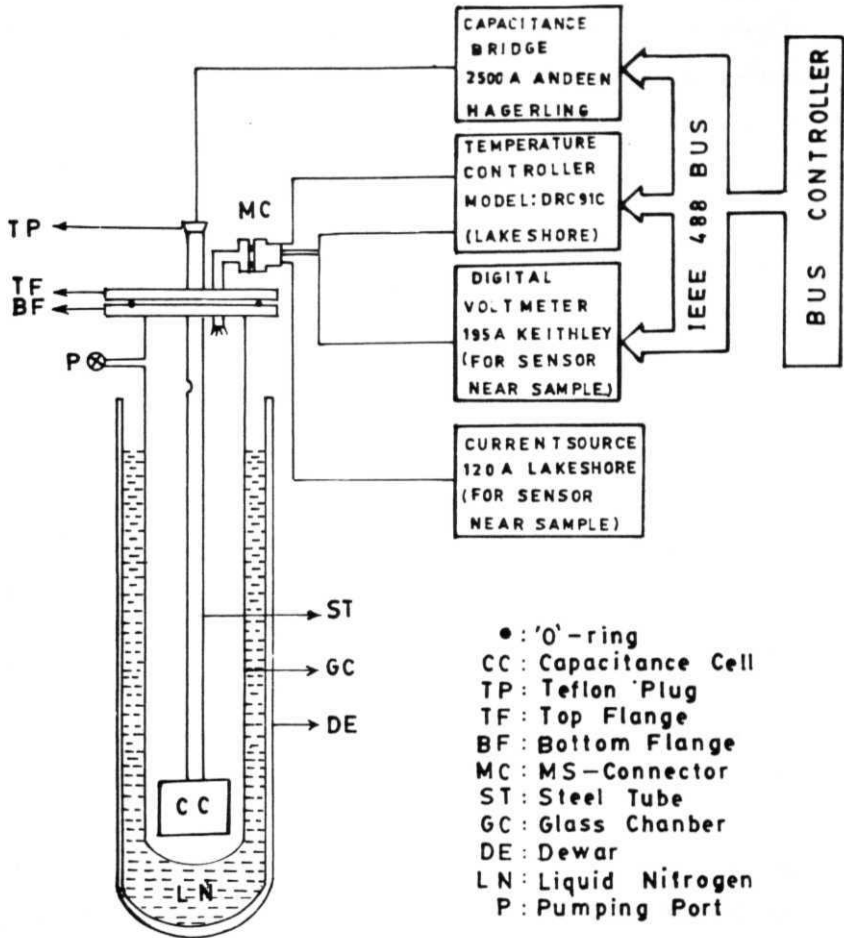
Fig.2.2 : Schematic block diagram of the cryostat and the insert used for thermal expansion measurements.

a small flange using four screws and an O'-ring and **the** small flange is connected to another steel tube which is also welded to the **top** flange of the insert. The electrical connections other than the capacitance leads from the cell are taken through the second tube and are connected to the MS connector. A small hole is drilled on **the** portion of the tube ST which lies inside the glass chamber to evacuate the inside of the cell. Fig.2.2 also shows the block diagram giving the interconnections of various measurement units.

2.4   Temperature and Capacitance Measurements

The glass chamber which houses the insert is first pumped through the port P and then liquid nitrogen (LN) is poured into the dewar. After waiting for about **three** hours for the insert to cool down to the liquid nitrogen bath temperature, the cell temperature is set to 78 K and controlled for half an hour before taking the first capacitance reading. The sample temperature is then scanned at the rate of $2 \, mK/sec$ using a Lakeshore model DRC91C temperature controller. Temperature values are recorded at the intervals of 4 sec using a Model 2500A automatic capacitance bridge from Andeen Hagerling. This bridge is designed to take three terminal capacitance measurement at a fixed frequency of 1 KHz with a true resolution of 0.5 attofarad (1 attofarad = 10^{-18} F). An average of fifty readings were taken to get the capacitance variation with temperature at 0.4 K intervals. To improve the quality of the data the bridge can be programmed to certain internal features. To avoid random noise peakup the bridge is programmed to sense the capacitance values at every 0.05 sec and average it out internally for 1 sec. To reject noise from external sources which generate signals at the same frequency and phase as the 1 KHz sine wave that the

instrument uses, the bridge is programmed to periodically alternate the applied signal to make it distinguishable from the synchronous noise signal. Also for rapidly changing capacitance values a track mode is used in which the bridge uses a high precision algorithm to take fast measurements. The measurement is carried out with an applied rms voltage of 15 volts on the capacitor plates.

The sample temperature measurement is carried out by sending a current of 1 mA through the PT2 sensor using a model 120A constant current source from Lakeshore Cryotronics and monitoring the voltage drop across the sensor using a model 195A digital multimeter from Keithley.

Mechanical vibrations generate a lot of scatter in the **capacitance** data due to microphonic effects. Care is taken to reduce those effects. The temperature setting. scanning and monitoring as well as capacitance measurements are fully automated using a 2AT6 computer. A program is written to automate the **experiment** which uses a IEEE-488 card.

2.5   Calibration and Standardisation of Data

For an ideal parallel plate capacitor the capacitance C is given by, $C = \epsilon A / L$, where A is the area of the capacitor plate. L is the distance between the two capacitor plates and t is the permittivity of the medium. If the medium does not change, then the change in the distance between the capacitor plates (ΔL) is related to the change in capacitance (AC) and the change in area (ΔA) of the capacitor plates as,

$$\frac{\Delta L}{L} = \frac{\Delta A}{A} - \frac{\Delta C}{C}$$

(2.1)

In the present cell design **the sample** is inserted between the capacitor plates and the length of the sample at any temperature is equal to the distance between **the** two plates at that temperature. Hence the fractional length change of the sample at any temperature T relative to the length at a reference temperature T_0 $\left(\frac{\Delta L(T)}{L(T_0)} = \frac{L(T) - L(T_0)}{L(T_0)}\right)$ is given in terms of the fractional area change, $[\Delta A(T)/A(T_0)]^P$ of the copper capacitor plates of **the** capacitance cell whose thermal expansion is known, as:

$$\left(\frac{\Delta L(T)}{L(T_0)}\right) = \left(\frac{\Delta A(T)}{A(T_0)}\right)^P - \left(\frac{\Delta C(T)}{C(T_0)}\right) = 2\left(\frac{\Delta L(T)}{L(T_0)}\right)^{Cu} - \left(\frac{\Delta C(T)}{C(T_0)}\right) \qquad \textbf{(2.2)}$$

The fractional length change data of any sample can thus be obtained from **the** measured fractional capacitance change data $(\Delta C(T)/C(T_0))$ as a function of temperature.

Equ.(2.2) holds for an ideal parallel plate capacitor and requires that the plates be perfectly parallel and flat. However in practice it is not possible to get a perfectly smooth finish of the plate surfaces and there can be some small non-parallelism between the plates. To correct for these effects experimentally, we first measure the thermal expansion of a standard copper sample of cylindrical cross section of diameter 3 mm and length 3 mm and compare the experimentally observed fractional length change data with the reported standard data of Kroeger and Swenson [29] which are obtained using an absolute expansion cell. Fig.2.3 shows a plot of $\left(\frac{\Delta L(T)}{L(T_0)}\right)_{reported}$ versus $\left(\frac{\Delta L(T)}{L(T_0)}\right)_{measured}$ for the standard copper sample. The plot is fitted to a straight line

$$\left(\frac{\Delta L(T)}{L(T_0)}\right)^{Cu}_{standard} = a\left(\frac{\Delta L(T)}{L(T_0)}\right)^{Cu}_{measured} + b$$
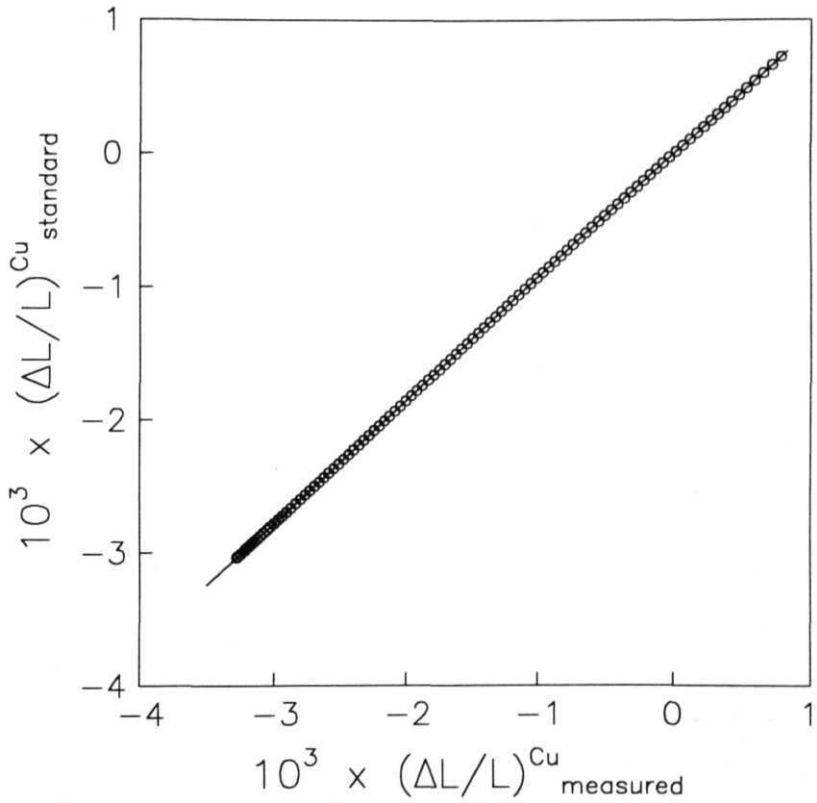
Fig.2.3 : Experimental fractional length change data of a standard copper sample obtained using our cell is plotted with the standard fractional length change data of Cu given by Kroeger and Swenson [29]. The solid line shows the linear fit to the plot.

giving a $= 0.9367$ and $b = -1.8$ x 10^{-8}. These values of a and b are taken to be the cell constants for our capacitance cell.

To test the performance of the cell, we have measured the thermal expansion of several other materials such as, aluminium (Al), silver (Ag), nickel (Ni) and iron (Fe) using our set up. These metal samples were annealed at $400°$ C for 24 hours to remove vacancies if any before recording the data. The experimentally observed thermal expansion data for these materials are found to be in excellent agreement with the data reported by other workers [1,36] and are compared in Fig.2.4a and Fig.2.4b.

2.6 Error Analysis

The resolution of the Model 2500A Andeen Hagerling three terminal capacitance bridge is 0.5 aF as given by the manufacturer. However due to the imperfect shielding of the capacitor cables and the microphonic noises there are fluctuations in the measured capacitance values which are more than the ultimate resolution that the instrument can provide. To estimate the experimental error in the capacitance measurements repeated observations of the capacitance values are carried out for the capacitance cell maintaining it at a fixed temperature with a stability of $\pm$ 10 mK. The standard deviation obtained from the distribution of the observed data is $\sigma_C = \pm 1$ aF. This is then taken to be the error in the capacitance measurement.

Using the error propagation formulae [37], the error in the measurement of $\Delta C(T)/C(T_0) = [C(T) - C(T_0)]/C(T_0)$ for a value of $C(T_0) = 5$ pF (typical value of the capacitance at $T_0 = 293$ K in our measurements) is 3 x 10^{-7}. From eqn.(2.2) the total error in $\Delta L(T)/L(T_0)$ comes from the error in the standard data of the
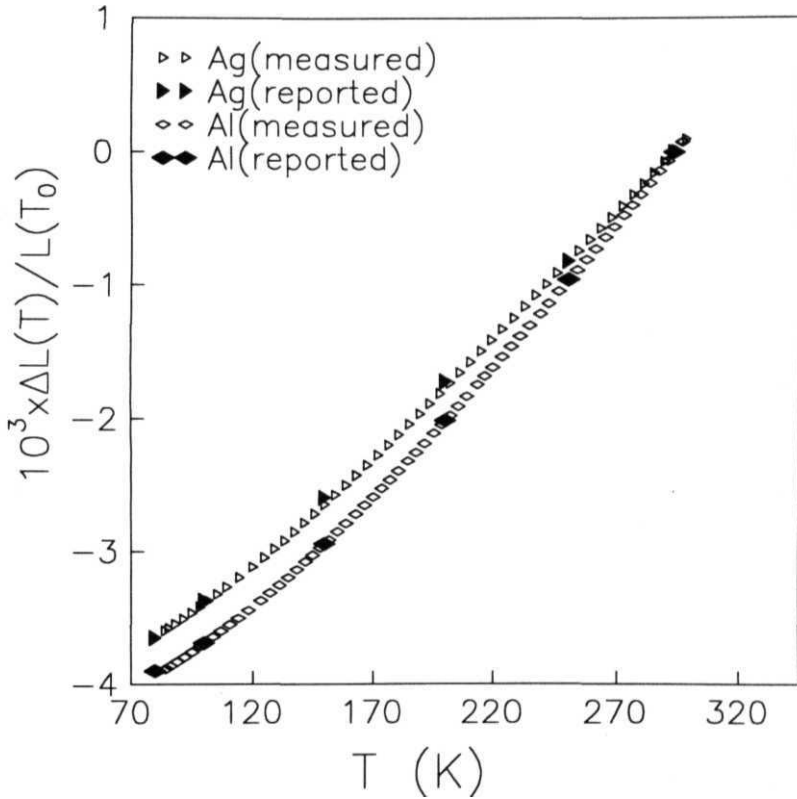
Fig.2.4a : The fractional length change data obtained from our experiments for Ag and Al (open data points) are plotted with the data taken from literature (filled data points) [1].
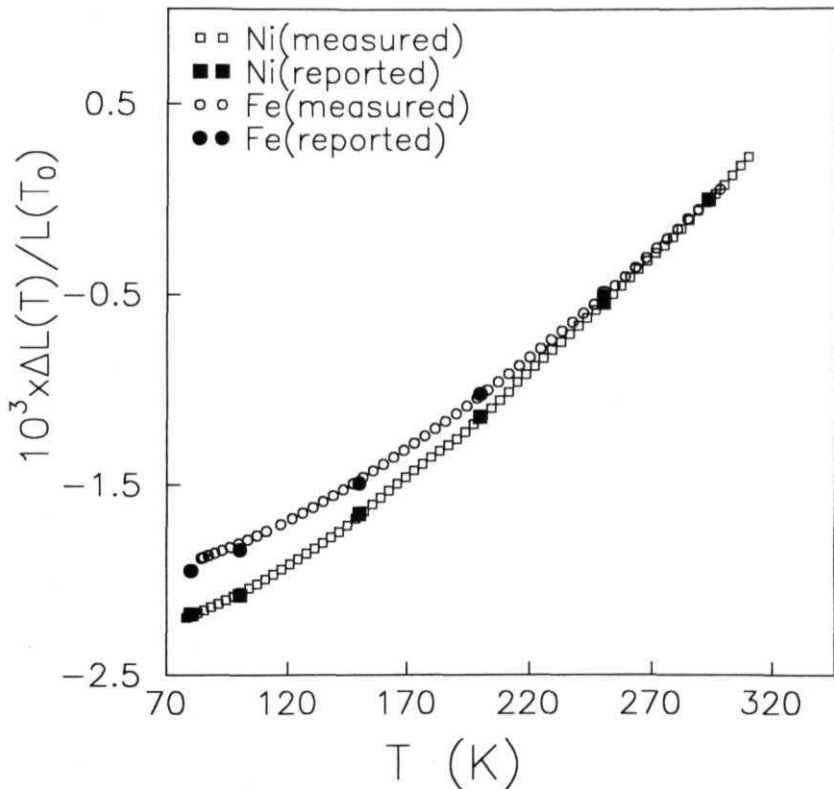
Fig.2.4b : The fractional length change data obtained from our experiments for Ni and Fe (open data points) are plotted with the data taken from literature (filled data points) [36].
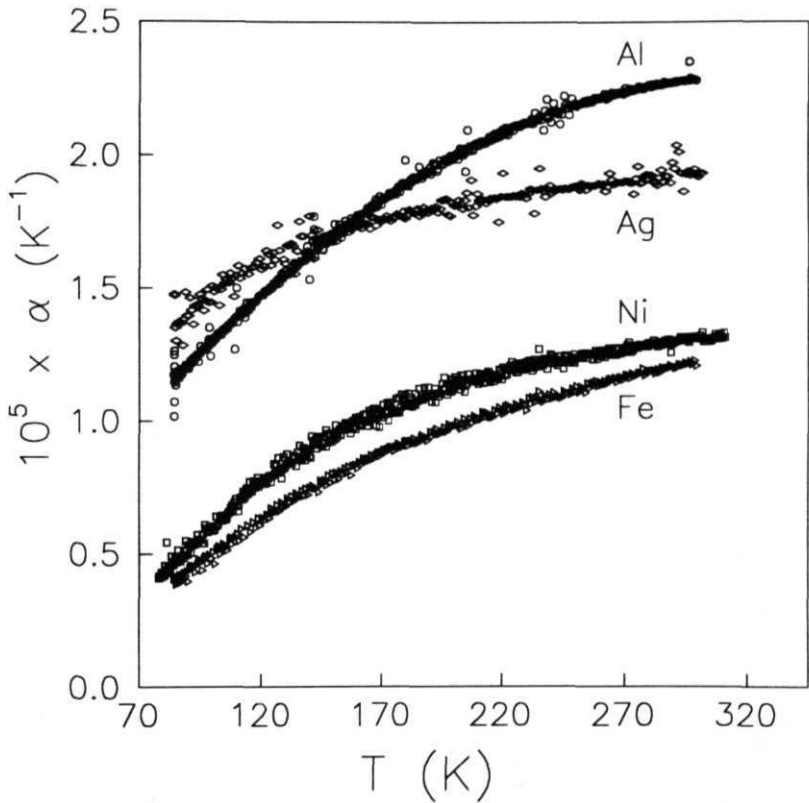
Fig.2.5 : Linear thermal expansion coefficient a obtained from the numerical three point differentiation of the measured fractional length change data obtained from our experiments for Al, Ag, Ni and Fe samples.

fractional length change for Cu reported by Kroeger and Swenson [29] and from the error in $\Delta C(T)/C(T_0)$ measurement done in our bridge. Thus the error in the fractional length change $\Delta L(T)/L(T_0)$ comes out to be 3.5 x 10^{-7} from our experiments.

The coefficient of thermal expansion o $= dlnL/dT$ is evaluated from the temperature dependence of the fractional length change $\Delta L(T)/L(T_0)$ by numerical three point differentiation. Fig.2.5 shows the temperature dependence of a for some of the test materials. The temperature stability of the cell is $\pm$ 10 $\mathbf{mK}$ and the experimental error in a is calculated to be σ_a — 4 x $10^{"8}$ $\mathbf{K}^{-1}$.

References

[1] Thermophysical Properties of Matter, Vol.12, eds.: Y.S. Touloukian, R.K. Kirby, R.E. Taylor and P.D. Desai, (IFI/Plenum, New York, 1977), p.17a.

[2] W.A. Plummer, AIP Conf. Proc. No.17 - Thermal Expansion. (AIP, New York, 1972), p.51.

[3] A. Baudran, Bull. S.F.C. 27, 13 (1955).

[4] M.H. Fizeau. Compt. Rend. 62, 1101 (1866).

[5] E. Reimerdes, Dissertation, University of Jena, 38 (1896).

[6] K. Scheel, Ann. Physik 9, 837 (1902).

[7] T. Rubin, H.W. Altmann and H.L. Johnston, J. Amer. Chem. Soc. 76, 5289 (1954).

[8] D.B. Fraser and A.C. Hollis Hallet, Proc. VII Int. Conf. Low Temp. Phys. (Univ. of Toronto Press, 1961), p.689.

[9] P.P.M. Meinke and G.E. Graham. Proc. VII Int. Conf. Low Temp. Phys. (Butterworths. London, 1963), p.401.

[10] T. Preston, The Theory of Heat (MacMillan and Company, London. 1904).

[11] L. Holborn and A. Day, Ann. Phys. 307, 505 (1900).

[12] H.L. Callendar, Phil. Trans. Roy. Soc. 178, 161 (1887).

[13] B.D. Rothrock and R.K. Kirby, J. Res. Natl. Bur. Stand. 71C, 85 (1967).

[14] R.O. Simmons and R.W. Balluffi, Phys. Rev. **117,** 52 **(1960).**

[15] P.S. Gaal, High Temp.-High Pres. 4, 49 (1972).

[16] J.B. Conway and A.C. Losekamp, Trans. Met. Soc. AIME 236, 702 **(1966).**

[17] A.L. Bowman, N.H. Krikorian and N.G. **Neveson,** AIP Conf Proc. No.3 (AIP, New York, 1972), p. 119.

[18] K. Becker, Z. Physik 40, 37 (1920).

[19] R.O. Simmons and R.W. Balluffi, Phys. Rev. 108, 278 (1957).

[20] B.F. Figgins, G.O. Jones and D.P. Riley, Phil. Mag. 1, 747 (1956).

[21] D.C. Schuele, Case Inst. of Technology, Ph.D. Thesis, 1962.

[22] G.K. White, Cryogenics 1, 151 (1961).

[23] J.S. Browder and S.S. Ballard, Appl. Opt. **8**, 793 (1969).

[24] W.F. Schlosser, G.M. Graham and P.P.M. Meinke, J. Phys. Chem. Solids 32, 927 (1971).

[25] R.H. Carr, Iowa State University, Ph.D. Thesis (1962).

[26] G.K. White, Nature **187,** 927 (1960); Phil. Mag. 6, 815 (1961).

[27] G.K. White and J.G. Collins, J. Low Temp. Phys. 7, 43 (1972).

[28] R.H. Carr and C.A. Swenson, Cryogenics 4, 76 (1964).

[29] F.R. Kroeger and C.A. Swenson, J. Appl. Phys. 48, 853 (1977).

[30] P.C. Wolfendale, J. Phys. E. 1, 817 (1968).

[31] R. Pott and R. Schefzyk, J. Phys. E **16,** 444 (1983).

[32] M.O. Steinitz, J. Genossar, W. Schnepf and D.A. Tindall, Rev. Sci. Instrum. 57, 297 (1986).

[33] P.W. Sparks and C.A. Swenson, Phys. Rev. **163,** 779 (1967).

[34] A.M. Thompson, I.R.E. Trans. on Instrumentation 1-7, 245 (1958).

[35] G.K. White, Private Communication.

[36] American Institute of Physics Handbook (1972).

[37] P.R. Bevington, Data Reduction and Error Analysis for the Physical Sciences, (Mc Graw-Hill, New York, 1969).

CHAPTER 3

THEORETICAL MODEL FOR THERMAL EXPANSION
AND ITS APPLICATION TO SIMPLE SYSTEMS

3.1   Introduction

In the first chapter, general macroscopic thermodynamic relations in connection with thermal expansion were discussed. There we have seen that thermal expansion can have contributions from various sources such as electrons, lattice, magnetic moments and so on. We have also pointed out that these contributions can be obtained essentially from the volume derivative of the respective entropies. We have not however discussed so far the actual microscopic mechanisms which are responsible for various contributions to thermal expansion. The purpose of the present chapter is to develop a microscopic theoretical model to describe these various contributions which will be useful to analyze the **thermal** expansion data.We shall present this theoretical model in section 3.2.

As is well known, the major contribution to thermal expansion comes from the lattice vibrations. In equilibrium, the atoms in a crystal vibrate about their mean positions. As the temperature is raised, more and more thermal energy is injected into the crystal and the atoms vibrate with greater and greater amplitude. Also the mean distance of separation between the atoms increases with the increase in temperature, which gives rise to the thermal expansion. Theoretically to understand this situation one can take a potential which is a function of atomic positions. If one takes the harmonic potential model where the positional dependence of the potential is quadratic in the atomic displacement, there will be no lattice expansion because of symmetrical displacements of the atoms about their equilibrium positions. Thus vibrational thermal expansion can be obtained only from the **anharmonic** lattice potential models. There have been a host of theoretical works on the vibrational thermal expansion of solids which are based on what are known as quasi-harmonic

models. In the quasi-harmonic theory [1,2] the vibration is still taken as **harmonic** but the thermal expansion is explained by assuming volume dependent frequencies $\omega_j(V)$ where the subscript j is for different modes of vibration. In this approximation the vibrational entropy S_{ph} is taken as a sum of contributions of various modes and is given by

$$S_{ph} = \sum_j S_J = \sum_j S(\hbar\omega_j/k_B T) \;, \tag{3.1}$$

where $S(\hbar\omega_j/k_B T)$ is the **vibrational** entropy function for a harmonic oscillator. The vibrational contribution to the thermal expansion coefficient can then be calculated by differentiating the entropy given by eqn.(3.1) with respect to volume. The quasi-harmonic theory is strictly valid in the limit of small oscillations [1]. Calculations show that **in** hard crystals the quasi harmonic harmonic theory works reasonably well only upto (1/6)th of the melting temperature [3]. However for soft rare gas crystals, the quasiharmonic approach is found to fall through even at low temperatures. In the extreme case of helium in which zero point quantum fluctuations are pretty large, the quasi-harmonic approach is found to be totally invalid at all temperatures, except at very high pressures. Thus theoretical calculations to obtain corrections to the quasi-harmonic models due to further anharmonic effects were called for. Various methods have indeed been suggested to deal with strongly anharmonic crystals (see references [3-5] for review). We have recently developed a very simple semiclassical anharmonic model for the vibrational contribution to thermal expansion [6-8] which we shall discuss in sub-section 3.2.1.

In metals, however, in addition to phonons, free conduction electrons also contribute to thermal expansion [1] which results from the volume dependence of the

conduction **electron** entropy. The Sommerfeld model of non-interacting free electrons suggests a linear temperature behaviour of the thermal expansion coefficient in lowest order [1]. We shall discuss this model in sub-section 3.2.2. In magnetic materials electron magnetic moments also contribute to thermal expansion through their mutual interaction. At low temperatures where the effects of lattice vibrations become very small, magnetic contributions to thermal expansion can be readily observed. The magnetic contribution to thermal expansion may come from both the itinerant and localized moments [1]. The itinerant moments contribution together with the free electron contribution is commonly referred to as the electron-magnetic contribution and can be described within the framework of Stoner-Wohlfarth model [9-12] which we shall present in sub-section 3.2.3. The localized electron moments in ferromagnetic metals and compounds would contribute to thermal expansion through the volume dependence of the magnon entropy [1]. We shall discuss the model for the magnon contribution to thermal expansion in sub-section 3.2.4.

In section 3.3 we apply our model to simple elemental metallic systems like Al and Cu to examine the validity of our theoretical approach. In the next section 3.4, the thermal expansion behaviour of ferromagnetic transition metals, namely Fe and Ni is studied within the framework of our theoretical model and the analysis of thermal expansion data of alkali halides is then taken up and presented in section 3.5. Finally we end this chapter by giving our concluding remarks in section 3.6.

3.2   Basis of the Model

The fractional length change of a solid at any temperature T with respect or a reference temperature T_0 can be defined as

$$\frac{\Delta L}{L(T_0)} = \frac{a(T) - a(T_0)}{a(T_0)} = \frac{\langle x \rangle_T - \langle x \rangle_{T_0}}{a(T_0)} \; , \tag{3.2}$$

where $a(T)$, the interatomic separation at temperature T, has been written as

$$a(T) = a(0) + \langle x \rangle_T \; . \tag{3.3}$$

$\langle x \rangle_T$ being the average lattice displacement at a temperature T. As alluded to in the introduction, eqn.(3.3) can have contribution from free electrons, anharmonic phonons, and itinerant and localized electron moments.

For a simple non-magnetic metallic system. $\langle x \rangle_T$ will have contributions from anharmonic phonons and free electrons. Hence we can write for simple metallic systems [1]

$$\langle x \rangle_T = \langle x \rangle_T^{el} + \langle x \rangle_T^{ph} \; . \tag{3.4}$$

where $\langle x \rangle_T^{p\prime}$ is the lattice vibrational contribution and $\langle x \rangle_T^{el}$ gives the contribution from free electrons. However for magnetic materials there will be in general additional contributions from the itinerant and localized electron moments. Thus we can write for magnetic materials

$$\langle x \rangle_T = \langle x \rangle_T^{el} + \langle x \rangle_T^{ph} + \langle x \rangle_T^{m} \; , \tag{3.5}$$

where $\langle x \rangle_T^{m}$ is the magnetic contribution to lattice displacement. As discussed in the introduction, $\langle x \rangle_T^{m}$ can be written as a sum of the itinerant moment contribution

$\langle x \rangle_T^{im}$ and the localized **moment** or **magnon** contribution $\langle x \rangle_T^{mag}$. We shall **write** $\langle x \rangle_T^{el}$ and $\langle x \rangle_T^{im}$ together as the electron-magnetic contribution ($\langle x \rangle_T^{em}$), i.e.,

$$\langle x \rangle_T^{em} = \langle x \rangle_T^{el} + \langle x \rangle_T^{im} \ . \tag{3.6}$$

Thus $\langle x \rangle_T$ for ferromagnetic materials can be finally written as

$$\langle x \rangle_T = \langle x \rangle_T^{em} + \langle x \rangle_T^{ph} + \langle x \rangle_T^{mag} \ . \tag{3.7}$$

3.2.1 Theory for Vibrational Contribution

The lattice contribution to thermal expansion originates from phonon-phonon interactions. These interactions arise from the anharmonic terms in an expansion of the lattice ion-ion interaction potential energy around the equilibrium configuration of the ions. In this anharmonic picture, a phonon has a finite life time and can decay into other phonons through multiphonon processes. One normally considers [13] in quantum mechanical model calculations three and four phonon interactions given by,

$$\begin{aligned}
\mathcal{H}' &= \frac{1}{3!} \sum_{qq'q''} \sum_{jj'j''} \frac{h^{\frac{3}{2}}}{2^{\frac{3}{2}} N^{\frac{1}{2}}} \frac{\phi(\vec{q}j, \vec{q}'j', \vec{q}''j'')}{\sqrt{\omega_{qj}\omega_{q'j'}\omega_{q''j''}}} \delta_{\vec{q}+\vec{q}'+\vec{q}'', \mathcal{K}_m} \\
&\times (a_{-\vec{q}j}^{\dagger} + a_{\vec{q}j})(a_{-\vec{q}'j'}^{\dagger} + a_{\vec{q}'j'})(a_{-\vec{q}''j''}^{\dagger} + a_{\vec{q}''j''}) \ ,
\end{aligned} \tag{3.8}$$

$$\begin{aligned}
\mathcal{H}'' &= \frac{1}{4!} \sum_{qq'q''q'''} \sum_{jj'j''j'''} \frac{h^2}{4N} \frac{\phi(\vec{q}j, \vec{q}'j', \vec{q}''j'', \vec{q}'''j''')}{\sqrt{\omega_{qj}\omega_{q'j'}\omega_{q''j''}\omega_{q'''j'''}}} \delta_{\vec{q}+\vec{q}'+\vec{q}''+\vec{q}''', \mathcal{K}_m} \\
&\times (a_{-\vec{q}j}^{\dagger} + a_{\vec{q}j})(a_{-\vec{q}'j'}^{\dagger} + a_{\vec{q}'j'})(a_{-\vec{q}''j''}^{\dagger} + a_{\vec{q}''j''})(a_{-\vec{q}'''j'''}^{\dagger} + a_{\vec{q}'''j'''}) \ ,
\end{aligned} \tag{3.9}$$

where $a_{\vec{q}}^{\dagger}$ ($a_{\vec{q}j}$) is the creation (annihilation) operator for a phonon of $j - th$ branch and wave vector $\vec{q}$ and frequency $\omega_{\vec{q}j}$, Φ's are related to the atomic force constant tensors, $\mathcal{K}_m$ is a reciprocal lattice vector and N is the number of allowed vectors. The

free energy is then calculated within **the** frame-work of **the** Rayleigh - Schrödinger perturbation theory using $\mathcal{H}' + \mathcal{H}''$ as a perturbation and finally the lattice constant is obtained as a function of temperature by minimizing the free energy with respect to it. This approach is, however, quite tedious and, in fact only for a **linear** chain explicit calculations are usually available in the literature. We shall therefore follow here a rather simple-minded semiclassical approach in which the effects of three and four-phonon interactions will be simulated by considering the anharmonic potential [14]

$$V(x) = cx^2 - gx^3 - fx^4 . \tag{3.10}$$

where c, g and f are constants, g and f measuring the strengths of the cubic and quartic anharmonicities respectively. The x^3 - term describes the asymmetry of the mutual ion-ion repulsive potential and the x^4 - term takes care of the flattening of the bottom of the potential well which gives mode softening at large amplitudes (see **Fig.3.1**). Classically, the average lattice displacement at temperature T for the above potential can be calculated using the Boltzman distribution [14], i.e..

$$\langle x \rangle_T^{ph} = \frac{\int_{-\infty}^{\infty} x e^{-(P^2/2m+V(x))/k_B T} dx dP}{\int_{-\infty}^{\infty} e^{-(P^2/2m+V(x))/k_B T} dx dP} . \tag{3.11}$$

Unfortunately, $\langle x \rangle_T^{ph}$ as given by eqn.(3.11) cannot be calculated exactly for the potential (3.10). However if the anharmonic terms are small in comparison to $k_B T$ we may expand the exponential function and simplify eqn.(3.11) as

$$\langle x \rangle_T^{ph} = \frac{\int_{-\infty}^{\infty} x e^{-(cx^2/k_B T)} \left(1 + \frac{gx^3 + fx^4}{k_B T} + \frac{(gx^3 + fx^4)^2}{2(k_B T)^2} + \frac{(gx^3 + fx^4)^3}{6(k_B T)^3} + \cdots\right) dx}{\int_{-\infty}^{\infty} e^{-(cx^2/k_B T)} \left(1 + \frac{gx^3 + fx^4}{k_B T} + \frac{(gx^3 + fx^4)^2}{2(k_B T)^2} + \frac{(gx^3 - fx^4)^3}{6(k_B T)^3} + \cdots\right) dx} . \tag{3.12}$$
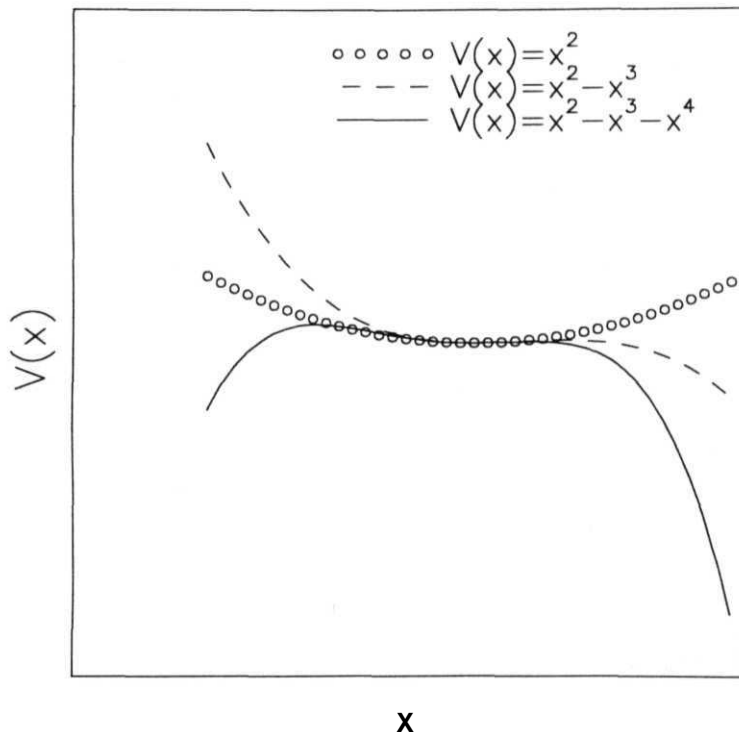
Fig.3.1 : Schematic representation of the anharmonic lattice potential.

The integrals appearing in the above equation can now be easily calculated to yield

$$\langle x \rangle_T^{ph} = \frac{3}{4}\frac{g}{c^2}(k_B T) \quad - \quad \frac{3}{4}\frac{g}{c^2}\left(\frac{15}{16}\frac{g^2}{c^3} - \frac{8f}{c^2}\right)(k_B T)^2$$
$$- \frac{105}{64}\frac{g}{c^2}\left(\frac{15}{4}\frac{g^2 f}{c^5} + \frac{3f^2}{c^4}\right)(k_B T)^3 , \qquad (3.13)$$

where terms higher than cubic in $(k_B T)$ have been neglected. In the present semi-classical scheme the classical thermal energy $k_B T$ is replaced by the average energy of a quantum oscillator. Employing the Debye model for the acoustic phonons and the Einstein approximation for the optical modes a semiclassical expression for the average vibrational lattice displacement can then be written as

$$\langle x \rangle_T^{ph} = \frac{3g}{4c^2}\left[\varepsilon - \left(\frac{15g^2}{16c^3} - \frac{8f}{c^2}\right)\varepsilon^2 - \frac{35}{16}\left(\frac{15}{4}\frac{g^2 f}{c^5} + \frac{3f^2}{c^4}\right)\varepsilon^3\right] . \qquad (3.14)$$

where,

$$\varepsilon = \left\{\left(\frac{3}{p}\right)3k_B T\left(\frac{T}{\Theta_D}\right)^3\int_0^{\frac{\Theta_D}{T}}\frac{z^3 dz}{e^z - 1} + \left(\frac{p-3}{p}\right)\frac{k_B \Theta_E}{e^{\frac{\Theta_E}{T}} - 1}\right\} , \qquad (3.15)$$

Θ_D and Θ_E are respectively the Debye and Einstein temperatures and p is the average number of phonon branches actually excited over the entire range of temperature. This way of approximating the acoustic and optical branches of a crystal is well known in the context of specific heat calculation. But to our knowledge such a scheme has not so far been used for the evaluation of thermal expansion.

The vibrational contribution to the linear thermal expansion coefficient (α_{ph}) can now be easily obtained using the equation

$$\alpha_{ph} = \frac{1}{a(T_0)}\frac{d\langle x \rangle_T^{ph}}{dT} . \qquad (3.16)$$

To determine the lattice vibrational Griineisen parameter (Γ_G^{ph}) one should also calculate for the anharmonic potential $V(x)$, the specific heat (at constant volume)

which is obtained as

$$C_{ph} = \frac{\partial}{\partial T}\langle[\frac{P^2}{2m} + V(x)]\rangle = \frac{\partial}{\partial T}\left[\frac{\int_{-\infty}^{\infty}\left\{\frac{P^2}{2m} + V(x)\right\}e^{-(P^2/2m-V(x))/k_B T}dxdP}{\int_{-\infty}^{\infty}e^{-(P^2/2m-V(x))/k_D T}dxdP}\right] \quad (3.17)$$

Using the same approximations and the philosophy as used in the case of eqns.(3.12) and (3.14) we simplify the calculation of C_{ph} and obtain

$$C_{ph} = 3\mathcal{N}\varepsilon' - 6\mathcal{N}\left(\frac{15g^2}{8c^3} - \frac{3f}{4c^2}\right)\varepsilon \times \varepsilon' . \quad (3.18)$$

where,

$$\varepsilon' = \left\{\left(\frac{3}{p}\right)3k_B\left(\frac{T}{\Theta_D}\right)^3\int_0^{\frac{\Theta_D}{T}}\frac{z^4e^z}{(e^z-1)^2}dz + \left(\frac{p-3}{p}\right)k_B\left(\frac{\Theta_E}{T}\right)^2\frac{e^{\frac{\Theta_E}{T}}}{(e^{\frac{\Theta_E}{T}}-1)^2}\right\} . \quad (3.19)$$

and $\mathcal{N}$ is the total number of atoms in the crystal. The lattice Griineisen parameter can then be calculated from

$$\Gamma_G^{ph} = \frac{\beta_{ph}B_T V}{C_{ph}} . \quad (3.20)$$

where β_{ph} is the vibrational contribution to the coefficient of volumetric thermal expansion and is given by $\beta_{ph} \; - \; 3\,\alpha_{ph}$, B_T is the total bulk modulus and V is the volume.

3.2.2 Free Electron Contribution to Expansion

In a simplified kinetic **picture,** the expansion due to free electrons can be interpreted physically as a change in volume of the lattice required to maintain a constant electron pressure when the temperature increases [15]. Quantitatively, the free electron contribution to the thermal expansion can be calculated from the volume dependence of the free electron entropy [16]. In the absence of any electron-phonon

interaction the electronic heat capacity (C_{el}) of a normal metal can be calculated from the Sommerfeld model of a nonint.eract.ing free electron gas. One obtains [14]

$$C_{el} = \frac{1}{3}\pi^2 g(\epsilon_0) k_B^2 T \; ,$$

(3.21)

for $T \ll \epsilon_0/k_B$ where ϵ_0 is the Fermi energy and $g(\epsilon_0)$ is **the** electron density of states at the Fermi level. The free electron entropy is now given by

$$S_{el} = \int_0^T \frac{C_{el}}{T} dT = \frac{1}{3}\pi^2 g(\epsilon_0) k_B^2 T \; .$$

(3.22)

The electronic contribution to linear thermal expansion coefficient α_{el} is then calculated as

$$\alpha_{el} = \frac{1}{3}\beta_{el} = \frac{1}{3B_T}\left(\frac{\partial S_{el}}{\partial V}\right) = \frac{2}{9}\left(\frac{1}{B_T V}\right)\left(\frac{1}{3}\pi^2 g(\epsilon_0) k_B^2\right) T = \gamma_{el} T \; ,$$

(3.23)

where β_{el} is the electronic contribution to volumetric thermal expansion coefficient. Hence the average lattice displacement due to free electrons in the case of a metal is given by

$$\frac{\langle x \rangle_T^{el}}{a(T_0)} = \frac{\gamma_{el}}{2} T^2 \; .$$

(3.24)

The free electron Grüneisen parameter (Γ_G^{el}) can also be obtained from the Sommerfeld model using the relation

$$\Gamma_G^{el} = \frac{\beta_{el} B_T V}{C_{el}} \; ,$$

(3.25)

which yields

$$\Gamma_G^{el} = \frac{2}{3} \; ,$$

(3.26)

which however is not found in general to be true experimentally. In the free electron model, the electron energy is purely kinetic and the electronic density of states is

proportional to the square root of the energy. When **the** effect of the periodic lattice potentials is taken into account the distribution of **the** electronic states gets modified giving rise to a series of energy bands which may be separate or overlapping with a density of states which may be a complicated function of energy unlike in the case of the free electron model where it is parabolic. The nonagreement of the free electron Grüneisen parameter value with the experimental values in case of several materials may thus be attributed to the non-parabolicity of the bands and band overlapping [1].

3.2.3   **Electron-magnetic contribution to** Thermal **Expansion**

The Heisenberg theory of ferromagnetism which is concerned with the direct exchange interaction between localized spins of nearest neighbours is a good enough theory for insulators. However it is certainly not quite valid for ferromagnetic metals and alloys where the electrons whose spin gives rise to ferromagnetism are not localized but itinerant. The most important group of ferromagnetic metals is the transition metals. The transition elements such as Fe, Co, Ni have 8, 9, 10 elections per atom respectively in the uppermost bands which are the superposition of 3d and 4s bands. It has been suggested that Cu and the transition metal elements have the similar band structure, and hence the similar density of states [17]. In Fig.3.2 we have shown schematically the density of states of Cu, Fe, Co and Ni where the elements are distinguished by the position of their respective Fermi energies relative to the band edges. For Cu, Fermi energy lies above the filled d-bands. The Fig.3.2 shows clearly that in the case of transition metals the overlapping d- and s-bands are only partially filled. Thus the d-band electrons also occupy the states near the Fermi energy. Efforts have been made to develop theories to explain ferromagnetism
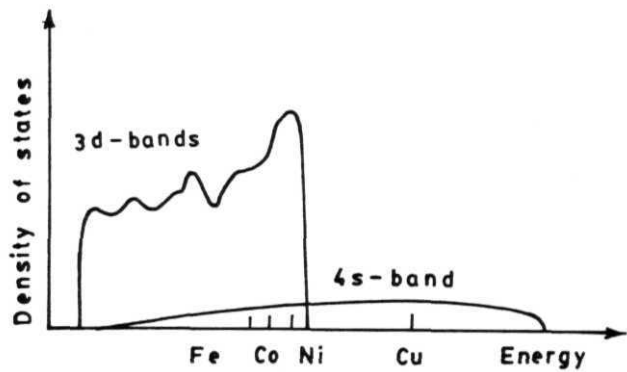
Fig.3.2 : Schematic representation of the density of states of the transition metals with the assumption that all thses elements have approximately the same band structure (rigid band model). The d-bands are filled to higher energies in Fe, Co and Ni according to the number of valence electrons. In Cu, the Fermi energy lies above the d-bands. in the 4s-band.
(From Introduction to Solid State Physics by 0. Madelung. Springer-Verlag, Berlin, 1978).

in transition metals considering **the** conduction electrons in unfilled bands. For iron group of elements the 4s-band electrons have been assumed not to contribute to ferromagnetism and the calculations have been done for the electrons in the partially filled 3d-band which have been considered responsible for ferromagnetism. Theories in which interactions between electrons have been considered have come to be known as the collective electron theories. The earlier theories however did not include the interactions of electrons with ion cores[18]. The calculations based on the band model were first performed by Slater [19], who obtained results for Ni which are in good agreement with the experimental values. **Stoner** has made a fairly detailed study of itinerant ferromagnetism in the transition metals on the basis of a collective electron model [10]. Later the Stoner model has been used and modified by Wohlfarth [11,12]. Since our calculation of the electron-magnetic contribution to thermal expansion will be based on the Stoner-Wohlfarth model we shall begin by presenting a detailed discussion of this model below.

(i) Stoner Model

The basic assumptions and the salient features of the Stoner's model are as follows:

1. The system under consideration is a set of N-electrons (or holes) in a partially filled 3d-band specified by the parameter ϵ_0, which denotes the maximum electron energy at T=0K in the absence of interaction (sec Fig.3.3a). The 3d-band is assumed to be parabolic near the Fermi level, i.e. the density of states $g(e)$ is given by the form,

$$g(e) \propto \epsilon^{1/2} .\qquad\qquad (3.27)$$
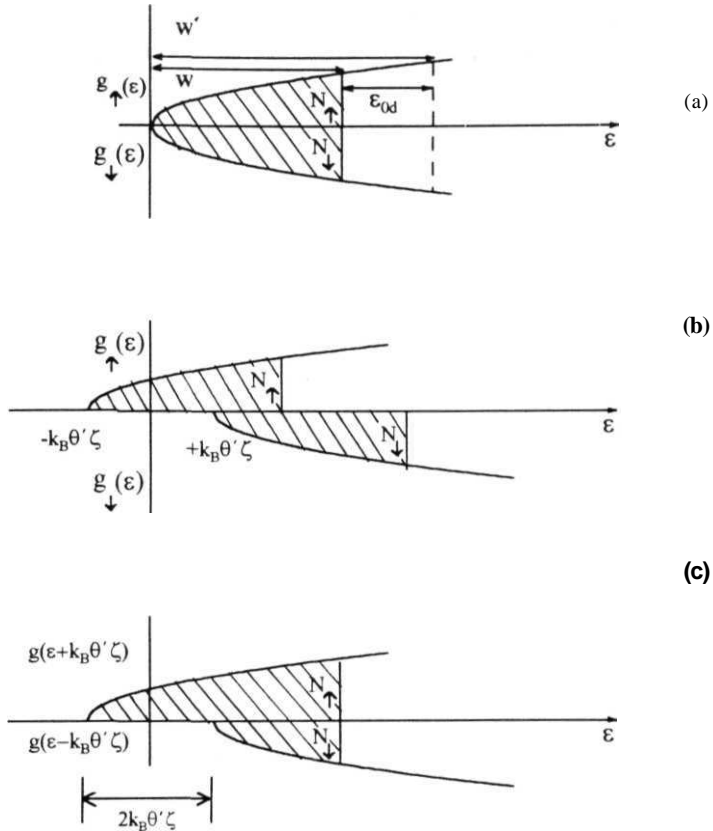
Fig 3.3: A schematic parabolic band structure of an itinerant ferromagnet at OK; (a) without interaction, (b) at the onset of exchange interaction and (c) after the exchange interaction showing an exchange splitting **of $2k_B\theta'\zeta$**.

The kinetic energy of the electrons is related to the wave vector k as

$$\epsilon(\vec{k}) = \frac{\hbar^2 k^2}{2m^*} ,$$
(3.28)

where m^* is the **Bloch** effective mass.

   2. The exchange interactions between the electrons can be treated in a mean field way by a Weiss-like molecular field. Thus the energy of an electron with spin parallel or antiparallel to the magnetization is given by [18]

$$\epsilon' = \mp N_u M \mu_B ,$$
(3.29)

where N_u is the molecular field constant and M is the resultant magnetic **moment** of **N-electrons** at a temperature T and μ_B is the Bohr magneton. Stoner has introduced the notations

$$\zeta = \frac{M}{N\mu_B} .$$
(3.30)

and

$$k_B \theta' = N_u N \mu_B^2 ,$$
(3.31)

where ζ is the relative magnetization, which is the ratio of the number of parallel spins to the total number of potentially effective spins [10]. Substituting eqns.(3.30) and (3.31) in (3.29), one obtains

$$\epsilon' = \mp k_B \theta' \zeta .$$
(3.32)

Since the maximum value of ζ is 1, $k_B \theta'$ gives a measure of the maximum quasi-magnetic interaction energy per electron [10]. The total energy of each electron is thus given by

$$\bar{\epsilon} = \epsilon + \epsilon' ,$$
(3.33)

which shows that the effect of the exchange interaction is to shift the up and down spin d-subbands energies by $-k_B\theta'\zeta$ and $k_B\theta'\zeta$ respectively leading to an exchange splitting of $2k_B\theta'\zeta$ between the upspin and and the downspin d-subbands (see **Fig**.3.3b). Consequently there will be a transfer of electrons from the down-spin subband to the up-spin subband resulting in a preponderance of upspin electrons and hence a spontaneous magnetic moment in the ground state. This is shown in Fig.3.3c.

We have shown in **Fig**.3.3 that in the presence of the exchange interactions the electronic density of states are modified. For **the** upspin and downspin electrons, the density of states can be written as

$$g_\uparrow(\epsilon) = g(\epsilon + k_B\theta'\zeta) \; , \tag{3.34}$$

and

$$g_\downarrow(\epsilon) = g(\epsilon - k_B\theta'\zeta) \;\; , \tag{3.35}$$

where the symbols $\uparrow$ and $\downarrow$ indicate up spin and down spin respectively and g is the single particle density of states for a non-interacting free electron gas. The number of electrons (or holes) in the upspin and downspin subbands can now be written as

$$N_\uparrow = \int_{-k_D\theta'\zeta}^{\infty} g_\cdot(\epsilon)f(\epsilon)d\epsilon \; . \tag{3.36}$$

and

$$N_\downarrow = \int_{k_D\theta'\zeta}^{\infty} g_\downarrow(\epsilon)f(\epsilon)d\epsilon \; , \tag{3.37}$$

where $f(\epsilon)$ is the Fermi distribution function given by

$$f(\epsilon) = \frac{1}{e^{(\epsilon-\mu)/k_BT} + 1} \; , \tag{3.38}$$

μ being the chemical potential. Using eqns.(3.34) and (3.38) and making the substitution $e + k_B\theta'\zeta = x$, we can write eqn.(3.36) as

$$N_\uparrow = \int_{-k_B\theta'\zeta}^{\infty} \frac{g(\epsilon + k_B\theta'\zeta)d\epsilon}{e^{(\epsilon-\mu)/k_BT} + 1} = \int_0^{\infty} \frac{g(x)dx}{e^{(x-k_B\theta'\zeta-\mu)/k_BT} + 1} \cdot \tag{3.39}$$

Similarly eqn.(3.37) becomes,

$$N_\downarrow = \int_{k_B\theta'\zeta}^{\infty} \frac{g(\epsilon - k_B\theta'\zeta)d\epsilon}{e^{(\epsilon-\mu)/k_BT} + 1} = \int_0^{\infty} \frac{g(x)dx}{e^{(x+k_B\theta'\zeta-\mu)/k_BT} + 1} \cdot \tag{3.40}$$

The total number of electrons (or holes) in the band is given by.

$$N = N_\uparrow + N_\downarrow. \tag{3.41}$$

Making the following substitutions

$$\frac{x}{k_BT} = y, \tag{3.42}$$

$$\frac{k_B\theta'\zeta}{k_BT} = \tau = \left(\frac{\theta'}{T}\right)\zeta, \tag{3.43}$$

and

$$\frac{\mu}{k_BT} = \lambda, \tag{3.44}$$

and using the expression for free electron density of states,

$$g(\epsilon) = \left(\frac{3N}{4}\right)\left(\frac{\epsilon^{1/2}}{\epsilon_0^{3/2}}\right) \cdot \tag{3.45}$$

we obtain from eqn.(3.41),

$$N = \frac{3}{4}N\left(\frac{k_BT}{\epsilon_0}\right)^{(3/2)} \left[F_{(1/2)}(\lambda + \tau) + F_{(1/2)}(\lambda - \tau)\right], \tag{3.46}$$

where

$$F_{(1/2)}(\lambda \pm \tau) = \int_0^{\infty} \frac{y^{1/2}dy}{e^{(y\mp\tau-\lambda)} + 1} \cdot \tag{3.47}$$

The resultant magnetic moment can be easily calculated. We obtain

$$M = \mu_B(N_\uparrow - N_\downarrow) \tag{3.48}$$

$$= \frac{3}{4}N\mu_B \left(\frac{k_BT}{\epsilon_0}\right)^{3/2} [F_{1/2}(\lambda + \tau) - F_{1/2}(\lambda - \tau)] . \tag{3.49}$$

Therefore the relative magnetization is given by,

$$\zeta = \frac{M}{N\mu_B} = \frac{F_{1/2}(\lambda + \tau) - F_{1/2}(\lambda - \tau)}{F_{1/2}(\lambda + \tau) + F_{1/2}(\lambda - \tau)} . \tag{3.50}$$

The total energy of the system can be written as,

$$E_{em} = \int_{-k_D\theta'\zeta}^{\infty} d\epsilon g_\uparrow(\epsilon)f(\epsilon)\epsilon + \int_{k_D\theta'\zeta}^{\infty} d\epsilon g_\downarrow(\epsilon)f(\epsilon)\epsilon + \frac{1}{2}Nk_B\theta'\zeta^2 . \tag{3.51}$$

where the third term in the above equation is the interaction energy. Using the expressions for $g_\uparrow(\epsilon)$, $g_\downarrow(\epsilon)$ and $f(\epsilon)$ the total energy of the system is obtained as.

$$E_{em} = \frac{3}{4}N\frac{(k_BT)^{5/2}}{\epsilon_0^{3/2}}[F_{3/2}(\lambda + \tau) + F_{3/2}(\lambda - \tau)] - \frac{1}{2}Nk_B\theta'\zeta^2 , \tag{3.52}$$

where

$$F_{3/2}(\lambda + \tau) = \int_0^{\infty} \frac{y^{3/2}dy}{e^{(y\mp\lambda-\tau)} + 1} \tag{3.53}$$

Eqn.(3.52) is a general expression for the electron-magnetic energy. It is not possible to obtain a simple analytical expression for the electron-magnetic energy at arbitrary temperatures. However in the limit $(k_BT/\epsilon_0) \ll 1$ or $A \gg 1$ (which will be a reasonable approximation for our systems) the Fermi integrals $F_{3/2}(\lambda \pm T)$ can be expanded in Taylor series and the electron-magnetic energy can be written in a simple analytical form. The series expansion for the general form of the Fermi-integral gives,

$$F_n(\lambda \pm \tau) = \int_0^{\infty} \frac{y^n dy}{e^{y-(\lambda\pm\tau)} + 1} = \frac{(\lambda \pm \tau)^{n+1}}{n + 1}\left\{1 + \sum_{\nu=1}^{\infty} a_{2\nu}^{(n)}(\lambda \pm \tau)^{-2\nu}\right\} \tag{3.54}$$

where

$$a_{2\nu}^{(n)} = 2(1 - 2^{1-2\nu})\varsigma(2\nu)(n+1)(n)(n-1)\cdots(n+2-2\nu),\qquad(3.55)$$

$\varsigma(2\nu)$ being the Riemann-Zeta function. Using eqn.(3.54), the electron-magnetic energy can be expressed as.

$$E_{em} = \frac{3}{4}N\frac{(k_BT)^{5/2}}{\epsilon_0^{3/2}} \quad \left[\frac{(\lambda+\tau)^{5/2}}{5/2}\left\{1 + \sum_1^\infty a_{2\nu}^{(3/2)}(\lambda+\tau)^{-2\nu}\right\} \right.$$
$$+ \left. \frac{(\lambda-\tau)^{5/2}}{5/2}\left\{1 + \sum_1^\infty a_{2\nu}^{(3/2)}(\lambda-\tau)^{-2\nu}\right\}\right]$$
$$- \frac{1}{2}Nk_B\theta'\zeta^2 .\qquad(3.56)$$

It is also possible to make the following inverse asymptotic expansion,

$$\lambda \pm \tau = \left\{\frac{3}{2}F_{1/2}(\lambda\pm\tau)\right\}^{2/3}\left\{1 - \sum_{\nu=1}^\infty a_{2\nu}^{(\frac{1}{2})'}\left[\frac{3}{2}F_{1/2}(\lambda\pm\tau)\right]^{-4\nu/3}\right\},\qquad(3.57)$$

where $a_2^{(\frac{1}{2})'} = \pi^-/12$, $a_4^{(\frac{1}{2})}$ - $\pi^4/80$ etc. The Fermi integrals $F_{1/2}(\lambda\pm T)$ can be written in terms of the relative magnetization ζ from eqns.(3.46) and (3.49) which give

$$F_{1/2}(\lambda\pm\tau) = \frac{2}{3}\left(\frac{\epsilon_0}{k_BT}\right)^{3/2}(1\pm\zeta) ,\qquad(3.58)$$

and the eqn.(3.57) then reduces to

$$\lambda \pm \tau = \left(\frac{\epsilon_0}{k_BT}\right)(1\pm\zeta)^{2/3}\left\{1 - \frac{\pi^2}{12}\left(\frac{k_BT}{\epsilon_0}\right)^2(1\pm\zeta)^{-4/3}\right.$$
$$\left. - \frac{\pi^4}{80}\left(\frac{k_BT}{\epsilon_0}\right)^4(1\pm\zeta)^{-8/3}\right\} .\qquad(3.59)$$

where terms upto fourth order in (k_BT/ϵ_0) have been retained. Substituting eqn.(3.59) in (3.56) and making some algebraic manipulations, we now obtain for the electron-magnetic energy to order $(k_BT/\epsilon)^4$,

$$E_{em} = \frac{3}{10}N\epsilon_0\left[\left\{(1+\zeta)^{5/3} + (1-\zeta)^{5/3}\right\} + \frac{5\pi^2}{12}\left(\frac{k_BT}{\epsilon_0}\right)^2\left\{(1+\zeta)^{1/3} + (1-\zeta)^{1/3}\right\}\right.$$

$$- \frac{31\pi^4}{384} \left(\frac{k_B T}{\epsilon_0} \right)^4 \left\{ (1+\zeta)^{-1} + (1-\zeta)^{-1} \right\} \Bigg] - \frac{1}{2} N k_B \theta' \zeta^2 \ . \tag{3.00}$$

The parameter & can also be written in a series in terms of $(k_B T/\epsilon_0)$. Using eqns.(3.43) and (3.59), we obtain

$$
\begin{aligned}
\theta' = \left(\frac{\tau}{\zeta} \right) T \ = \ & \frac{1}{2\zeta} \left(\frac{\epsilon_0}{k_B} \right) \left[\left\{ (1+\zeta)^{2/3} - (1-\zeta)^{2/3} \right\} \right. \\
& - \frac{\pi^2}{12} \left(\frac{k_B T}{\epsilon_0} \right)^2 \left\{ (1+\zeta)^{-2/3} - (1-\zeta)^{-2/3} \right\} \\
& \left. - \frac{\pi^4}{80} \left(\frac{k_B T}{\epsilon_0} \right) \left\{ (1+\zeta)^{-2} - (1-\zeta)^{-2} \right\} \right] \ .
\end{aligned}
\tag{3.61}
$$

Substituting eqn.(3.(il) in (3.60) and differentiating E_{em} with respect to temperature we now obtain the total electron-magnetic specific heat as,

$$
\begin{aligned}
\frac{C_{em}}{N k_B} \ = \ & \frac{\pi^2}{4} \left(\frac{k_B T}{\epsilon_0} \right) \left\{ (1+\zeta)^{1/3} + (1-\zeta)^{1/3} \right\} - \frac{31\pi^4}{320} \left(\frac{k_B T}{\epsilon_0} \right)^3 \left\{ (1+\zeta)^{-1} + (1-\zeta)^{-1} \right\} \\
& + \frac{1}{2} \frac{\epsilon_0}{k_B} \left[\frac{\pi^2}{6} \left(\frac{k_B T}{\epsilon_0} \right)^2 \left\{ (1+\zeta)^{-2/3} + (1-\zeta)^{-2/3} \right\} \right. \\
& \left. + \frac{39\pi^4}{640} \left(\frac{k_B T}{\epsilon_0} \right)^4 \left\{ (1+\zeta)^{-2} + (1-\zeta)^{-2} \right\} \right] \frac{\partial \zeta}{\partial T} \ .
\end{aligned}
\tag{3.62}
$$

At low temperatures. $\frac{k_B T}{\epsilon_0} \ll 1$ and since in the low-temperature limit ζ can be replaced by its zero temperature saturation value ζ_0, the electron-magnetic contribution to the specific heat at low temperature can be approximately written as,

$$
C_{em} = \frac{(\pi k_B)^2}{4} \frac{N}{\epsilon_0} \left\{ (1+\zeta_0)^{1/3} + (1-\zeta_0)^{1/3} \right\} T \ . \tag{3.63}
$$

(ii) Calculation of Thermal Expansion using Stoner-Wohlfarth Model

In the present work we are interested in the thermal expansion of transition metals such as Fe, Ni and their alloys in which the particles responsible for ferromagnetism are holes in the d-band. Indeed, Wohlfarth [11] has shown that most of the thermal

and magnetic properties of Ni could be interpreted satisfactorily through **the** presence of holes in the unfilled d-band. Therefore the number of particles N appearing in eqn.(3.63) should refer in the case of transition metals to the total number of holes in the 3d-band and ϵ_0 will refer to the zero temperature hole band width in the absence of interaction. In what follows we shall denote the hole band width by ϵ_{0d}, d referring to the d-band. Furthermore, as we have discussed above, the Stoner model calculations are based on the assumption **that** the energy bands are parabolic. Band structure calculations however show that electron density of states in transition metals can in general be quite complicated. Wohlfarth has modified [12] the Stoner model by taking a generalized band with the energy density of states give by

$$g(\epsilon) \propto \epsilon^{m} \tag{3.64}$$

where m lies between 0 and 1/2. The Stoner-Wohlfarth model yields for the electron-magnetic specific heat

$$C_{em} = \gamma_{em} T . \tag{3.65}$$

with

$$\gamma_{em} = \left(\frac{m+1}{6}\right) \frac{(\pi k_B)^2}{\epsilon_0 d} N_a N_{0d} \left[(1+\zeta_0)^{\frac{m}{m-1}} + (1-\zeta_0)^{\frac{m}{m+1}}\right] . \tag{3.66}$$

where N_{0d} is the total number of holes in **the** d-band per atom and N_a is the Avogadro number. If $N_{0d\uparrow}$ and $N_{0d\downarrow}$ are the number of the holes per atom in the up-spin and down-spin d-subbands respectively at T = OK and n_{0d} is the zero temperature magneton number per atom, then

$$n_{0d} = N_{0d\downarrow} - N_{0d\uparrow} , \tag{3.67}$$

and

$$N_{0d} = N_{0d\downarrow} + N_{0d\uparrow} \; . \tag{3.68}$$

Then the relative magnetization at T — OK is given by

$$\zeta_0 = \frac{n_{0d}}{N_{0d}} = \frac{N_{0d\downarrow} - N_{0d\uparrow}}{N_{0d\downarrow} + N_{0d\uparrow}} \; . \tag{3.69}$$

The electron-magnetic entropy (S_{em}) can be easily calculated from eqn.(3.65) and is given by

$$S_{em} = \int_0^T \frac{C_{em}}{T} dT = \gamma_{em} T \; . \tag{3.70}$$

Taking the volume dependence of ϵ_{0d} to be of the form, $\epsilon_{0d} \propto V^{\,\xi}$ (which is more general than what is obtained from the free electron model) and assuming that ζ_0 is independent of volume. we can calculate the electron-magnetic contribution to the coefficient of linear thermal expansion (α_{em}) using the relation

$$\alpha_{em} B_T = \frac{1}{3} \left(\frac{\partial S_{em}}{\partial V} \right) \; , \tag{3.71}$$

which gives

$$\alpha_{em} = \gamma'_{em} T \; . \tag{3.72}$$

where

$$\gamma'_{em} = \left(\frac{\delta}{3 B_T V} \right) \gamma_{em} \; . \tag{3.73}$$

The electron-magnetic contribution to the average lattice displacement is thus given by

$$\frac{\langle x \rangle_T^{em}}{a(T_0)} = A \left[(1 + \zeta_0)^{\frac{m}{m+1}} + (1 - \zeta_0)^{\frac{m}{m+1}} \right] T^2 \tag{3.74}$$

$$= \frac{\gamma'_{em}}{2} T^2 \; , \tag{3.75}$$

where

$$A = \frac{\delta}{6} \left(\frac{m+1}{6} \right) \frac{\pi^2 k_B^2}{\epsilon_{0d}} \frac{N_a N_{0d}}{B_T V} \ .$$ (3.76)

The electron-magnetic **Grüneisen** parameter can be obtained from the relation

$$\Gamma_G^{em} = \frac{\beta_{em} B_T V}{C_{em}} \ ,$$ (3.77)

where $\beta_{em} - 3\alpha_{em}$.Eqn.(3.77) yields

$$\Gamma_G^{em} = \delta \ .$$ (3.78)

Therefore, we can directly calculate the value of Γ_G^{em} from the thermal expansion measurements and eqn.(3.76) knowing the values of N_{0d} and ϵ_{0d}, which can be obtined from the band **structure** calculations.

3.2.4   The Magnon Contribution

The localized moment contribution to the thermal expansion can be obtained from the **Bloch spin-wave** theory which gives for **the** magnon specific heat of an **isotropic** cubic system [17]

$$C_{mag} = \gamma_{mag} T^{3/2} \ .$$ (3.79)

with

$$\gamma_{mag} = \left[\frac{N}{4\pi^2} \left(\frac{k_B}{2JS} \right)^{3/2} k_B \int_0^\infty \frac{x^{3/2} dx}{e^x - 1} \right] \ ,$$ (3.80)

where S is the spin. J is the exchange integral and N is the number of localized spins. The magnon entropy can be easily calculated as

$$S_{mag} = \int_0^T \frac{C_{mag}}{T} dT = \frac{2}{3} \gamma_{mag} T^{3/2} \ .$$ **(3.81)**

Taking the volume dependence of J to be of the form. $J \propto V$ ", the magnon contribution to the linear thermal expansion coefficient (α_{mag}) can now be obtained from the relation

$$\alpha_{mag} = \frac{1}{3}\beta_{mag} = \frac{1}{3B_T}\left(\frac{\partial S_{mag}}{\partial V}\right) ,$$ (3.82)

where β_{mag} is the magnon contribution to **the** volumetric **thermal** expansion coefficient, Eqn.(3.82) yields

$$\alpha_{mag} = \gamma'_{mag}T^{3/2} .$$ (3.83)

where

$$\gamma'_{mag} = \left(\frac{\eta}{3B_T V}\right)\gamma_{mag} .$$ (3.64)

The **magnon** contribution to **the** average lattice displacement can thus be written **as**

$$\frac{\langle x\rangle_T^{mag}}{a(T_0)} = \frac{2}{5}\gamma'_{mag}T^{5/2} .$$ (3.85)

It immediately follows from **the** relation

$$\Gamma_G^{mag} = \frac{\beta_{mag}B_T V}{C_{mag}} .$$ (3.86)

that η can be identified as the **magnon Grüneisen parameter.**

In terms of γ'_r and η, the magnon entropy is given by a simple relation :

$$S_{mag} = 2\left(\frac{\gamma'_{mag}B_T V}{\eta}\right)T^{3/2} .$$ (3.87)

which will be later used to determine η.

3.3   Tests of the Model

To examine the validity of our theoretical model we first make thermal expansion measurements on Al and fit our observed fractional lengtli change data (discussed in section 2.5) and the corresponding standard data of Cu [20] to eqn.(32). Since these are non-magnetic metals we include in $\langle x \rangle_T$ only the electronic and phonon contribution given by eqns.(3.24) and (3.14) respectively. Furthermore as **these** systems are monoatomic solids they are not expected to have any optic modes in lattice vibrations. Hence the fits have been performed without the Einstein term and by taking $p = 3$ in the Debye term and with $g' - g/c^2 a(T_0), g'' = g^2/c^3, f - //c^2$ and Θ_D as parameters. A non-linear least square fit has been done using the grid search technique [21] where the optimum value of every parameter is found by varying each parameter separately. The fits are found to be excellent (see Fig.3.3). Table-3.1 gives the values of the parameters that give the best fit. The percentage r.m.s. deviation is found out to be less than 0.3% for both the fits. The values of Θ_D obtained from the fits of Cu and Al are respectively (344.5 ± 0.8) K and (423.3 ± 0.4) K which compare well with the corresponding reported values 345 K and 428 K. The values of the coefficient of the electronic contribution to thermal expansion (γ_{el}) obtained from our fits are (2.60 ±0.08) x 10^{-10}K^2 and (9.13 ±0.04) x 10^{-10}K^{-2} for Cu and Al respectively which also agree with the reported values. The comparison is shown in Table-3.1. This impressive agreement between our fitted values and the ones given in the literature imparts a fair amount of confidence in our approach.

In the following section. we shall use our model to analyze the thermal expansion data of ferromagnetic transition metals where the electron-magnetic and magnon terms also contribute. This is followed by application of the model to alkali halides.
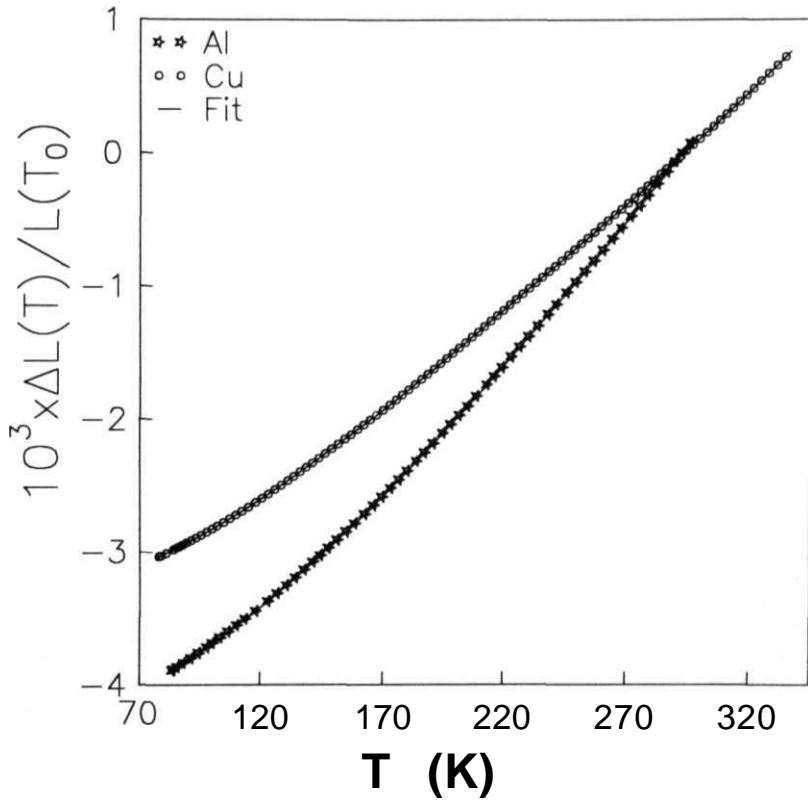
Fig.3.4 : Fractional length change data of Copper and Aluminum with the fits to the eqn.(3.2) shown as the solid lines.

Sample	Copper	Aluminum
g' (eV^{-1})	0.265±0.008	0.370 ± 0.004
g'' (eV^{-1})	$(8.86\pm0.2)\times10^{-6}$	$(7.85\pm1.3)\times10^{-6}$
f' (eV^{-1})	$(1.04\pm0.02)\times10^{-6}$	$(9.20\pm1.53)\times10^{-7}$
Θ_D (K)	344.5±0.8 [345]	423.3±0.4 [428]
γ_{el} (K^{-2})	$(2.60 \pm 0.0.08) \times 10^{-10}$ [2.54 x 10^{-10}]	$(9.13 \pm0.04) \times 10^{-10}$ [9.20 x 10^{-10}]

Table-3.1 : Values of anharmonicity parameters and characteristic temperatures obtained by fitting the fractional length change data of Cu and Al. The values of Θ_D and γ_{el} in the square brackets are reported values obtained from specific heat data [1,14].

3.4 Measurement and Analysis of Thermal Expansion of Nickel and Iron

Interest in the transition metal elements has continued unabated for several decades for their interesting magnetic and thermal properties several of which have remained hitherto elusive. Experimentally, ferromagnetic **transition** metals are found **to** show in addition to a vibrational contribution a linear-T dependence in their low temperature thermal expansion behaviour which is believed **to** include both the pure electronic contribution and a contribution from the itinerant electron moments. As we have already mentioned in subsection 3.2.3, this linear-T term in the thermal expansion coefficient is commonly referred to as the electron-magnetic contribution and can be explained within the framework of the collective electron model of Stoner and Wohlfarth. There have been a host of experimental reports giving the values of electron-magnetic Grüneisen parameter Γ_G^{em}. But accurate theoretical calculation of Γ_G^{em} is certainly very difficult for these elements because of their complicated band structure and complex magnetic behaviour. To our knowledge, there has been only one calculation of Γ_G^{em} [22] which predicted $\Gamma_G^{em} = 5/3$ from a simplified model for magnetic properties of electrons in isolated d-bands based on the works of Lang and Ehrenreich [23] and Heine [24]. However there seems to be no justification for this model to apply in general.

We have also discussed in the subsection-3.2.4 that in the transition metals and alloys the magnetic contribution to the thermal expansion may come from the localized spin moments too which we have termed as magnon contribution. To our knowledge, for these materials there exists no estimation of the magnon Grüneisen

parameter (Γ_G^{mag}), which is essentially given by **the** volume derivative of **the Heisen-**berg interaction energy J, again a quantity difficult **to** calculate theoretically.

The aim of the present section is to show that our model can be used together with the band structure results to analyze the thermal expansion data of transition metals to yield reliable estimates of characteristic temperatures, various contributions to specific heat and the Griineisen parameters. For this purpose we have performed thermal expansion measurements on two transition metals, namely nickel and iron for which accurate band structure calculations are available. We have already discussed in detail in Chapter 2 our thermal **expansion** measurement procedure and have also presented our fractional length change data of Fe and Ni in 2.5 for the sake of comparison with **the** reported data. In the following subsections (3.4.1 and 3.4.2), we shall present **the** analysis of these data using our model.

3.4.1   Nickel

Band structure calculations for Ni [25,26] show that the 3d-band electron wave functions overlap strongly with 4s-band electrons. It has been found that at zero temperature the outermost electrons are distributed so that the Ni d-band contains 9.4 electrons per atom and s-band contains 0.6 electrons per atom. The upspin d-subband is completely filled up with 5 electrons per atom while the downspin d-subband has 4.4 electrons per atom. Thus the d-band contains 0.6 holes' per atom which are the participating particles in the ferromagnetism of Ni. Therefore

$$\zeta_0 = \frac{n_{0d}}{N_{0d}} = \frac{N_{0d\downarrow} - N_{0d\uparrow}}{N_{0d\downarrow} + n_{0d\uparrow}} = \frac{0.6}{0.6} = 1 \ . \tag{3.88}$$

which explains why Ni is considered a strong itinerant ferromagnet [27]. Furthermore, the occupied part of the up-spin d-subband has a width of 4.6 eV and that

of the down-spin d-subband has a width of 4.08 eV with an exchange splitting of 0.52 eV.

To analyze the thermal expansion behaviour of Ni we have fitted the fractional length data to eqn.(3.2) with the total average lattice displacement $\langle x \rangle_T$ given by eqn.(3.7) and $\langle x \rangle_T^{em}$, $\langle x \rangle_T^{mag}$ and $\langle x \rangle_T^{ph}$ obtained from eqns.(3.74), (3.85) and (3.14) respectively. Fits have been performed with Co $= 1$ and with $g' = g/c^2a(T_0)$, $g'' = g^2/c^3$, $l' = l/c^2$, Θ_D, Θ_E, p, A, m and $7'$ as parameters. It is observed that $p = 3$ gives the best fit. This shows the absence of optical modes in the present system. Furthermore, the magnon contribution also turns out to be negligibly small. In the final fit, therefore, the Einstein and the magnon terms have been dropped altogether. The fit is shown in Fig.3.5. It is clear that the fit is excellent over the entire range of temperature. The percentage r.m.s. deviation is found to be about 0.7%. Table-3.2 gives the parameter values for the best fit. Interestingly enough, the value of the Debye temperature obtained from our fit is 450 K which is exactly-identical to the value reported in the literature [14]. Using the fitted values of the anharmonic parameters and the Debye temperature and with the total number of atoms, $.V - 6.023 \times 10^{23}$, we now obtain the molar vibrational specific heat (C_{ph}) from eqn.(3.18). Γ_G^{ph} is then calculated from eqn.(3.20) using $B_T - 1.86 \times 10^{11}$ Nm^{-2} [14]. $V = 6.59$ cc (molar volume) and the above value of $\mathcal{N}$. It is observed that $\Gamma_G^{p'}$ remains essentially constant, independent of temperature in the range 80 - 300K and we find its value to be equal to 2.0 which compares quite favourably with the value 1.6 (see Table-3.3) which is the reported lattice Grüneisen parameter for Ni at low temperature [1].

The value of m obtained from fitting is 0.497 which suggests that in the case of Ni the energy band is almost parabolic. Using the fitted values of m, A and ζ_0 =
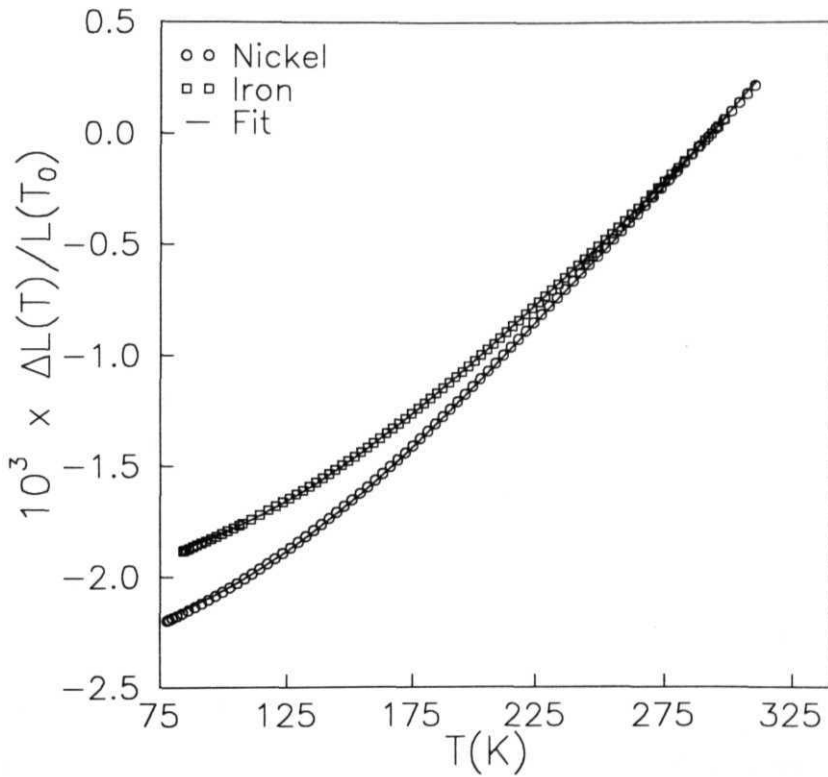
Fig.3.5 : Fractional length change data of Iron and Nickel with the fits to the eqn.(3.2) shown as the solid lines.

1 we find $\gamma'_{em} = 3.1 \times 10^{-9}$ K^2 which is in excellent agreement with the reported value, 3.8×10^{-9} K^{-2} [1]. To obtain the electron-magnetic specific heat and Γ_G^{em} we need to know the value of the hole band width, ϵ_{0d}. In the absence of exchange interactions each d-subband of Ni contains 4.7 electrons at OK within a band width of 4.34 eV. If w' is the total band width of the d-band (i.e., the width including the occupied electron band and the hole band) at T = OK in the absence of exchange interactions, then we can write

$$\frac{5}{4.7} = \frac{\int_0^{w'} \epsilon^m d\epsilon}{\int_0^{4.34} \epsilon^m d\epsilon} \; , \tag{3.89}$$

which yields $w' — 4.523$ eV and thus ϵ_{0d} is obtained as

$$\epsilon_{0d} = (4.523 - 4.340)eV = 0.183eV \; . \tag{3.90}$$

Using this value of ϵ_{0d} and $N_{0d} = 0.6$, $B_T = 1.86 \times 10^{11}$ Nm^{-2}, $V = 6.59$ cc (molar volume) and the fitted values of A and m we obtain from eqn.(3.76), $\delta = 1.97$ which is in excellent agreement with the reported experimental electron-magnetic Griineisen parameter value 2.1 (see Table-3.3) [1]. The coefficient of the molar electron-magnetic specific heat can now be easily calculated from eqn.(3.73). We get $\gamma_{em} = 7.243$ mJ/mol K^2 which agrees remarkably well with the reported experimental value, 7.02 mJ/mol K^2 [14] lending credence to our theoretical analysis.

3.4.2 Iron

Band structure calculations on iron by Callaway and collaborators [28,29] suggest that at zero temperature the upspin d-subband of iron contains 4.6 electrons per atom within a band width of 4.7 eV and the downspin d-subband contains 2.4 electrons within a width of 3.4 eV with an exchange splitting of 1.3 eV. We thus

Sample	Nickel	Iron
g' (eV^{-1})	0.21 ± 0.02	0.16 ± 0.02
g'' (eV^{-1})	$(3.24\pm0.2)\times10^{-3}$	$(2.63\pm0.2)\times10^{-3}$
f' (eV^{-1})	$(3.83\pm0.2)\times10^{-4}$	$(3.092\pm0.2)\times10^{-4}$
Θ_D $(\mathbf{K})$	450.0 ± 0.7 [450]	$\mathbf{469.7\pm0.7}$ [470]
m	0.497 ± 0.002	0.489 ± 0.002
A (K^{-2})	$(1.23\pm0.7) \times 10^{9}$	$(1.95\pm0.6) \times 10^{9}$
γ'_{em} (K^{-2})	3.1×10^{-9} [3.8×10^{-9}]	4.9×10^{9} [3.2×10^{-9}]
γ'_{mag} $(K^{-5/2})$	-	$(2.9\pm0.6) \times 10^{10}$

Table-3.2 : The fitted parameter values for Ni and Fe. The values of Debye temperatures inside the square brackets are taken from ref.14 and the values of γ'_e inside square brackets are taken from ref.l.

have $N_{0d\uparrow} = 0.4$ and $N_{0d\downarrow} = 2.6$ and **therefore** the relative magnetisation for iron at T = OK is given by

$$\zeta_0 = \frac{n_{0d}}{N_{0d}} = \frac{2.2}{3.0} = 0.73 ,$$

which implies that iron is not a strong itinerant ferromagnet [27]. The fractional length change data for iron are fitted to eqn.(3.2) with the above value of ζ_0 and with g', $9''$, f', Θ_D, Θ_E, p, A, m and γ_{mag} as fitting parameters. It is again observed that $p = 3$ gives the best fit. So the final fit has been carried out without the Einstein term. It is however interesting to note that it was not possible to fit the data with reasonable accuracy without the magnon term which is however consistent with the observation that $\zeta_0 < 1$ for iron. The fit is shown in Fig.3.4. Clearly the fit is excellent. The percentage r.m.s. deviation is found to be about 0.3%. Table-3.2 gives the parameter values from the best fit. The value of Θ_D obtained from the fit is 469.7 K which is again in excellent agreement with the value quoted in the literature (see Table-3.2) [14].

We calculate Γ_G^{ph} for Fe in the same way as we have discussed for Ni. We find for Fe, $\Gamma_G^{ph} = 1.485$ which agrees quite remarkably with the reported value 1.3 [1]. From the fitted values of m and A and with Co = **0.73,** we obtain $\gamma'_{em} = (4.956 \pm 0.6)$ x 10^{-9} K $^{-2}$. which compares reasonably with the reported value (3.2 ± 0.4) x 10^{-9} K^{-2} [1] In the absence of exchange interactions each d-subband of Fe contains 3.5 electrons at OK within a band-width of 4.05 eV. Using the same prescription as was followed in the case of Ni, we find for Fe, $w = 5.146$ eV and thus $\epsilon_{0d} = 1.096$ eV. Using this value of ϵ_{0d}, and $N_{0d} = 3.0$, $B_T = 1.683$ x $10^{11} Nm^{-2}$ [14], $N_a = 6.023$ x 10^{23}, $V = 7.09$ cc (molar volume) and the fitted values of A and m, we obtain from eqn.(3.77), $6 = 2.01$ which is fairly close to the reported experimental value 2.4

Sample	γ_{em} $(mJ/molK^2)$	Γ_G^{ph}	Γ_G^{em}	G
Nickel	7.243 [7.02]	2.00 [1.6]	1.97 [2.1]	
Iron	8.829 [4.980]	1.48 1.3]	2.01 [2.4]	4.01

Table-3.3 : The estimated values of the electron-magnetic contribution to specific heat and Gruneisen parameters of Ni and Fe. The values of γ_{em} inside the square brackets are taken from ref.14 and the values of Gruneisen parameters inside square brackets are taken from ref.1.

[1]. From eqn.(3.73) we now get $\gamma_{em} = 8.829$ mJ/mol $\mathbf{K^3}$ **which is** somewhat higher than the only reported value 4.98 mJ/mol K^2 [1]. As has already been alluded to above, we have obtained a nonvanishing magnon contribution to the thermal expansion of iron with $\gamma'_{mag} = 2.878$ x 10^{-10} K-5/2. Using the expression (3.87) and the prescription that the magnon entropy should continuously go over to the paramagnetic value *Rln2* at $T - T_C$, η is then found to be equal to 4.01. Eqn.(3.84) then yields, $\gamma_{mag} = 0.257$ mJ/mol $K^{-5/2}$ **which** is about an order of magnitude larger than the only reported value [32]. So it seems that more accurate measurements together with careful analysis of data are called for to verify **the** magnon contribution to the specific heat and thermal expansion of Iron.

Thus we find that our method provides us with very accurate values of the Debye temperature, yields estimates of the anharmonicity parameters of the lattice potential, gives correct values the Griineisen parameters and suggests the nature of the energy bands. We show that both nickel and iron have almost parabolic bands. We furthermore show that the electron-magnetic moments in nickel are all itinerant while those in iron are not. We would like to point **out** that in addition to the assumption of volume independence of ζ_0, we have made a few more assumptions in our analysis for the sake of mathematical simplicity. For instance, we have used the low-temperature limit of the Stoner model. This, we believe, will introduce only a small error in our result because for both nickel and iron the temperature range considered in our work is much below the transition temperature. Secondly, we have neglected a small electronic contribution which would come from the s-band. We have also neglected the band transfer effect, which is proportional to $(k_B T/\epsilon_{0d})^2$ and is therefore very small in the present case for both iron and nickel. Finally, the expression for the magnon contribution used in our analysis is rigorously

valid only at long wavelengths and at low temperatures at which the system can have only low-lying excitations. In practice however this turns out to be a good enough approximation in many cases. Incorporation of the contributions from the s-band and the band transfer effect and the higher-order electron-magnetic **and magnon** terms will certainly improve our analysis. We however do not anticipate any significant qualitative difference to show up, although a marginal change in the model parameters might be expected.

3.5   **Thermal** Expansion Analysis of Alkali Halides

The temperature variations of thermal expansion and specific heat at constant volume of KBr and NaCl have been studied by Kwon [30] by incorporating the local dynamics of the lattice into the original Einstein model. Though for NaCl the modified Einstein model of Kwon agrees with the experimental data, the fits are not very impressive for KBr. In the present section we shall analyze the thermal expansion data of four alkali halides KBr, KCl, KI and NaCl our semiclassical model described in section 3.2.

As the alkali halides are non metals only the vibratioiial part of the fractional length change expression is used for the fit using g', g'', f, Θ_D, Θ_E, and p as parameters. The experimental data for these materials have been taken from Ref.31. The plots are shown in Figs.3.6, 3.7, 3.8 and 3.9 and the values of the parameters are quoted in Table-3.4. Fig.3.6 shows the variation of the thermal expansion of potassium bromide with temperature. It is clear that the fit is excellent over the wide range of temperature. The value of Debye temperature predicted from our fit is 173.7 ± 1.2 K which is very close to the reported value of **174** K. However the
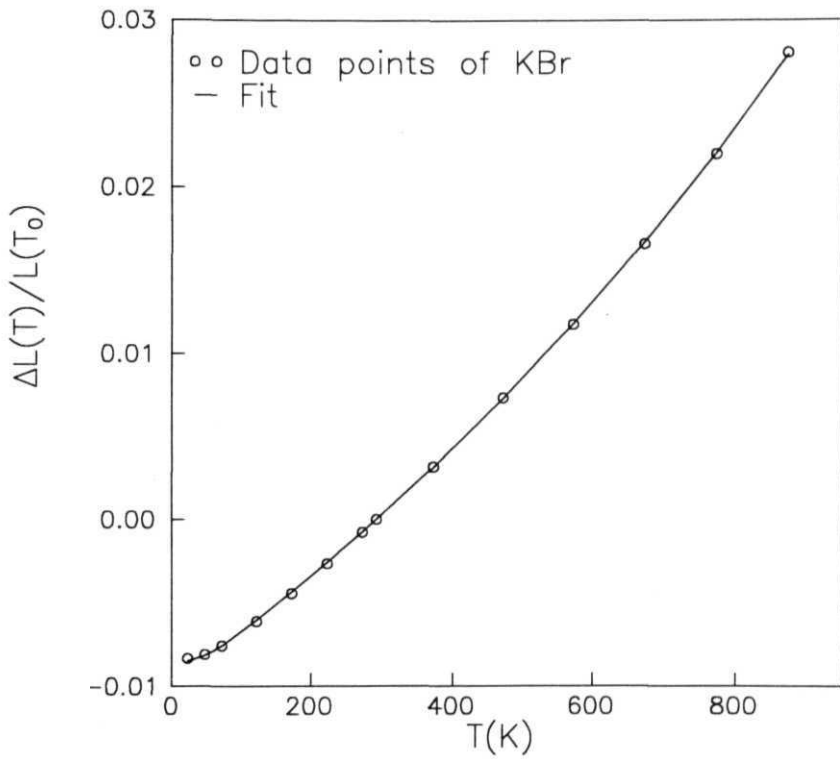
Fig.3.6 : Temperature variation of fractional length change data of KBr with the solid line showing the fit to the data.
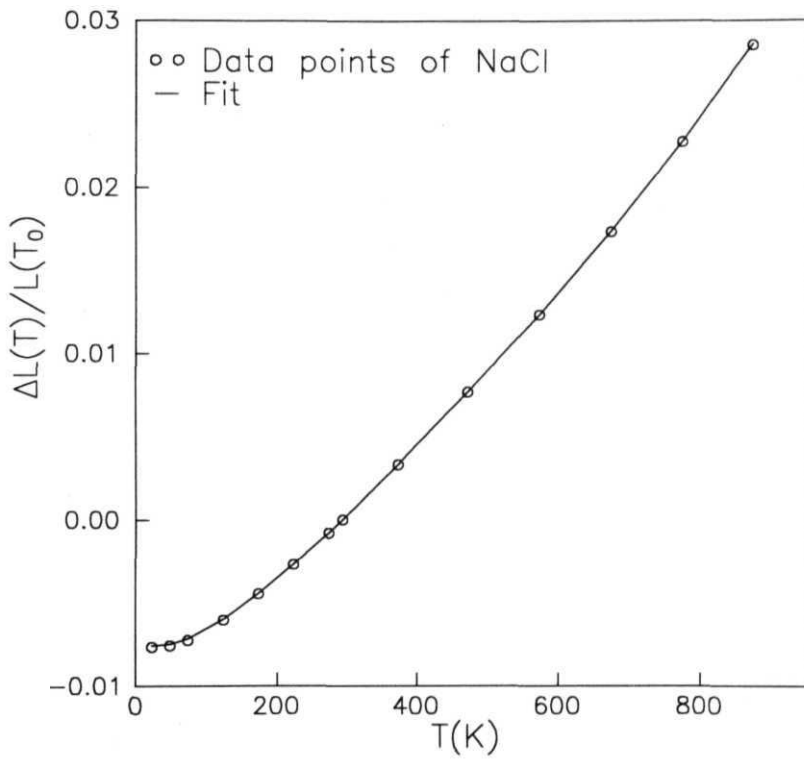
Fig.3.7 : Temperature variation of fractional length change data of NaCl with the solid line showing the fit to the data.
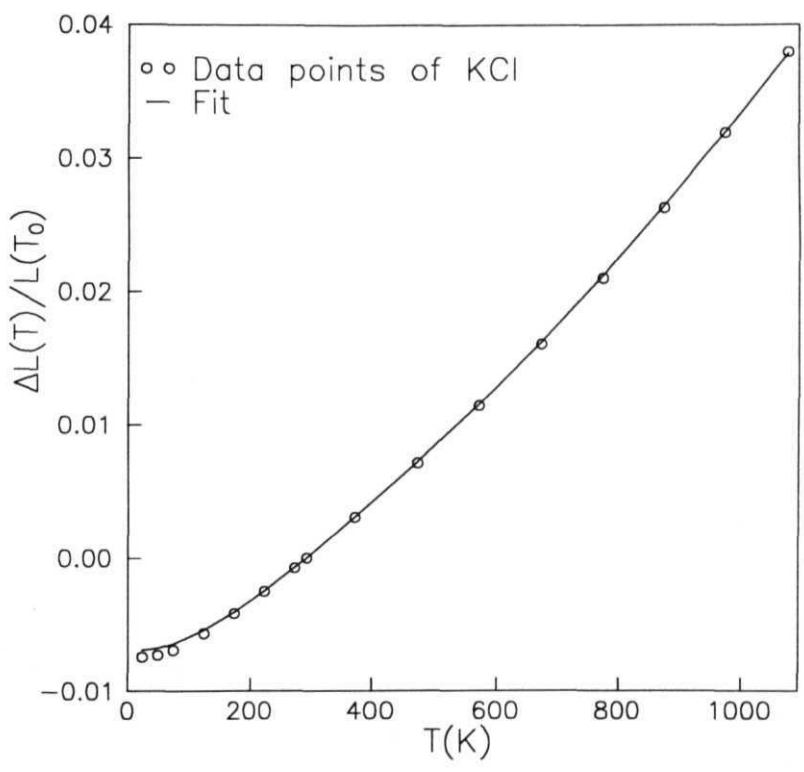
Fig.3.8 : Temperature variation of fractional length change data of KCl with the solid line showing the fit to the data.
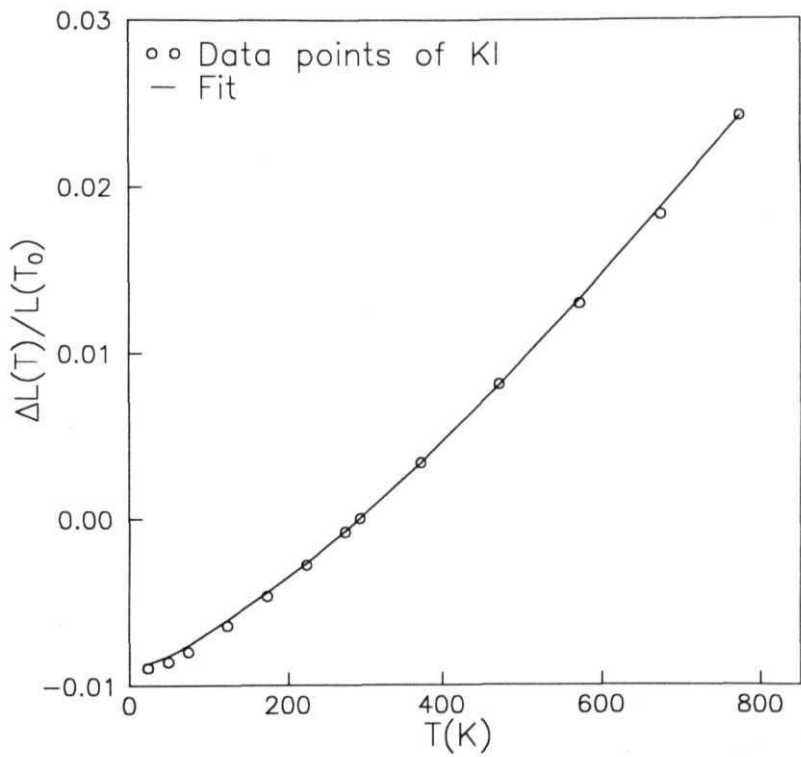
Fig.3.9 : Temperature variation of fractional length change data of KI with the solid line showing the fit to the data.

fit did not show the **presence of** any optical modes. In Fig.3.7 the data of NaCl is plotted with the fit which is given by the solid line. The fit is quite **impressive** over the complete temperature range The average number of phonon branches p in this case, however, comes out **to** be a **fraction,i.e.,** 3.2 which is probably because the parameter p is kept fixed over the entire range of temperature while in reality the number of phonon branches excited in different temperature ranges could be different. Interestingly, however. the value of Debye temperature obtained from our fit is 321.0 ± 1.3K which is identical to the value reported in **literature.** The value of Einstein temperature **returned** by the fit is 649.8 ± 1.3 K. Fig.3.8 shows the variation of thermal expansion of potassium chloride with temperature. Evidently the fit is fairly good over the entire temperature range and the value of Debye temperature obtained from our analysis is 236.6 ± 0.8 K which is again quite close to the reported value 235 K. The average number of phonon branches **in** this case came out to be 5 with the Einstein temperature as 540.2 ± 0.8 K. Finally in Fig.3.9 the behaviour of the thermal expansion data of potassium iodide is plotted as a function of temperature. The fit is quite impressive at the complete temperature range. The value of Debye temperature predicted from the fit is exactly identical to the value quoted in literature which is 132.0 K. But the total number of branches came our to be 3. Thus in general the above semiclassical theory seems to agree quite well with the experimental results. One can see the distinct advantage of this model is that it predicts the values the Debye and Einstein temperatures from the thermal expansion data quite accurately. Hence the same model can be used to calculate the vibrational specific heat and the vibrational entropy using the fitted parameters from the fit of the thermal expansion data.

3.6   Conclusion

In this chapter we have developed a new microscopic **theoretical** model **to** obtain the vibrational, electron-magnetic and magnon contributions to the coefficient of thermal expansion. The model has been applied to analyze the thermal expansion behaviour of simple elemental metallic systems like Cu and Al, ferromagnetic transition metals such as Fe and Ni and alkali halides. It has been shown that the present model provides us with estimates of anharmonicity parameters of the lattice potential and also gives very accurate values of the characteristic Debye and Einstein temperatures. We have furthermore shown that we are able to obtain from our approach quite successfully the values of the various Griineisen parameters. The model developed in the present chapter will be used to analyze the thermal expansion behaviour of more complicated systems in the subsequent chapters.

References

[1] T.H.K. Barrou, J.G. Collins and G.K. White, Adv. Phys. 29. 609 (1980).

[2] G. Leibfried and W. Ludwig, Solid State Phys. 12, 276 (1961).

[3] H.R. Glyde and M.L. Klein, Crit. Rev. Solid St. Sci. **2**, 18 **(1971).**

[4] G.K. Horton and A.A. Maradudin, Dynamical Properties of Solids, Vols.l and 2 (Amsterdam, North Holland. 1974, 1975).

[5] M.L. Klein and J.A. Venables (editors), Rare Gas Solids, Vol.1 (Academic-Press. London. 1976).

[6] G.D. **Mukherjee,** C. Bansal and Ashok Chatterjee, Mod. Phys. Lett. B 8, 425 (1994).

[7] G.D. Mukherjee, Ashok Chatterjee and C Bansal, Physica C **232,** 241 (1994)

[8] G.D. Mukherjee, C. Bansal and Ashok Chatterjee, Phys. Rev. Lett. 76, 1876 (1996).

[9] G.D. Mukherjee, C. Bansal and Ashok Chatterjee, *Vibrational and magnetic contribution to entropy of an $L1_2$ ordered and a partially ordered Ni_3Mn alloy : results from thermal expansion measurements and model calculations,* submitted for publication.

[10] E.C. Stoner, Proc. Roy. Soc. **A165,** 372 (1938); **A169,** 339 (1939).

[11] E.P. Wohlfarth, Proc. Roy. Soc.(London) **A195.** 434 (1949); Proc. Phys. Soc. 60, 360 (1948).

[12] E.P. Wohlfarth, Phil. Mag. 42, 374 (1951).

[13] O. Madelung, Introduction to Solid State Physics (Springer, Berlin, Heidelberg, 1978), p.314.

[14] C. Kittel, Introduction to Solid State Physics (Wiley Eastern Univ. Edition, 1977).

[15] J.G. Collins and G.K. White, Prog. Low temp. Phys. 4, 40 (1964).

[16] D.C. Wallace, J. Appl. Phys. 41, 5055 (1970).

[17] A.H. Morrish, The Physical Principles of Magnetism, (Robert E. Kreiger Publishing Co., Inc., 1980).

[18] F. Bloch, Z. Physik 57. 545 (1929); L. Brillouin, J. Phys. Radium 3, 565 (1932).

[19] J.C. Slater, Phys. Rev. 49, 537 (1936); 49, 931 (1936); 52, 198 (1937); Revs. Mod. Phys. 25, 199 (1953)

[20] F.R. Kroeger and C.A. Swenson. J. Appl. Phys. 48. 853 (1977).

[21] P.R. Bevington, Data Reduction and Error Analysis for the Physical Sciences, (Mc Graw Hill, New York, 1969), p.204.

[22] M. Shimuzu, Phys. Lett. A 50, 93 (1974).

[23] N.D. Lang and H. Ehrenreich, Phys. Rev. 168, 605 (1968).

[24] V. Heine, Phys. Rev. 153, 673 (1967).

[25] J. Callaway and C.S. Wang, Phys. Rev. B 7, 1096 (1973).

[26] C.S. Wang and J. Callaway. Phys. Rev. B **9,** 4892 (1974).

[27] E.P. Wohlfarth, Ferromagnetic Materials, vol.1 (ed. E.P. Wohlfarth. North-Holland, Amsterdam, 1980), p.1.

[28] R.A. Tawil and J. Callaway, Phys. Rev. B 7, 4242 (1973).

[29] J. Callaway and C.S. Wang. Phys. Rev. B 16, 2095 (1977).

[30] T.H. Kwon, Phil. Mag. Lett. 65. 261 (1992); Solid State Commun. **82.** 1001 (1992).

[31] R.K. Kirby, T.A. Hahn and B.D. Rothrock. Thermal **Expansion,** American Institute of Physics Handbook, 3rd Edition. ed. D.E. Gray. 4-119 (1972).

[32] M. Dixon, F. Hoare, T.M. Holden and D.E. Moody, Proc. Roy. Soc. **A285, 561** (1965).

CHAPTER 4

THERMAL EXPANSION STUDY OF ORDERED AND
DISORDERED Fe$_3$Al AND Ni$_3$Mn ALLOYS

4.1   Introduction

Binary and multicomponent alloys are important for technological and commercial applications. The basic physical understanding of these alloys is necessary for their designing, processing and improvement in performance. As these solid solutions can have many phases present for different concentrations of alloy components and temperatures, the actual phase diagrams need to be calculated to know the stability of the phases. Hence there have been many attempts to obtain the free energy functions ab initio, from which **the** phase diagrams can be calculated. The free energy functions use the entropy values of the system. Therefore the calculation of vibrational and electronic entropies together with the configurational entropy for any system is required to get the correct total entropy values. In this Chapter, it is shown that the thermal expansion measurements can be used as an effective method to calculate the various contributions to total entropy correctly both in ordered and disordered state of the alloy. Besides this accurate values of characteristic Debye and Einstein temperatures can be obtained from the thermal expansion measurements [1].

4.1.1   Order-Disorder Transformation in Alloys

A homogenous alloy is formed by dissolving an atom species into another where both the species of atoms are distributed over the crystal lattice positions. In some alloys at higher temperatures the atoms are distributed randomly which are known as the disordered states and at lower temperatures they are ordered at specific lattice sites. The evidence of ordered arrangements in an alloy is given by the presence of superlattice lines in X-ray diffraction patterns taken on the alloy [2].

In alloys which show order-disorder transformations, the formation of a perfect superlattice occurs at lower temperatures in which the unlike atoms tend to be close together and the atoms of the same kind move distant to each other. Therefore in thermodynamic equilibrium the ordered arrangement must be favoured energetically than the random distribution of atoms. But as the temperature is increased, the amplitude of thermal vibrations will become more and more and in the process they acquire sufficient energy to break away from their original places in the lattice and exchange positions. Hence according to free energy considerations at higher temperature the disordered phase be more stable than the ordered one. Therefore above a critical temperature, which can be termed as order-disorder transition temperature, the alloy will become completely disordered.

4.1.2   Role of Vibrational Entropy in the Order-Disorder Transitions

The phase diagrams and hence the thermodynamic stability of the ordered alloys have allways been obtained using the free energy that includes only the configurational entropy, S_{config} [3,4], calculated from the combinatorics of arranging the atoms on the crystal lattice sites, given a particular state of order [5-7]. Recently, it is seen that by including the vibrational entropy for the calculation of Gibb's free energy, the temperatures of the phase boundaries shift by as much as 20 % [8,9]. Therefore considerable effort has gone into the understanding the role of the lattice vibrations in thermodynamics of chemical ordering in binary substitutional alloys [9-15]. It has been suggested [14,15] that the contribution of vibrational entropy to phase stability in alloys can be quite significant. Historically, however Nix and Shockley [17] first pointed out the importance of vibrational entropy in the context of order-disorder transformations. They suggested that the state of order could

affect the lattice vibrations through a change in the Debye temperature. Using a simple physical argument based on the number of ways of distributing the energy among the vibrational modes they were also able to derive an expression **for** the vibrational entropy difference (ΔS_{ph}) between the ordered and the disordered phase of an alloy,

$$\Delta S_{ph} = S_{ph}^D - S_{ph}^O = 3Rln\left(\frac{\Theta^O}{\Theta^D}\right) \tag{4.1}$$

where Θ^C and Θ are the Debye temperatures for the ordered and disordered alloy respectively. Later several theoretical calculations [18-23] have followed emphasizing the significance of vibrational entropy. It has also been shown that the incorporation of vibrational entropy term in the free energy can lead to a sizeable reduction in **the** critical temperature for ordering [18-20,23]. Experimentally, however, no direct evidence for the importance of vibrational entropy was available mainly because of the inherent difficulty in its measurement. But for the calculations of phase diagrams and to know the stability of phases from the ab-initio free energy considerations, the vibrational entropy contribution needs to be measured carefully. Very recently Fultz et.al. [14,15,24] have made an attempt in this direction.

As mentioned earlier thermal expansion measurements can be used to serve as one direct and useful method of studying the vibrational entropy and this technique is used in the present work for disordered and ordered Fe_3Al and Ni_3Mn alloys.

4.2   Order-Disorder in Fe_3Al Alloy

The phase diagram of Fe-Al alloy is given in Fig.4.1 [25]. Fe- 25 at% Al alloy assumes the b.c.c. lattice structure. At high temperature, the Fe_3Al alloy is completely disordered and is given by the notation A2. Fe_3Al can be melt quenched to retain
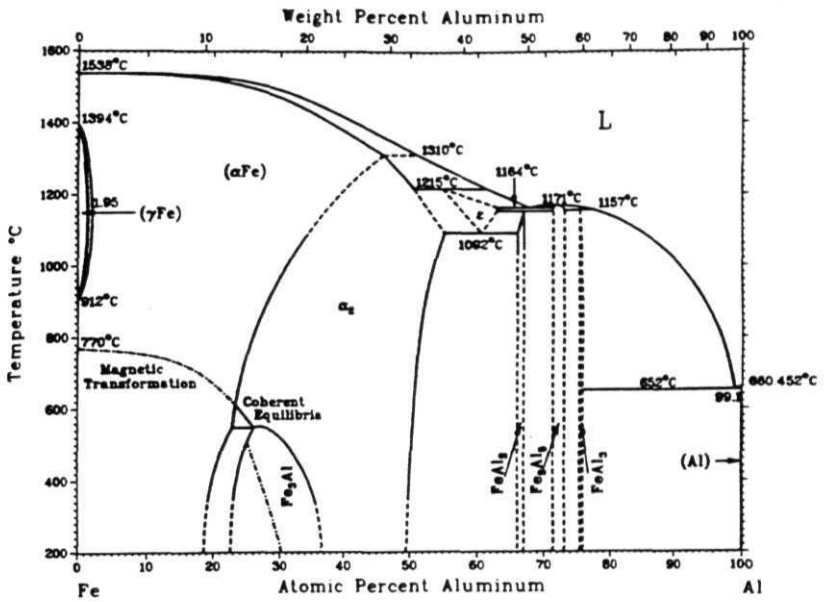
Fig.4.1 : Thermodynamic equilibrium phase diagram for Fe-Al alloy $(\alpha:A2,\alpha_2:B2,$
$Fe_3Al:DO_3)$, taken from ref.25.

the A2 structure. To consider the state of order, the b.c.c. structure of Fe_3Al can be best described with four interpenetrating f.c.c. sublattices. The structure is shown in **Fig**.4.2a. The four interpenetrating sublattices are labelled as A, B, C and **D**, shifted along the body diagonal and having origins at (0,0,0), (1/4,1/4,1/4), (1/2,1/2,1/2) and (3/4,3/4,3/4). In the disordered state (A2), there is no preference of Fe atom or the solute atom Al for any of the four sublattices. Here the atoms occupy all lattice sites randomly. Fe_3Al can order in B2. DO_3 or B32 structures. Below 800° C the order is B2. In this order, **the** two non-adjacent sublattices (e.g. B and D) are occupied by **Fe-atoms** exclusively, and the other two are occupied by 50 % Fe, 50 % Al atoms randomly (see Fig.4.2b(i)). Due to this random occupancy of one of its sublattices, **the** B2 structure can not be a ground state for Fe_3Al stoichiometry. Below 550° C, the DO_3 structure is the equilibrium state for Fe_3Al. For the DO_3 order, A, B, and C sites are occupied by Fe atoms and the D sites are occupied by Al atoms (see Fig.4.2b(ii)). But during cooling from the melt, the Fe_3Al sometimes can also form a transient B32 order which could arise from very small antiphase domains of either DO_3 or B2 order [26]. This B32 order is also not an equilibrium state of Fe_3Al alloy. For this B32 order, two adjacent sublattices are occupied by Fe atoms exclusively. and the other two are occupied by 50% Fe and 50% Al solute atoms randomly (Fig.4.2b(iii)).

4.2.1   Sample Preparation and Characterization

An alloy sample of Fe- 25 at% Al composition was prepared from 4N purity metals by arc melting under an argon atmosphere in an Edmund Buhler D-7400 arc melting furnace. The sample was melted repeatedly a few times to get a good homogenous solution. The weight loss of the final alloy was negligible. A sample of cuboid shape,
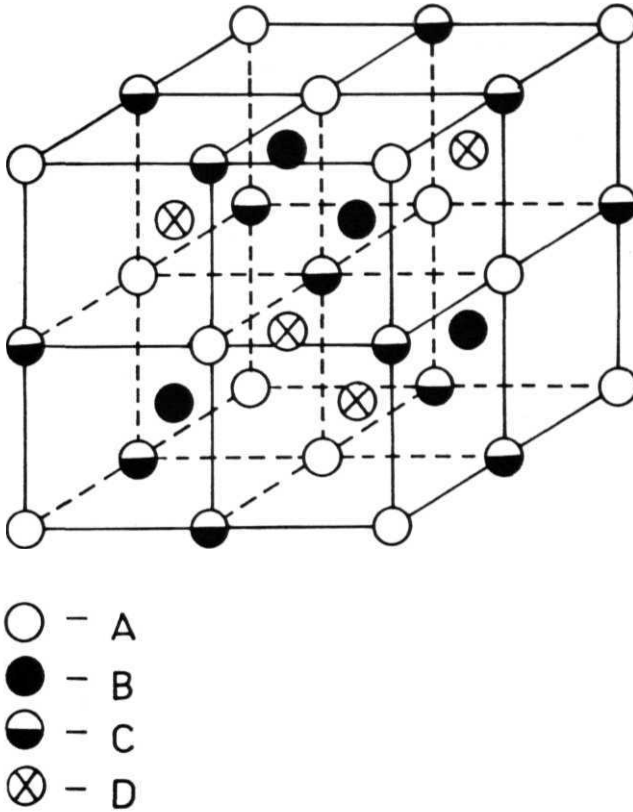
Fig.4.2a : DO_3 structure with A. B, C and D sublattices having origins at $(0\ 0\ 0)$ $(\frac{1}{4},\frac{1}{4},\frac{1}{4})$, $(\frac{1}{2},\frac{1}{2},\frac{1}{2})$ and $(\frac{3}{4}, j,)$ along the body diagonal.

A: Fe
B: Fe, Al
C: Fe
D: Fe, Al

B2 (i)

A: Fe
B: Fe
C: Fe
D: Al

DO3 (ii)

A: Fe
B: Fe
C: Fe, Al
D: Fe, Al

B32 (iii)

● Fe,   ○ Al,   ⊘ Fe or Al

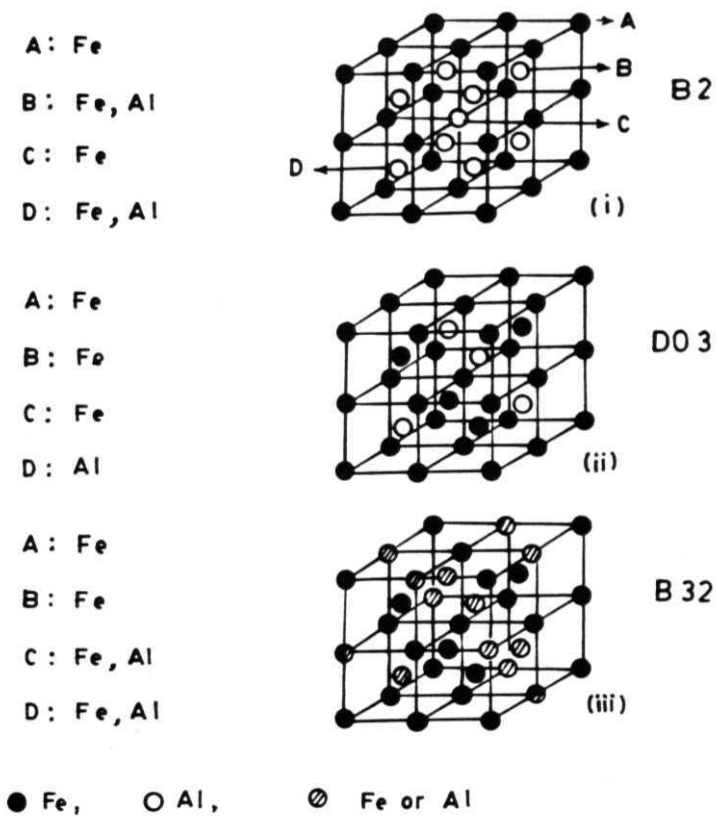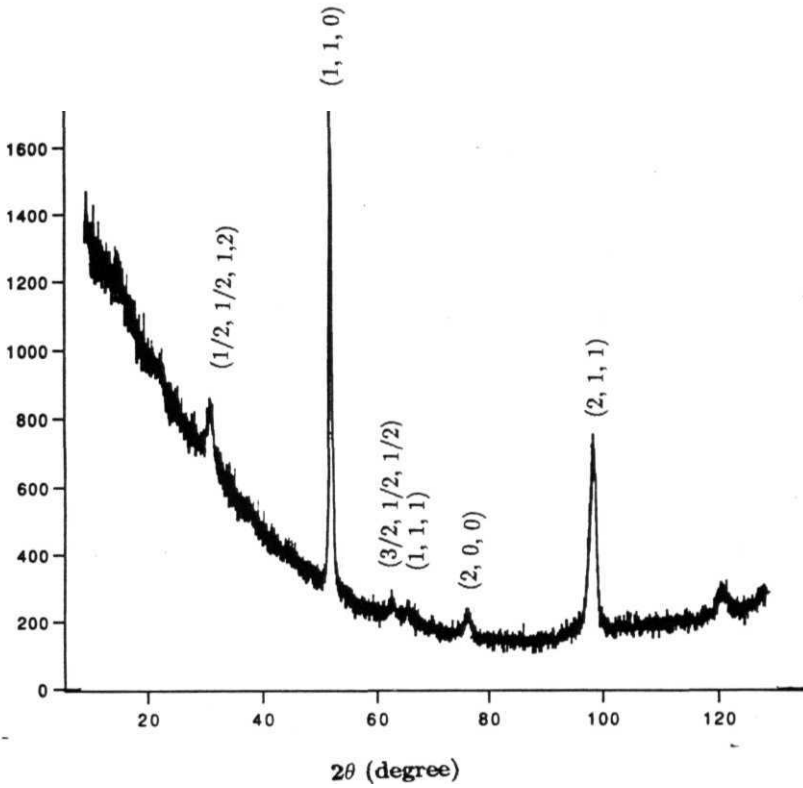Fig.4.2b : The possible ordered structures in bcc Fe₃Al (i) B2; (ii) DO₃; (iii) B32.

Fig.4.3 : X-ray diffraction pattern of the quenched Fe_3Al alloy.

$3 \times 2 \times 2\,mm^3$ dimensions was cut from the arc melted ingot. It was quenched from 1200^{ν} C by dropping into liquid nitrogen in an attempt to get chemical disorder. However due to the bulk nature of the sample it was not possible to get a fully disordered alloy sample. The sample passes through the temperature range 800^{ν} C - 550^{ν} C where the equilibrium state is B2 order aud below 550° C where the equilibrium state is DO_3 order. The X-ray diffraction pattern for the quenched sample shows lines corresponding to B32 phase (see Fig.4.3). However due to requirement of bulk sample in the thermal expansion measurement, the quenched alloy is assumed to be disordered in this thesis work, although it may have some incipient order. After completing the thermal expansion measurements on this sample it was ordered by annealing at 500" C for 24 hours followed by 450^{ν} C for one week, which produced a DO_3 ordered sample. From the density measurements the molar volume of the ordered and the disordered samples were found out to be 28.53 cc and 28.96 cc respectively.

4.2.2   Thermal Expansion Measurements

Thermal expansion measurements were carried out in the temperature range 80 - 300 K using the three terminal capacitance dilatometer described in Chapter 2. The sample temperature was scanned at a rate of 2 mK/Sec and the capacitance values were recorded at 4 Sec intervals. An average of fifty readings was taken to get the capacitance variation with temperature at 0.4 K intervals. Then by using the standardisation procedure described in Chapter-2 the values of $\Delta L/L(T_0)(T_0 = 293$ K) were obtained.

Fig.4.4 shows the observed temperature dependence of the fractional length change $\Delta L/L(T_0) = [L(T) - L(T_0)]/L(T_0)$ where the reference temperature $T_0 =$
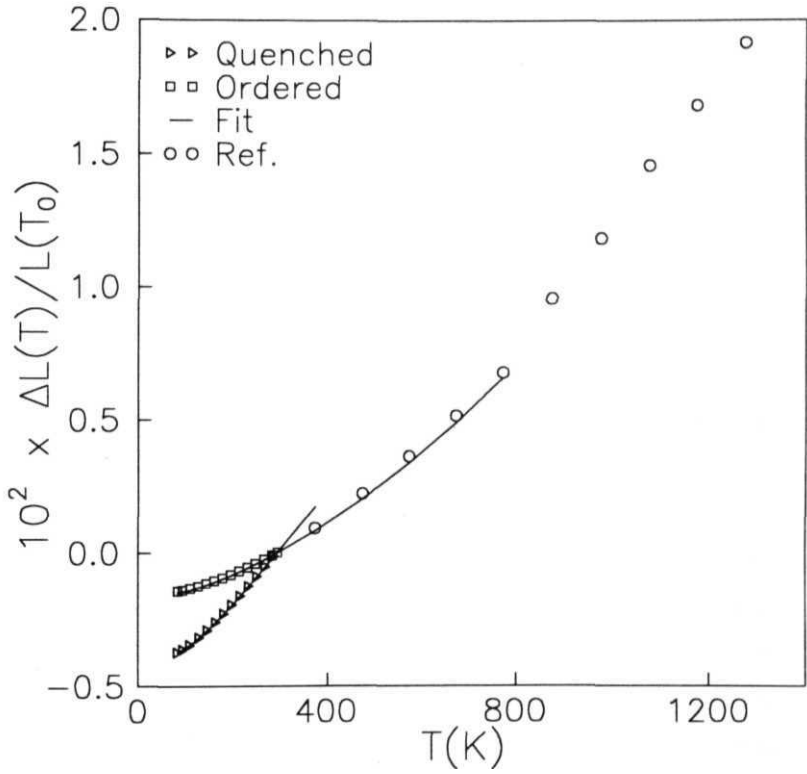
Fig.4.4 : Fractional length change data of ordered and disordered Fe_3Al alloy. The high temperature data above 400 K are taken from ref.27. Solid lines show the fits to the data.

293 K, for the quenched and DO_3 ordered Fe_3Al alloy in the temperature range 80 - 300 K together with the previously reported data [27] recorded at higher temperatures (300 K - 1273 K). The high temperature data shows discontinuities in $\Delta L/L(T_0)$ about thetransition temperatures (at 823 K for transition from DO_3 ordere to B2 order and at 1073 K from B2 order to complete disorder) reflecting changes in state of order. In the present work **the high** temperature disordered state is retained by quenching **the** sample from above 1073 K and the thermal expansion of the disordered sample is measured in the temperature range 80 - 300 K. Data for the ordered alloy are also recorded in the same temperature range and a direct comparison between the ordered and the disordered states of the alloy is therefore possible.

4.2.3   Thermal Expansion Data Analysis

To understand and analyze the observed thermal expansion behaviour of this alloy we note that in the temperature range 80 - 300 K there are three contributions to thermal expansion - the vibrational part due to the lattice. the electronic part due to the free electrons and the magnetic part due to the presence of ferromagnetism below 720 K. As we have discussed in Chapter-3, the ferromagnetic contribution to thermal expansion comes from the itinerant electron moments and localized electron moments. As the free electron contribution and the itinerant electron moment contribution, both give linear-T terms to the thermal expansion coefficient, together they are termed as the electron-magnetic contribution (eqn.(3.6)). The theoretical expression for the electron-magnetic term is given by eqn.(3.74) and it requires an estimate of the relative magnetization at 0 K. ζ_0 which can be calculated with a knowledge of the band structure of the system. Ishida et.al. [28] have done band

structure calculations on **the** ordered Fe_3Al alloy and have shown that there is a total of 18.65 electrons per cell of Fe_3Al in the d-band. As a cell of Fe_3Al contains three iron atoms, it can have a maximum of 30 electrons per cell in the d band. Hence total number of holes present in the d-band per cell is, $N_{0d} = (30 - \mathbf{18.65)} = 11.35$. Neutron diffraction measurements on Fe_3Al alloy gives a net magnetic moment of 5.18 μ_B with the Fe D-site carrying a moment of 2.18 μ_B and **the** Fe A, C-sites carrying 1.50 μ_B moment each [29]. Hence the value of net magnetic moment, n_{0d} is 5.18. Thus the value of relative magnetization at absolute zero is, Co - (5.18/11.35) = 0.456. Using the above value of ζ_0, $\Delta L/L$ data of DO_3 ordered Fe_3Al are fitted to eqn.(3.2), where we include in $(x)r$ the vibrational, electron-magnetic and magnon contributions given by eqns.(3.14), (3.74) and (3.85) respectively. Fig.4.4 shows **the** the fits to the experimentally obtained data of DO_3 ordered Fe_3Al alloy using g'. $/'$. g'', p, $0/;$, Θ_E, A, m and γ'_{mag} as parameters. But for the disordered Fe_3Al the band structure data is not available, and the value of Co is not known. Therefore for the quenched sample the quantity $(\gamma'_{em}/2) = A \left[(1 + \zeta_0)^{\frac{m}{m+1}} + (1 - \zeta_0)^{\frac{m}{m+1}} 1 \right]$ is treated as a single parameter. Table-4.1 gives the values of the parameters that give the best fit. The percentage r.m.s. deviation is found to be 0.2% for both the fits. It is evident from the **Fig**.4.4 that the data for the DO_3 ordered Fe_3Al in the temperature range 80 -300 K match smoothly with the data at high temperatures [27]. In fact, the extrapolated curve obtained from eqn.(3.2) with the same parameter values as used in fitting the DO3 phase data (in the range 80 - 300 K) agrees very well with the high temperature data [26] upto 823 K, the temperature of phase transformation from DO_3 to B2 phase. Fig.4.5 shows the variation of the thermal expansion coefficient $\alpha(T)$ $\left(= \frac{\Delta'}{\Delta'J(T)} \right)$ as a function of temperature as obtained directly from the measured fractional length

Sample	Fe$_3$Al (Quenched)	Fe$_3$Al (Ordered)
g$'$ (eV^{-1})	.431±.003	.1001.002
g$''$ (eV^{-1})	(2.22±.03)×10^{-3}	(4.66± 02)×10^{-3}
f$'$ (eV^{-1})	(2.57±.03)×10^{-4}	(5.34±.02)×10^{-4}
0D(K)	431.0±0.3 [423.0]	376.7±0.3 [377.0]
P	30	4.1±.02
Θ_E (K)		507.910.4 [519.0]
A (K^{-2})	-	(2.653± 03)×10^{-9}
m	-	0.3641003
γ'_{em} (K^{-2})	(-1.58±.03)×10^{-8}	(1.037±.03)×10^{-8}
γ'_{mag} (K$^{-5/2}$)	-	(2.237±.04)×10^{-10}

Table-4.1 : Values of **anharmonicity** parameters and characteristic temperatures obtained by fitting fractional length change data of orederd and disordered **Fe$_3$Al** alloy. Also the elecctron-magnetic and magnon contribution to the thermal expansion obtianed from the same fit are **given** The values of Debye and Einstein temperatures given inside square brackets are taken from **ref**.15.
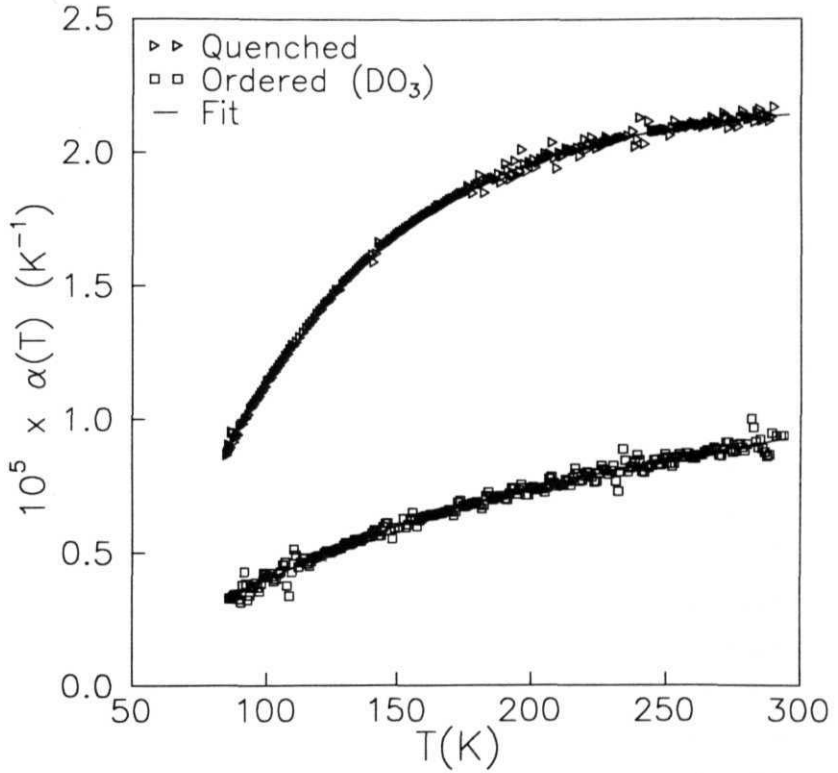
Fig.4.5 : Temperature variation of thermal expansion coefficient (α) of ordered and disordered Fe$_3$Al sample.

change data by numerical differentiation. The solid **line** through data is obtained by analytically differentiating the eqn.(3.2), with respect to temperature using for $\langle x \rangle_7$ the theoretical expression in eqns.(3.14), (3.75)and (3.85) with the same parameter values as obtained from the fitting of the fractional length change data.

(a) Analysis of Vibrational Contribution and Calculation of Vibrational Entropy

The thermal expansion data of quenched Fe_3Al could be fitted well with only three acoustic branches ($p = 3$) and $\Theta_D = 431$ K which corresponds to **the** Debye cutoff frequency ν_D — 8.96 THz. Fits carried out with **the** Einstein term present and a variable p yielded $p = 3$, thereby showing the absence of optical modes. In the case of DO3 ordered Fe_3Al, however, both acoustic and optical modes were required to fit the data with a value of p close to 4 which suggests that **in** DO3 ordered phase an optical branch develops together with the three acoustic branches. The values of Θ_D and Θ_E obtained in this case are 376.7 K (ν_D - 7.85 THz) and 507.9 K (Einstein frequency, ν_E — 10.58 THz) respectively. The values of the Debye cutoff frequency obtained from thermal expansion data for ordered as well as disordered Fe_3Al and the Einstein frequency for the ordered Fe_3Al are in remarkably good **agreement** with those determined from the Density of State (DOS) calculations by Fultz et.al. [15] using Born - von Karman force constants obtained by Robertson [30] from inelastic neutron scattering measurements on disordered and ordered Fe_3Al. For disordered Fe_3Al the values are Debye like with a maximum frequency of 8.8 THz (corresponds to a Debye temperature of 423.0 K) whereas for ordered Fe_3Al the maximum frequency of Debye like mode decreases to 7.85 THz (corresponds to a Debye temperature of 377.0 K) but an additional peak is observed at a frequency

of 10.8 THz (corresponds **to** an Einstein temperature **of** $519.0K$). The presence **of** an additional Einstein frequency **for ordered** Fe_3Al has been physically attributed to the formation of sublattices in the DO_3 ordered structure with the D sublattice being rich in Al which has a lower mass and a correspondingly a higher vibrational frequency.

The vibrational specific heats C_{ph}^O and C_{ph}^D for ordered and disordered Fe_3Al respectively are calculated using the eqn.(3.18) with the characteristic Debye and Einstein temperatures and **the anharmonic** parameters obtained from the fits. The vibrational entropy is calculated using the relation $S_{ph} = \int_0^{\cdot} (C_{ph}/T)dT$ at any temperature T for both ordered and disordered samples. In Fig.4.6a the temperature dependence of $\Delta C_{ph} = C_{ph}^D - C_{ph}^O$ is plotted. The difference in vibrational entropy ΔS_{ph} $(= S_{ph}^D - S_{ph}^O)$ between the disordered and ordered Fe_3Al is calculated and is plotted in Fig.4.6b with respect to temperature. The vibrational entropy difference at the order-disorder transition temperature (T — 1073 K) comes out to be 0.113 $k_B/atom$ (3.76 $J/molK$)[1]. This is in very good agreement with the value 0.10 ± 0.03 $k_B/atom$ obtained by Fultz et.al. [15] from DSC measurements. The value of ΔS_{ph}^{DO} is about 20 % of the configurational entropy value 0.56 $k_B/atom$ which is quite large. This can very well influence the ordering transition and the phase stability of the system. From the calculation of the vibrational specific heat and the vibrational contribution to the thermal expansion α_{ph} we have calculated the vibrational contribution to the Gruneisen parameter $\Gamma_G^{p_l}$, using the molar volumes. 28.53 cc for the ordered alloy and 28.96 cc for the disordered alloy found out from the density measurements. The value of Γ_{ph} has remained largely constant in the temperature range 80-300K at 0.80 for the ordered and 3.48 for the disordered Fe_3Al alloy.
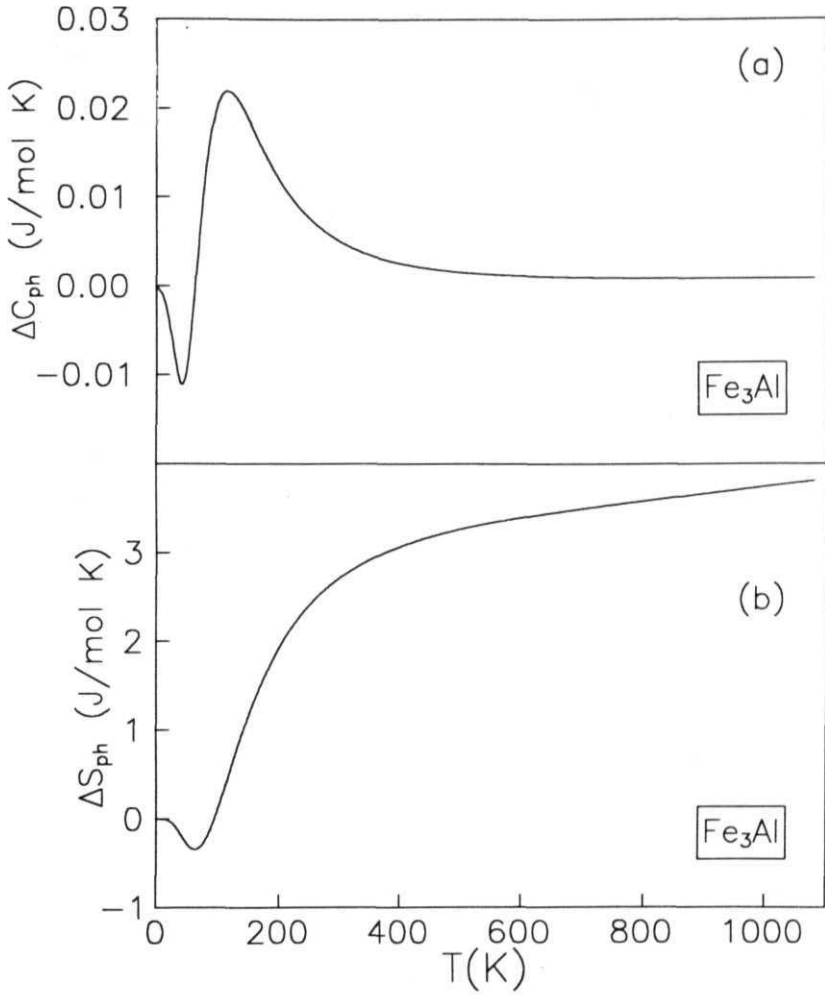
Fig.4.6 : (a) The vibrational specific heat difference (ΔC_{ph}) and (b) the vibrational entropy difference (ΔS_{ph}) between disordered and ordered Fe_3Al.

(b) Analysis of Electron-Magnetic Contribution

Prom the electron magnetic contribution to **the** thermal expansion the fit returned the value of m to be 0.364. For Fe_3Al alloy, in the absence of interaction at absolute zero the up spin and down spin d- sub bands each has **9.325** electrons per **cell. In** Chapter-3 we have seen that in the absence of exchange interactions one Fe atom has 3.5 electrons in each of **the** d sub bands contained in a width of 4.05 eV with a value of m — 0.489. Assuming the d-band width in **the** absence of interaction in the ordered Fe_3Al system is w, then we can **approximately** write (following eqn.(3.89))

$$\frac{9.325}{4 \times 3.5} = \frac{w^{1.364}/1.364}{(4.05)^{1.489}/1.489} \tag{4.2}$$

which gives $u' = 3.205$ eV. In a similar way one can also find **the** total width of **the** Fe_3Al d-band u'' i.e., including **the** unoccupied part of the d band width which can contain 15 electrons,

$$u' = 3.205 \times \left(\frac{15}{9.325}\right)^{\frac{1}{1.364}} = 4.541 eV$$

Therefore the width occupied by 11.35 holes per cell is, $\epsilon_{0d} = $ tt$^{1'}$ - u' = 1.336 eV. Using this value of $\epsilon_{0d} = 1.336$ eV, $N_{0d} = 11.35$ and $n, = 0.364$. the linear electron-magnetic coefficient for specific heat γ_{em} is calculated using eqn.(3.66) to be 26.574 mJ/mol K^2. It compares excellently well with the experimental value of 29.23 mJ/mol K^2 obtained by Okamoto and Beck [31]. Then using the above value of ϵ_{0d}, and with the bulk modulus $B_T = 1.443 \times 10^{11} Nm^{-2}$, $V = 28.531$ cc, $N_{0d} = 11.35$ holes per cell, $A = 2.653 \times 10^{9} K^{-2}$ and $m = 0.364$ for the ordered sample, 6 is found out to be 4.82 (using eqn.(3.76)) which is the electron-magnetic Griineisen constant.

The linear electron-magnetic (γ'_{em}) contributions to the thermal expansion co-efficient for both the ordered and disordered Fe_3Al alloys are in the same order of

magnitude, but becomes negative in the case of quenched Fe_3Al (see Table-4.1). This is because the electron-magnetic contribution to thermal expansion coefficient is related to the electron-magnetic Grüneisen parameter Γ_G^{em} by,

$$\Gamma_G^{em} = \frac{3\gamma'_{em} V B_T}{\gamma_{em}}$$ (4.3)

and is negative in the case of disordered Fe_3Al alloy. The electron-magnetic Griineisen parameter is given by,

$$\Gamma_G^{em} = \frac{\partial ln g(\epsilon_0)}{\partial ln V}$$ (4.4)

where $g(\epsilon_0)$ is the electronic density of state at the Fermi energy. Thus γ'_{em} can be negative in the systems in which the electronic density of states has a largo peak near Fermi energy. The change in the sign of the γ'_{em} due to order-disorder transition is related to the change in band structure.

(c) Analysis of Magnon Contribution

The fit returned the value of the magnon contribution to thermal expansion for the ordered Fe_3Al sample to be $\gamma_{mag} = 2.237 \times 10^{10}$ K $^{5/2}$. By stipulating that the magnon entropy should be equal to the paramagnetic value $3Rln2 = 17.28\ J/molK$ at the ferromagnetic transition temperature $T_C = 720$ K, eqn.(3.87) gives. $\eta = \Gamma_G^{mag} = 2.06$ for the ordered sample. But the fitting of the thermal expansion data of the disordered sample gave a very small value of γ'_r which is negligible. And also as the ferromagnetic T_C of the disordered Fe_3Al is not known we could not give the value of Γ_G^{mag}.

The electron-magnetic and magnon contributions to the entropy are calculated for the ordered Fe_3Al sample using the respective Gruneisen constants, $\Gamma_G^{em} = 4.822$
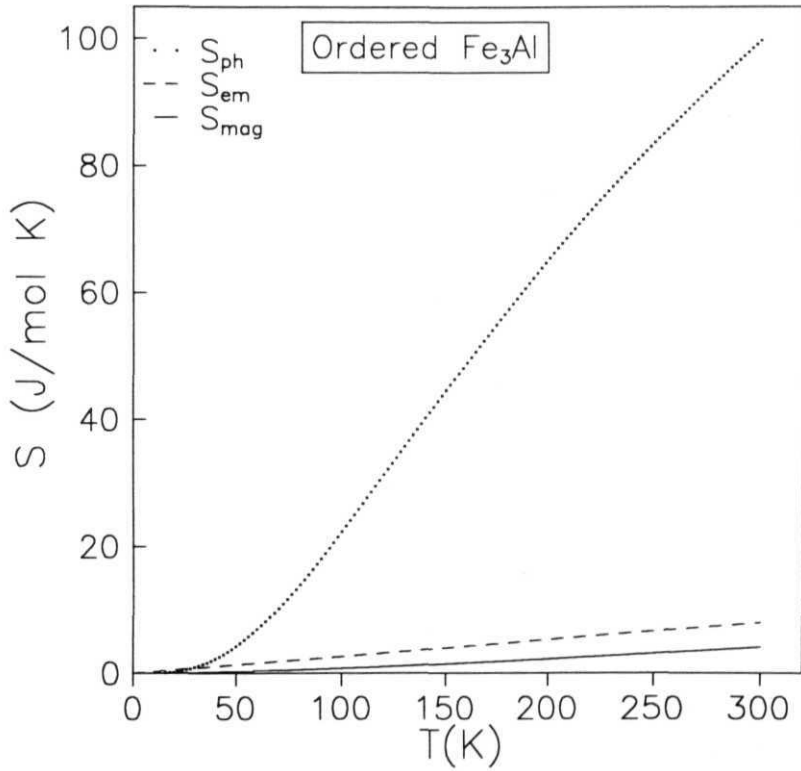
Fig.4.7 : Vibrational, electron-magnetic and magnon contributions to entropy (S_{ph}, S_{em} and S_{mag} respectively) of ordered Fe_3Al.

and Γ_C^{mag} = 2.06. In Fig.4.7 S_{ph}^O is plotted with the electron-magnetic entropy S_{em}^O and the **magnon** entropy S_{mag}^O with temperature for the ordered Fe_3Al alloy. One can see that the magnetic entropies are very small compared to the vibrational entropy. Also as the ferromagnetic Curie temperature (720 K) is below the order-disorder transition temperature (820 K) they do not affect the ordering transition.

4.3 Ni_3Mn- Ordered and Disordered Alloy

The next binary alloy system in both ordered and disordered states considered is Ni_3Mn alloy. The Ni-Mn alloy system is known to exhibit complex magnetic properties which are extremely sensitive to the state of atomic order and the Mn concentration in the vicinity of the stoichiometric composition Ni_3Mn[32-38]. The Ni_3Mn alloy orders to a $L1_2$ structure at about 753 K. It is more interesting in the sense that this alloy is ferromagnetic in a perfectly ordered state with a T_C of 700 K [32]. However with a decrease in chemical order this system shows a remarkable change in the magnetic order also [32-37]. The magnetization curves for the disordered and partially ordered Ni_3Mn alloys however look rather complex [33] and consist of two distinctly different temperature behaviour possessing two different Curie temperatures T_C and T_C'. Though magnetization does decrease as the lower Curie temperature T_C is approached from below. it still remains nonzero, albeit small, at T_C and vanishes only at a higher temperature T_C'. It has been postulated that the equilibrium phase between T_C and T_C' is nonhomogeneous consisting of long-range order domains in a matrix of short-range order [35]. The magnetic phase diagram of disordered Ni-Mn alloys with different Mn concentrations near 25 at.% of Mn have revealed that in these alloys competing magnetic interactions

coexist leading to a reentrant spin glass behaviour with **the** ferromagnetic Curio temperature T_C decreasing with the increase of **Mn** concentration [36].

Although a large amount of literature has piled up on **the** magnetic properties of Ni_3Mn alloy system, very little is known about its thermodynamic properties. Therefore thermal expansion measurements have been performed on both an $L1_2$ ordered and a partially ordered Ni_3Mn alloy, and the proposed theoretical model described in Chapter-3 is applied to separate and calculate the vibrational and magnetic contributions to thermal expansion and entropy **for** the two phases with a view to ascertaining the effects of lattice vibrations and magnetic interactions on the order-disorder transformation of this alloy system.

4.3.1   Alloy Preparation and Expansion Measurements

An alloy sample of nominal composition Ni_3Mn was prepared from 99.99 % purity metals by arc melting under an argon **atmosphere** in Model AF 92 arc furnace from Materials Research Corporation. The sample was repeatedly melted to get a good homogenous solution. The weight loss of the final ingot was less than 2 %. Then the ingot was sealed in a evacuated quartz tube and homogenized at $800°$ C for one week to get a good homogenous alloy. A sample of cuboid shape, $3 \times 2 \times 2$ mm^3 in dimensions, was cut from the homogenized ingot. It was then quenched from $900°$ C by dropping into the brine solution to get disorder. The susceptibility measurements on the quenched sample however yielded a ferromagnetic T_C = 267 K (see **Fig**.4.8) suggesting that the disorder achieved was only partial. An explanation of this partial disorder is that the quenching rate is probably slower than that would be necessary to **get** a complete disorder for a sample as large as used in this work. Accurate thermal expansion measurements were taken on the above sample in the
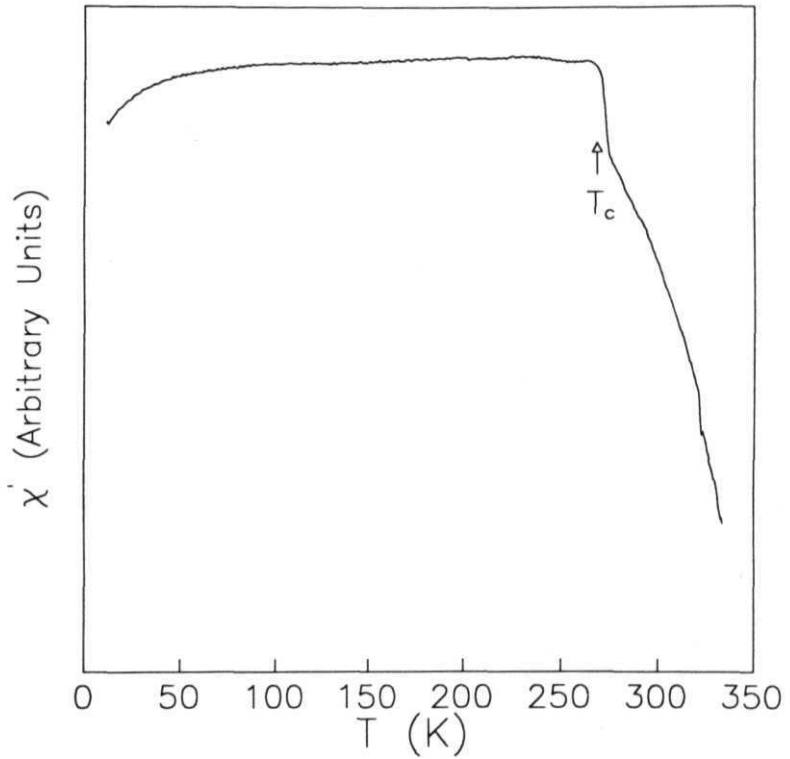
Fig.4.8 : Variation of a.c. susceptibility (χ') with temperature for quenched Ni_3Mn alloy. The arrow indicates T_C at 267 K.

temperature range 80 - 300 K. The expansion data were recorded at intervals of 0.4 K. After completing the measurements on the disordered sample it was ordered by annealing successively at 550° C for one day, **then** at 490° C for 11 days, then at 420° C for another 11 days and finally at 400" C for 10 days. A total number of 33 days anneal was done by sealing the sample in a evacuated quartz tube. **Fig**.4.9 shows the temperature dependence of the fractional length change $\Delta L/L(T_0)=$ $[L(T) - L(T_0)]/L(T_0)$ where the reference temperature $T_0 = 293$ K for both the quenched and the ordered alloys. The thermal **expansion** data **for** the quenched alloy did not show any observable change at $T_{C} = 267$ K probably because of the presence of an inhomogeneous magnetic phase above T_{C} **which** is also corroborated by the susceptibility measurements. From the density measurements the molar volume of the samples in **the** ordered and disordered states were found out to be 32.81 cc and 35.58 cc respectively.

4.3.2   Results and Discussion

Taking the average Ni and Mn moments in the ordered Ni_3Mn to be 0.3 μ_B and 3.18 μ_B respectively as suggested by the neutron diffraction data [36] and assuming that both Ni and Mn atoms contribute 0.3 electrons per atom to the s band [39] the value of ζ_0 has been calculated. Mn atom has 7 electrons in its outermost shell and as in the alloy it gives 0.3 electron to the s band, it will contribute 6.7 electrons per atom in the d-band of the alloy. From the average magnetic moment of 3.18 μ_B of Mn in the alloy, the contribution of Mn atom to the upspin d-subband of the alloy is 4.94 electrons per atom and to the downspin d-subband of the alloy is 1.76 electrons per atom. Similarly the average magnetic **moment** of Ni in the alloy is 0.3 μ_B and as it contributes 0.3 electrons to the s-band of the alloy it will contribute
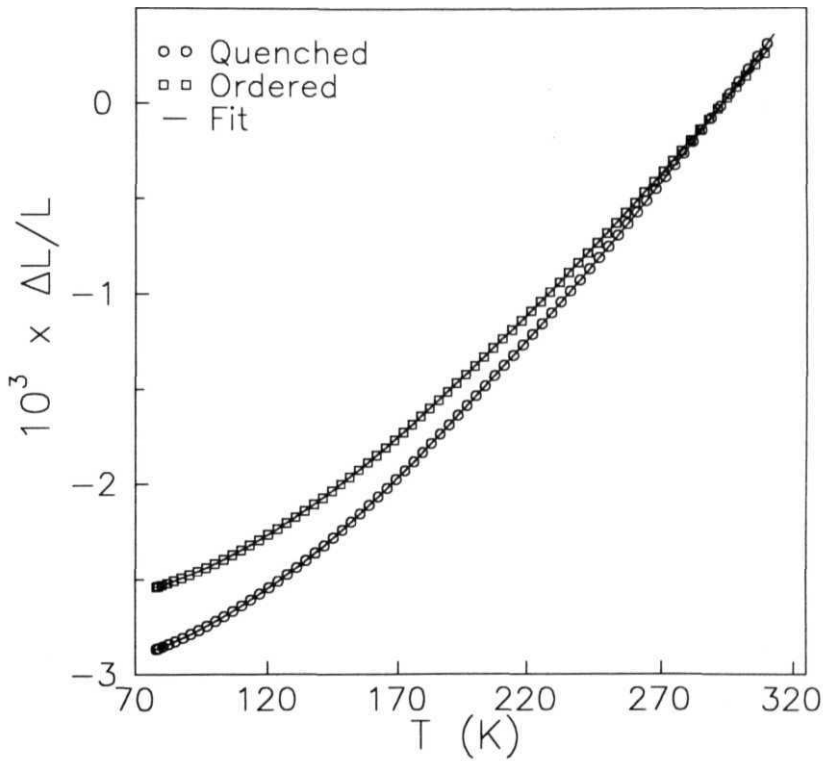
Fig.4.9 : Fractional length change data of ordered and disordered Ni_3Mn alloy. The solid lines indicate the fits to the data.
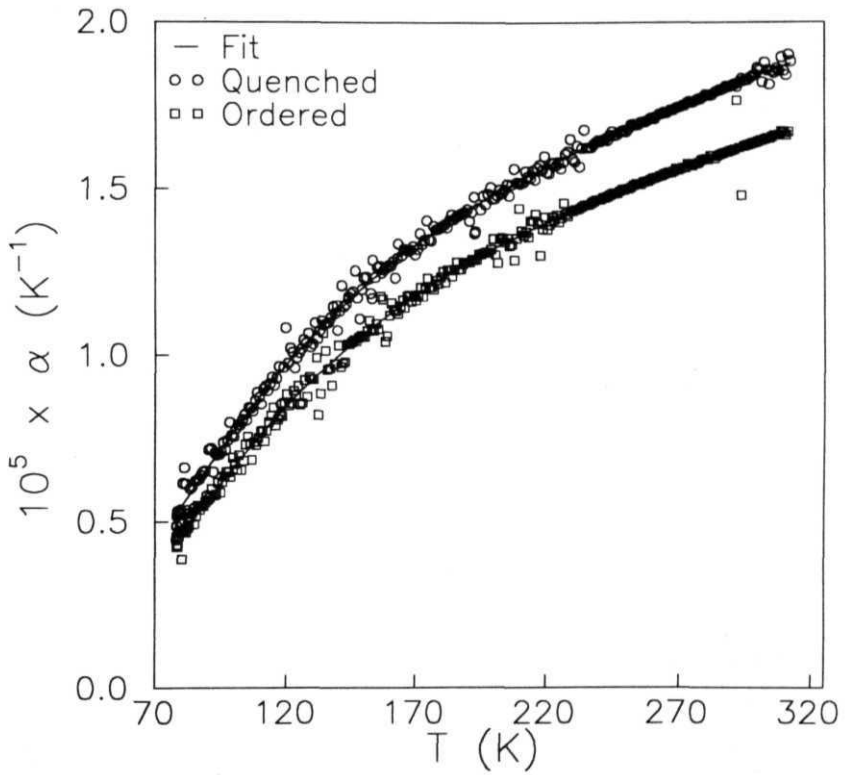
Fig.4.10 : The thermal expansion coefficient of ordered and disordered Ni_3Mn alloy with temperature.

on average 4.7 electrons per atom in **the downspin** d-subband and 5 electrons per atom in the upspin d-subband of the alloy. From these contributions one can easily find out that the Ni_3Mn alloy contains on average 3.965 electrons per atom in the downspin d-subband and 4.985 electrons per atom in the upspin d-subband. This gives that downspin d-subband contains 15.86 electrons per cell and upspin d-subband contains 19.94 electrons per cell. So number of holes per cell present in the downspin d- and upspin d-subbands are 4.14 and 0.06 respectively. Therefore N_{0d} = (4.14 + 0.06) = 4.2 and n_{0d} = (4.14 - 0.06) = 4.08. Finally the value of Co is found out to be, Co = (4.08/4.2) = 0.97.

The total fractional length change data **the** ordered alloy are then fitted to eqn.(3.2) with g''. g''. $/'$, Θ_D, Θ_F, p, A, m and γ'_i as **parameters.** However for the quenched alloy, the quantity γ'_{em} given in eqn.(3.75) is treated as a single **parameter** as Co is not known for this sample. The fits are shown in Fig.4.9 with the best fit parameters given in Table-4.2. The data of disordered alloy is fitted upto 267 K which is the T_C for the sample. The percentage r.m.s. deviation is found to be about 0.3% for both the fits. Fig.4.10 shows the variation of linear thermal expansion coefficient ($\alpha(T)— \frac{1}{L(T_o)}\frac{\Delta l}{\Delta T}$) as a function of temperature as obtained by numerical differentiation of the experimentally obtained fractional length change data. The solid line through the data points is obtained by analytically differentiating the theoretical expression for $\Delta L/L$ with respect to T using the fitted parameter values. The fits carried out with the Einstein term present and a variable p yielded, $p = 3$ for the quenched sample with a Debye temperature $\Theta_D = 451.0$ K. However for the annealed sample, both acoustic and optical modes were required **to** fit the data with. $p = 3.6$, $\Theta_E = 502.0$ K and $\Theta_D = 439.0$ K suggesting the presence of optical modes in the $L1_2$ ordered Ni_3Mn alloy. No experimental values for the characteristic

temperatures of Ni_3Mn are available. The Debye temperature of ordered Ni_3Mn alloy can however be calculated theoretically using the expresssion given by Giri and Mitra [41]. They have shown that the Debye temperature (Θ_{AB}) of any binary alloy of two metals A and B, combined in **the** atomic **proportion** p:q such that $p+q=1$ can be calculated using **the** expression,

$$\Theta_{AB}^2 M_{AB(pq)} = pM_A\Theta_A^2 + qM_B\Theta_B^2 \tag{4.5}$$

where Θ_A and Θ_B are **the** Debye temperatures of the **component** metals A and B of atomic mass M_A and M_B respectively and $M_{AB(pq)}$ $-pM_A + qM_B$ is **the** effective mass of the binary alloy. Using **the** above equation we have calculated the Debye temperature of Ni_3Mn alloy **to** be 441.0 K which is in close agreement with our result. The anharmonicity parameter values are larger in the case of quenched alloy which shows that the phonon anharmonicity increases with atomic disorder. With the fitted parameter values the vibrational specific heat C_{ph} and vibrational **entropy** S_{ph} are calculated for the ordered and the quenched samples and we obtain $\Delta S_{ph} = S_{ph}^D - S_{ph}^O$, where D and O refer to the disordered and the ordered phases of the alloy respectively. In Fig.4.11 we have plotted C_{ph} in both the ordered and disordered states as a function of temperature and $\Delta C_{ph} = C_{ph}^D$ - C_{ph}^O is shown as an inset. From the calculation of C_{ph}^O, the vibrational contribution **to the** thermal expansion coefficient α_{ph}^O, and using the value of the bulk modulus, B_1 — 1.544 x 10^{11} N/m^2 (taking a weighted average of the bulk moduli of Ni and Mn), molar volume $V = 32.81$ cc, the vibrational contribution to the Gruneisen parameter is calculated to be, Γ_{ph} = 2.23 for the ordered Ni_3Mn alloy. For the disordered alloy the value of Γ_{ph} came out to be 2.56 from the calculated values of C_{ph}^D and α_{ph}^D and using the experimental molar volume $V = 35.58$ cc.

Sample	Ni$_3$Mn (Quenched)	Ni$_3$Mn (Ordered)
g$'$ (eV^{-1})	.240±.005	.226±.006
g$''$ (eV^{-1})	$(3.00±.05)×10^{-3}$	$(4.79±.06)×10^{-3}$
f$'$ (eV^{-1})	$(3.62±.05)×10^{-4}$	$(2.44±.06)×10^{-4}$
Θ_D (K)	451.0±0.5	439.0±0.6 [441.0]
p	3.0	3.6±.06
Θ_E (K)	-	502.0±0.6
A (K^{-2})	-	$(1.10±.06)×10^{-9}$
m	-	0.200±.006
γ'_{em} (K^{-2})	$(5.28±.05)×10^{-9}$	$(3.70±.06)×10^{-9}$
γ'_{mag} (K$^{-5/2}$)	$(5.28±.05)×10^{-10}$	$(4.30±.06)×10^{-10}$

Table-4.2 : Values of **anharmonicity** parameters and characteristic temperatures obtained by fitting fractional length change data of orederd and disordered Ni$_3$Mn **alloy** Also the **elecctron-magnetic** and magnon contribution to the thermal expansion obtianed from the same fit are **given** The value of Debye temperature given inside square brackets has been calculated using the expression given by Giri and Mitra.
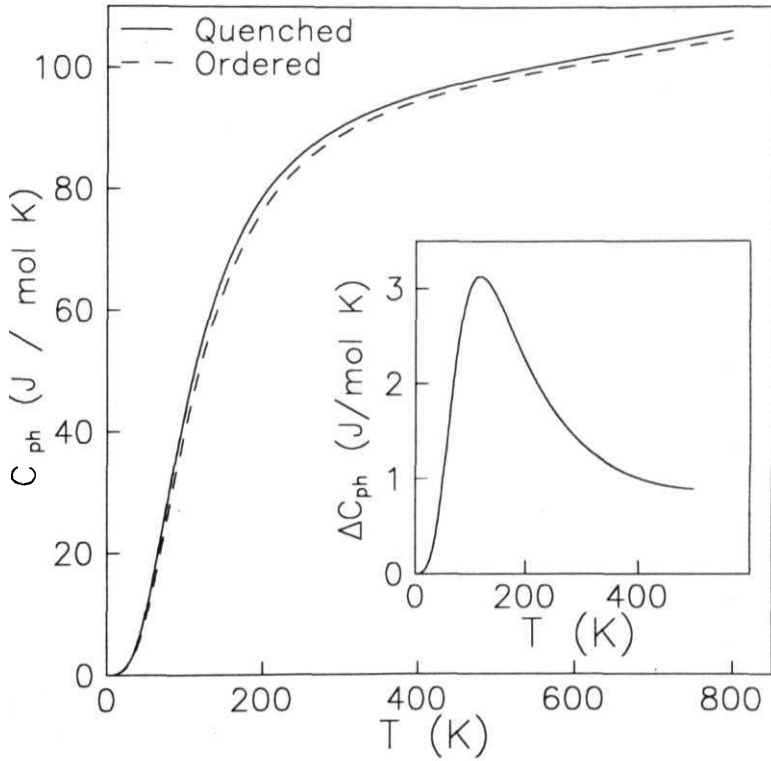
Fig.4.11 : Variation of vibrational specific heat (C_{ph}) with temperature of ordered and disordered Ni_3Mn alloy. The inset shows the vibrational specific heat difference with temperature.

It is interesting **to** note that it was not possible to fit **the** thermal expansion data without the magnon term. In Fig.4.12 we have plotted the electron-magnetic **and** magnon contributions to thermal **expaqnsion** coefficient (α_{em} and α_{mag} respectively) with temperature, which shows that both **the** contributions are of same order of magnitude. This together with the observation that ζ_0 is finite in an ordered and partially ordered Ni_3Mn alloy suggests that **the** magnetic moments in this system in general possess both an itinerant and a localized character. The coefficients of the electron-magnetic term γ'_{em} of $\Delta L/L(T_0)$ for the ordered and the quenched alloys are respectively 3.70 x 10^{-9} K^{-2} and 5.28 x 10^{-9} $K"^2$ while those of the magnon term γ_{mag} **for** the **corresponding** phases are 4.300 x 10^{-10} K $^{5/2}$ and 5.280 x $10^{-5/2}$. Thus at a given temperature both the electron-magnetic and the magnon contributions to the thermal expansion are larger **in the** quenched **phase** than in the $L1_2$ ordered phase. A higher electron-magnetic contribution clearly implies a lower value of ζ_0 if we assume that the band structure of the disordered alloy does not differ much from the ordered system and consequently a reduction in the itinerant character of the moments. Thus it appears that the atomic disorder in a Ni_3Mn alloy tends to suppress the itinerant character of its magnetic moments. Since the state of disorder in the quenched sample was not known. it was not possible **to** find the value of ζ_0 for this sample. It is however expected that the electron-magnetic Gruneisen parameter Γ_G^{em} for a partially ordered alloy should not be much different from that of an ordered alloy. Therefore the same value of Γ_G^{em} is assumed for the quenched sample as calculated for the ordered one. For the ordered system fitting gives m $= 0.2$ while for the elemental Ni the energy band seems to be almost parabolic with m =0.497 (see Chapter 3). In the absence of exchange interactions, each d subband of Ni contains 4.7 electrons per atom within a band width of 4.34
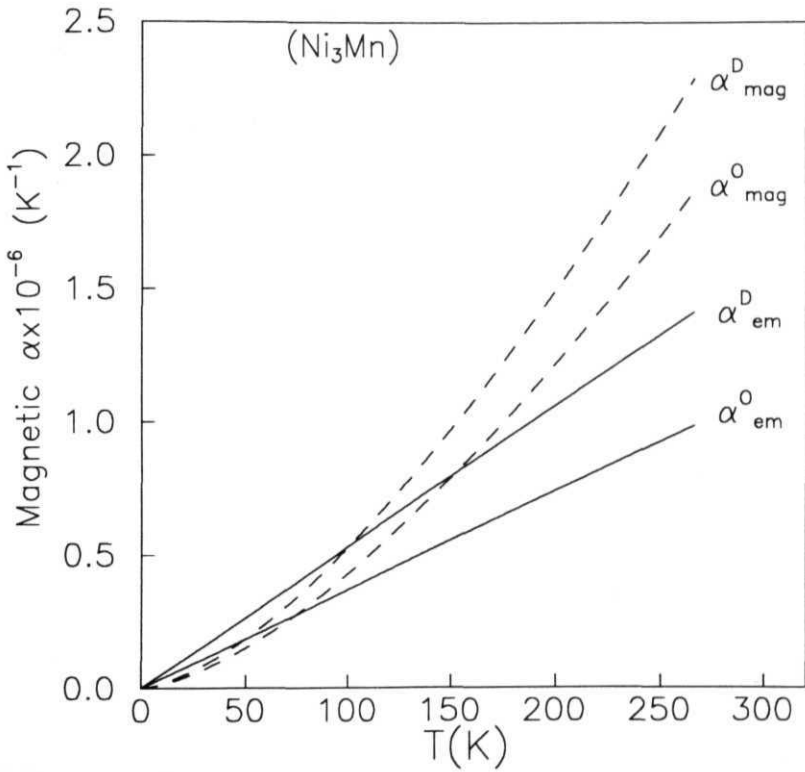
Fig.4.12 : Temperature variation of electron-magnetic and magnon contributions to thermal expansion of Ni_3Mn alloy.

eV. During the calculation of ζ_0 we have seen that there are a total number of 35.8 electrons per cell in the d-band of the Ni_3Mn alloy. In the absence of interaction 35.8 electrons per atom are equally distributed in the two d-subbands with each one containing 17.9 electrons per atom. If the occupied d-band width of the alloy in the absence of interactions is taken to be w, then from the occupied d-band width of Ni atom one can write

$$\frac{17.9}{4 \times 4.7} = \frac{w^{1.2}/1.2}{(4.34)^{1.497}/1.497} \tag{4.6}$$

which gives w — 4.983 eV. In a similar way the total width (w') of the 3d band of the Ni_3Mn alloy including the unoccupied portion of the band, is calculated to be

$$w' = 4.983 \left(\frac{20}{17.9}\right)^{\frac{1}{1.2}} eV = 5.466eV \tag{4.7}$$

Thus $\epsilon_{0d} = w' - w$ — 0.483 eV. Using this value of ϵ_{0d}, and with $B_T = 1.544$ x $10"$ Nm^{-2} (taking a weighted average of the bulk moduli of Ni and Mn), V — 32.81 cc (molar volume), N_{0d} — 4.2 holes per cell and the fitted values of m and A. for the ordered sample, we find b — 2.72 using eqn.(3.76). The electron-magnetic entropy now can be calculated for both the ordered and the quenched samples using the relation (3.70) and the difference $\Delta S_{em} = S_{em}^D - S_{em}^O$, can be obtained. For the quenched sample $V = 35.58$ cc (molar volume) is taken which is found out from the density measurements. For the ordered and the quenched samples the values of γ_{em} are found out to be 20.517 $mJ/molK^2$ and 30.4 $mJ/molK^2$ respectively which are compared with the experimental values 19.6 $mJ/molK^2$ and 35.4 $mJ/molK^2$ [40]. Evidently the **agreement** in the case of ordered sample is excellent and in the case of quenched alloy the slight **disagreement** is may be due to the presence of partial order in our sample. That the value of γ_{em} for the quenched alloy is

larger than the ordered alloy again suggests that **the** quenched alloy is a weaker itinerant ferromagnet as compared to the ordered alloy. To obtain ΔS_{mag} the value of the magnon Griineisen parameter η for both the phases of the alloy are needed By stipulating that the magnon entropy should go over to the paramagnetic value $4Rln2$ at the ferromagnetic T_C, eqn.(3.87) gives, $\eta = 3.5$ for the ordered sample and $\eta = 1.05$ for the quenched sample. The vibrational, electron-magnetic and magnon Griineisen parameters of Ni_3Mn alloys are summarized in Table-4.3 along with that of ordered Fe_3Al alloy. Also γ_{em} values obtained from our analysis are given in Table-4.3 for ordered and disordered Ni_3Mn and ordered Fe_3Al alloys. We have calculated γ_{mag} using eqn.(3.84) and S_{mag}^{D}, S_m^{O} using eqn.(3.81) and the difference ΔS_{mag}. In Fig.4.13 we have plotted the vibrational, electron-magnetic and magnon contributions to entropy with temperature for both in the ordered and disordered phases of Ni_3Mn alloy.

In Fig.4.14 the vibrational entropy difference ΔS_{ph} between the ordered and the disordered phases of the alloy Ni_3Mn is plotted with respect to temperature with ΔS_{em} and ΔS_{mag}. It is observed that ΔS_{ph} at the order-disorder transition temperature is 5.40 $J/molK(0.16\ k_B\ /\ atom)$ which is a sizable contribution as compared to the configurational entropy of mixing $(0.56\ k_B/atom)$. This shows that the vibrational entropy contributes significantly to the thermodynamics of the chemical ordering of the Ni_3Mn alloy. However the electron-magnetic entropy difference ΔS_{em} is much smaller than ΔS_{ph} over the temperature range shown. At the ordering transition temperature ΔS_{em} will be simply given by the free electron entropy difference and is therefore not expected to be large. The variation of ΔS_{mag} is however interesting. It increases initially with increasing temperature, attains a maximum value at T = 267 K, and then decreases monotonically to zero at T = 700

Sample	γ_{em} (mJ/mol K^2)	Γ_G^{ph}	Γ_G^{em}	Γ_G^{mag}
Fe$_3$Al (Ordered)	26.574 **(29.23)**	0.80	4.82	206
Ni$_3$Mn (Ordered)	20.517 (19.6)	2.23	**2 72**	**3 5**
Ni$_3$Mn (Quenched)	30400 (35.4)	2.56	2.72	**1.05**

Table-4.3 : The values of electron-magnetic contribution to specific heat γ_{em} calculated from our thermal expansion data anlysis of ordered Fe$_3$Al alloy and the ordered and disordered Ni$_3$Mn alloys The γ_{em} values inside the brackets are the experimental values given in literature Also the values of the vibrational, electron-magnetic and magnon contribution to the Gruneisen paprameter are given
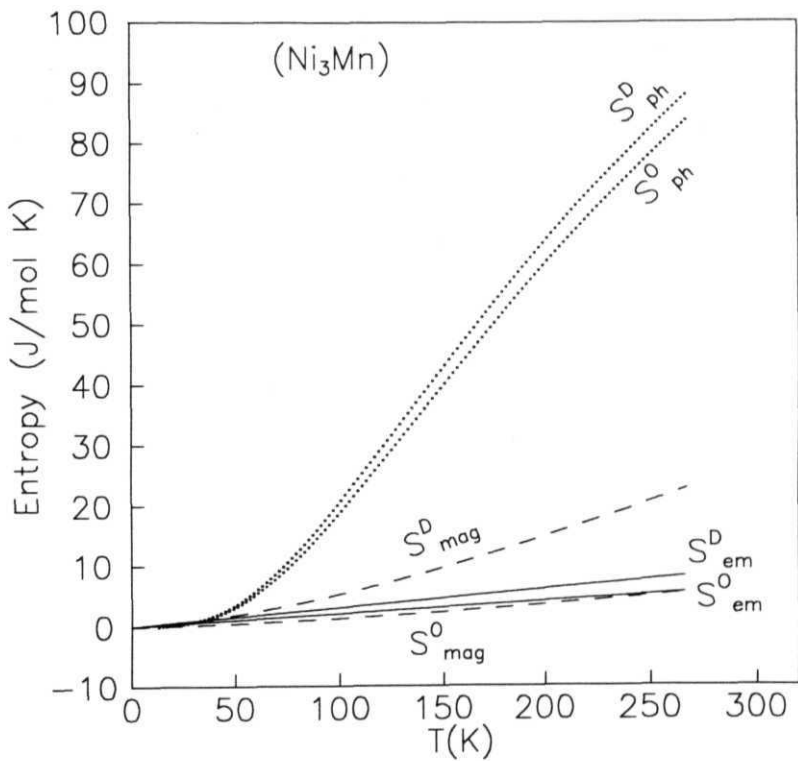
Fig.4.13 : Temperature variation of vibrational, electron-magnetic and magnon entropies of Ni_3Mn alloy in ordered and disordered states.
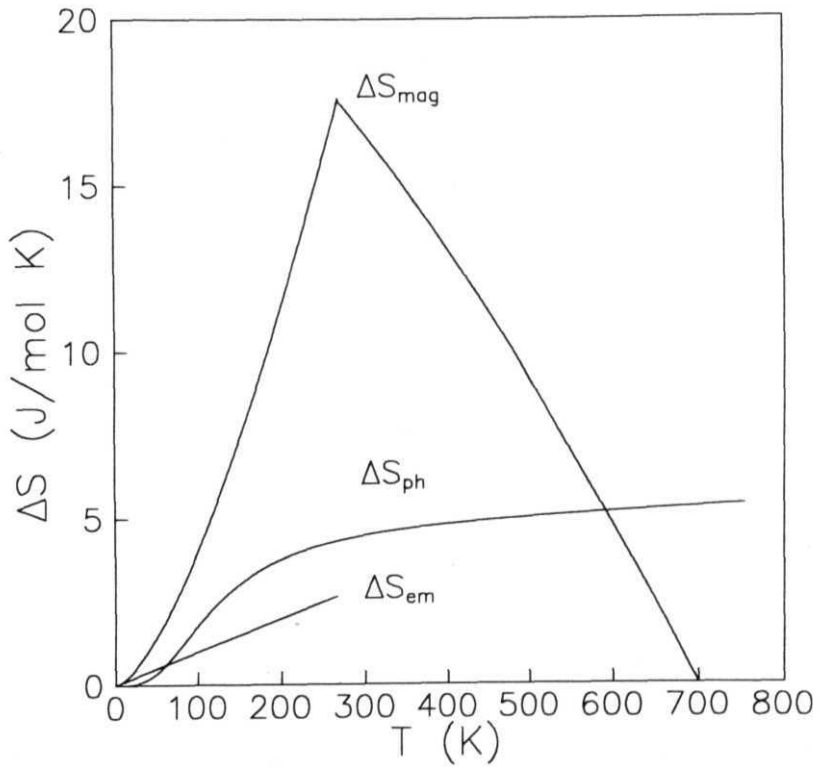
Fig.4.14 : Temperature variation of vibrational, electron-magnetic and magnon entropy differences between disordered and ordered Ni_3Mn alloy.

K. However here S^D_{mag} is overestimated by neglecting the non-homogenous magnetic phase above T = 267 K which yielded a smaller value of η. But the important point is that ΔS_{mag} vanishes near order-disorder transition temperature which suggests that magnon entropy does not play any role in the ordering transformation.

4.4 Conclusion

In conclusion we would like to emphasize that the thermal expansion measurements together with our theoretical model can serve as an effective approach to study the changes in the vibrational properties of alloys due to chemical order-disorder transformations. The vibrational entropy difference between the quenched and ordered Fe_3Al and Ni_3Mn alloys are found to be about 20 % and 28.6 % respectively of the configurational entropy of mixing and are substantially large. This suggests that the lattice vibrations will play a rather important role in the order-disorder transformation of these binary alloys and would contribute significantly to their phase stability. This method also provides reliable estimates of characteristic temperatures (Θ_D and Θ_E), cubic and quartic anharmonicity parameters in the lattice potential energy, and the vibrational contribution to entropy. Also it is shown that the thermal expansion measurements together with the proper band structure data can be effectively used to study the effect of magnetic interactions on the thermodynamic properties of magnetic alloys. In this connection the above analysis revealed that an $L1_2$ ordered Ni_3Mn alloy contains both itinerant and localized moments and the effect of atomic disorder is to suppress the itinerant character of the moments. This method provides reliable estimates of electron-magnetic and magnon Griineisen parameters.

References

[1] G.D. Mukherjee, C. Bansal and Ashok Chatterjee, **Phys.** Rev. Lett. **76,** 1876 (1996).

[2] T. Muto and Y. Takagi. Solid State Physics, Vol.1, eds: F. Seitz and D. Turnbull (Academic Press, New York, 1955), p. 193

[3] E. Ising. Z. Phys. **31,** 253 (1925).

[4] W.L. Bragg and E.J. Williams, Proc. Roy. Soc. London **A145**, 699 (1934).

[5] D. de Fontaine, Solid State Phys. 34, 73 (1979)

[6] F. Ducastelle, Order and Phase Stability in Alloys (North-Holland, Amsterdan, 1991).

[7] K. Terakura, T. Oguchi, T. Mohri and K. Watanabe, Phys. Rev. B **35.** 2169 (1987); A.A. Mbaye, L.G. Ferreira and A. Zunger, Phys. Rev. Lett. 58, 49 (1987); A.E. Carlsson and J.M. Sanchez, Solid State Commun. 65, 527 (1988); M. Sluiter, D. de Fontaine, X.Q. Gao, R. Podloucky and A.J. Freeman, Phys. Rev. B42, 10460 (1990).

[8] J.M. Sanchez, J.P. Stark and V.L. Moruzzi, Phys. Rev. B44, 5411 (1991).

[9] T. Mohri, S. Takizawa and K. Terakura. J. Phys. C**5**, 1473 (1993).

[10] B.N. Persson, Phys. Rev. B40, 7115 (1989).

[11] C.V. Krishnamurthy and Y.V.G.S. Murti, Phys. Rev. B43, 14206 (1991).

[12] K. Nakamura and T. Mohri, Modelling Simul. Mater Sci. Eng. 1, 143 (1991).

[13] M. Asta, R. Mc Cormack and D. de Fontaine, Phjs. Rev. B48, 748 (1993).

[14] L. Anthony, J.K. Okamoto and B. Fultz, Phys. Rev. Lett. 70, 1128 (1993).

[15] B. Fultz, L.J. Nagel, L. Anthony and J.K. Okamoto, Phys. Rev. Lett. 73. 3034 (1994).

[16] G.D. Garbulsky and G. Ceder, Phys. Rev. B49, 6327 (1994).

[17] F.C. Nix and G. Shockley, Rev. Mod. Phys. 10, 1 (1938).

[18] C. Booth and J.S. Rowlingson, Trans. Faraday Soc. 51, 463 (1955).

[19] P.J. Wojtowicz and J.G. Kirkwood, J. Chem. Phys. 33, 1299 (1960).

[20] H. Bakker, Phil. Mag. A45. 213 (1982).

[21] J.A.D. Mathew. R.E. Jones and V.M. Dwyer, J. Phys. F 13, 581 (1983).

[22] H. Bakker and C. Tuijn, J. Phys. C 19, 5585 (1986).

[23] C. Tuijn and H. Bakker, Phys. Status Solidi(b) 155, 107 (1989).

[24] B. Fultz, L. Anthony and L.J. Nagel, Phys. Rev. B 52, 3315 (1995).

[25] Binary Alloy Phase Diagrams, Vol.1 ed : T.B. Massalski, H. Okamoto. P.R. Subramanyam and L. Kacprzak. (A.S.M. International, 1990).

[26] Z.Q. Gao and B. Fultz, Phil. Mag. B 67, 787 (1983); L.B. Hong, L. Anthony and B. Fultz, J. Mater. Res. 10, 126 (1995); L. Anthony, Ph.D. Thesis, California Inst. of Technology (1993).

[27] Thermophysical Properties of Matter, Vol.12. eds.: Y.S. Touloukin. R.K. Kirby, R.E. Taylor and P.D. Desai, (IFI/Plenum, New York. 1995), p.437.

[28] S. Ishida. J. Ishida, S. **Asano** and J. Yamashita, J. Phys. **Soc.** Japan 41. 1570 (1976).

[29] S.J. Pickart and R. Nathans, Phys. Rev. **123,** 1163 (1961).

[30] I.M. Robertson, Solid State Commun. 53, 901 91985).

[31] H. Okamoto and P.A. Beck, Monatsch. Chem. 103, 907 (1972).

[32] S. Kaya and A. Kussmann. Z. Phys. 72, 293 (1931).

[33] M.J. Marcinkowski and N. Brown, J. Appl. Phys. 32, 375 (1961).

[34] M.J. Marcinkowski and R.M. Poliak. Phil. Mag. 8, 1023 (1963).

[35] A. Paoletti, F.P. Ricci and L. Passari, J. Appl. Phys. **37**. 3236 (1966).

[36] R.L. Streever, Phys. Rev. **173,** 591 (1968).

[37] P.J. Caplan and R.L. Streever, Phys. Rev. B 2, 3449 (1970).

[38] W. Abdul-Razzaq and J.S. Kouvel, J. **Appl.** Phys. 55, 1623 (1984).

[39] J.E. Goldman, Rev. Mod. Phys. 25. 108 (1953).

[40] W. Proctor. R.G. Scurlock and E.M. **Wray,** Proc. Phys. Soc. 90, 697 (1967).

[41] A.K. Giri and G.B. Mitra, Physica **138B,** 41 (1986).

CHAPTER 5

THERMAL EXPANSION BEHAVIOUR OF CHEMICALLY
ORDERED $Fe_{3-x}Mn_xSi$ AND $Fe_{3-x}Mn_xAI$ ALLOYS

5.1 $Fe_{3-x}Mn_xSi$ Alloys

Binary Fe-Si alloys near their stoichiometric composition Fe_3Si and their ternary alloys with Mn addition have always been subjected to considerable experimental and theoretical investigations because of their unusual magnetic and thermal properties [1-13]. Fe_3Si is a ferromagnet with $T_C = 830$ K and Mn_3Si is an antiferromagnet with the Neel temperature, $T_N = 25.8$ K [14]. By forming solid solutions of Fe_3Si and Mn_3Si, the state of magnetic order of $Fe_{3-x}Mn_xSi$ changes from ferromagnetic for $x < 0.75$ to a complex one for $x > 0.75$ due to the presence of mixed ferromagnetic and antiferromagnetic interactions. Single phase alloys in this system are formed in a wide concentration range $0 < x < 1.8$ with the end members Fe_3Si and Mn_3Si both as stable DO.) ordered phases. The DO_3 ordered structure has been discussed earlier in Chapter-4. In DO_3 ordered Fe_3Si. A,B and C sites are occupied by Fe atoms and the D sites are occupied by Si atoms. The chemically and magnetically equivalent A and C sites have identical first near neighbour enviornment with four Fe atoms at B site and four Si atoms at D site. The B site Fe atom has eight iron neighbours belonging to the A and C sites. This different site enviornments give rise to different magnetic moments on the A, B and C sites. Polarized neutron beam diffraction experiments have shown that Fe A and C sites have a magnetic moment of $1.2\,\mu_B$ each whereas Fe B site has a moment of $2.4\,\mu_B$. Si A sites do not show any detectable moment [6].

Magnetization and neutron diffraction studies on $Fe_{3-x}Mn_xSi$ [4] show that the average magnetic moment falls approximately linearly with Mn concentration for $x < 0.75$. Fe at B sites are preferentially substituted by Mn upto this concentration and the magnetic moment of this site stays nearly constant at about 2.4 μ_B, whereas

the A,C site moments decrease **to** 0.4 μ_B. Above $x = 0.75$, the A,C sites also start getting occupied by Mn atoms and B site moment decreases rapidly due to Mn first neighbours. Since the A,C site enviornment does not change anymore, the moment at these sites remain constant at about 0.4 μ_B.

The ferromagnetism in Fe_3Si can come from the localized as well as the itinerant electrons. The neutron diffraction measurements have shown the presence of spin waves in Fe_3Si alloy [15-17]. But the low temperature specific heat [8] and thermal expansion measurements [9] on Fe_3Si did not show any spin wave contribution within the experimental accuracy. The specific heat measurements on $Fe_{3-x}Mn_xSi$ compounds [10] showed two **transitions.** The higher transition temperature *(Tc)* is the one where the paramagnetic to ferromagnetic transition takes place. The other one is at very low temperature at T_R giving a transforniation from ferromagnetic to spin glass like behaviour. Miles et.al. [9,11] have done thermal expansion studies on Fe_3Si and Fe_2MnSi and have tried to understand the magnetic behaviour in it with the addition of Mn. They have used the data of Fe_3Si as a background to estimate the magnetic contribution of other $Fe_{3-x}Mn_xSi$ alloys [11], assuming the magnetic contributions to thermal expansion and specific heat in the range 0 - 300 K for Fe_3Si are negligible. But **as** Fe_3Si is a ferromagnet the above assumption invites a lot of criticism. In this work, the semiclassical model for the thermal expansion which is described in Chapter-3 has been used effectively to estimate the vibrational back ground correctly. Also the band structure calculations have been used to find out the relative magnetization ζ_0 needed for the calculation of the electron-magnetic part of the thermal expansion. The magnon part is separated out using the Heisenberg interaction model for the localized spins. The respective Grüneisen parameters have been calculated and they are used to find out the specific

heat and entropy of the systems coming from different contributions.
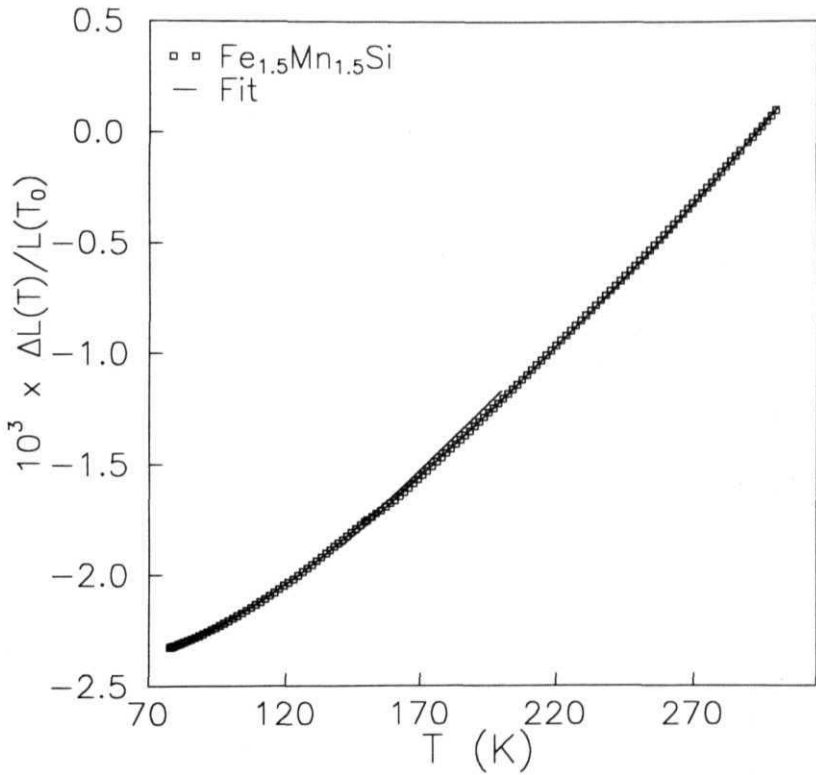
5.1.1   Experimental

Three alloy samples of compositions $Fe_{1.8}Mn_{1.2}Si$ $Fe_{1.5}Mn_{1.5}Si$ and $Fe_{1.2}Mn_{1.8}Si$ were prepared by arc melting by taking requisite quantities of metals of 4N purity. They were homogenized at 800° C for a week to get good homogenized samples. Small rectangular pieces of cuboid shapes of dimensions 2 x 2 x 2mm^3 were cut from the ingots and were annealed at 400° C for one week to get good ordered samples. From the density measurements the molar volumes are found out to be 27.475 cc, 28.18 cc and 27.43 cc for x = 1.2, 1.5 and 1.8 respectively. AC susceptibility measurements gave the ferromagnetic Curie temperatures to be 188 K and 157 K for x = 1.2 and x=1.5 alloys respectively. The alloy sample of x = 1.8 came out to be non-magnetic in the temperature range 80 - 300 K. Then thermal expansion measurements were done on these samples and the Figs.5.1a to 5.1c show the observed fractional length change data with temperature. Fig.5.2 shows the variation of linear thermal expansion coefficient (a) data obtained by the numerical differentiation of $\Delta L/L$, with temperature. The data of Fe_3Si are taken from literature [9].

5.1.2   Disussion of Fe_3Si alloy

There are few band structure calculations available in literature on Fe_3Si [18-20]. From these Switendick [18] was the first to show that the energy band calculations, based on a rigid-level spin-polarized model, were capable of explaining different magnetic moments on different sites. Switendick's calculation gives that there are a total of 14.5 electrons per cell in the upspin d-subband and 9.5 electrons per cell in the downspin d-subband with a total number of 24 electrons per cell in the d-band.
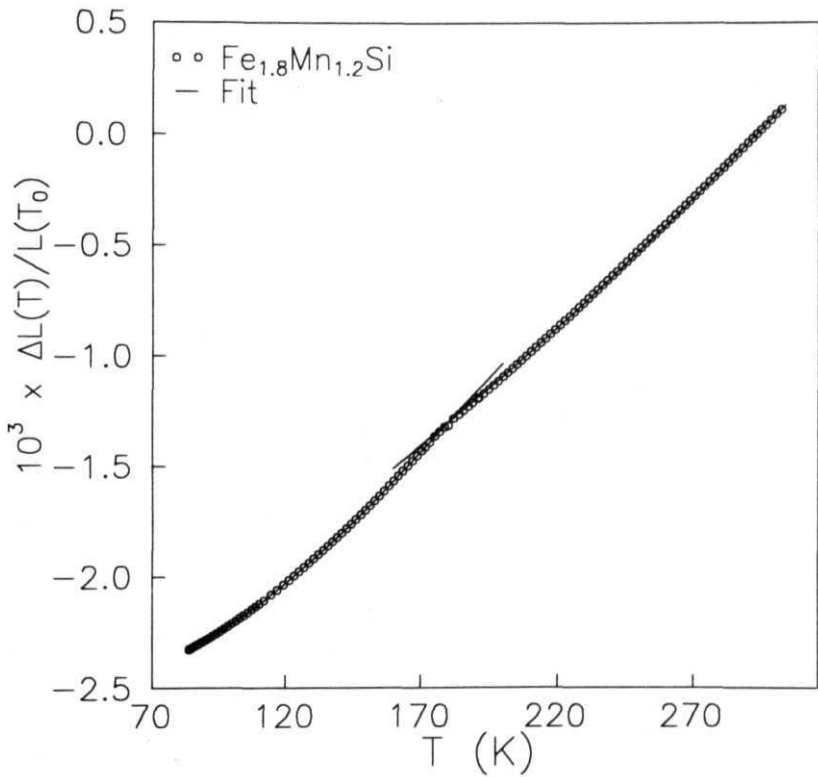
Fig.5.1a : Fractional length change data of $Fe_{1.8}Mn_{1.2}Si$ alloy. The solid lines show the fits of the experimental data points in the temperature range below and above T_C separately.

Fig.5.1b : Fractional length change data of $Fe_{1.5}Mn_{1.5}Si$ alloy. The solid lines show the fits of the experimental data points in the temperature range below and above T_C separately.
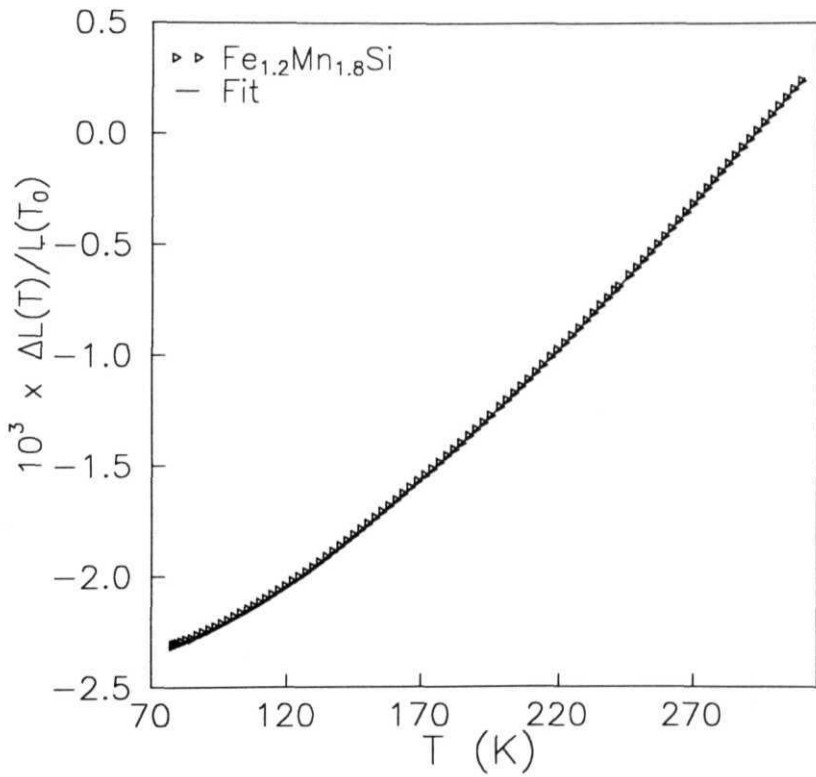
Fig.5.1c : Fractional length change data of $Fe_{1.2}Mn_{1.8}Si$ alloy with the solid line showing the fit to the experimental data points with single set of parameter values in the complete temperature range.
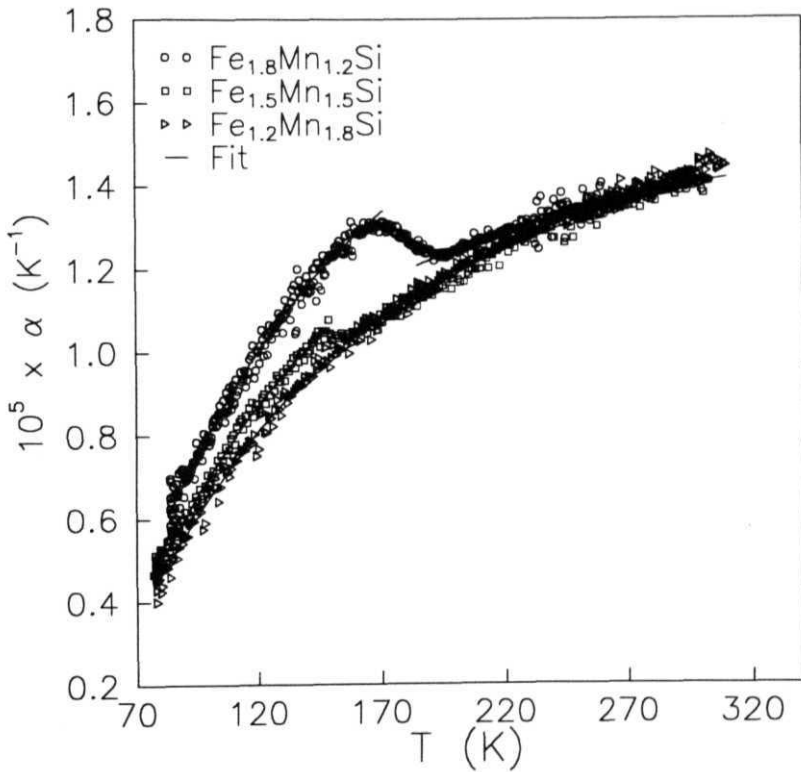
Fig.5.2 : Temperature variation of linear thermal expansion coefficient α for $Fe_{1.8}Mn_1$ $Fe_{1.5}Mn_{1.5}Si$ and $Fe_{1.2}Mn_{1.8}Si$ alloys. The solid lines are obtained from the analytical derivative of eqn.(3.2) using the same parameter values obtained from the fits of the respective alloys.

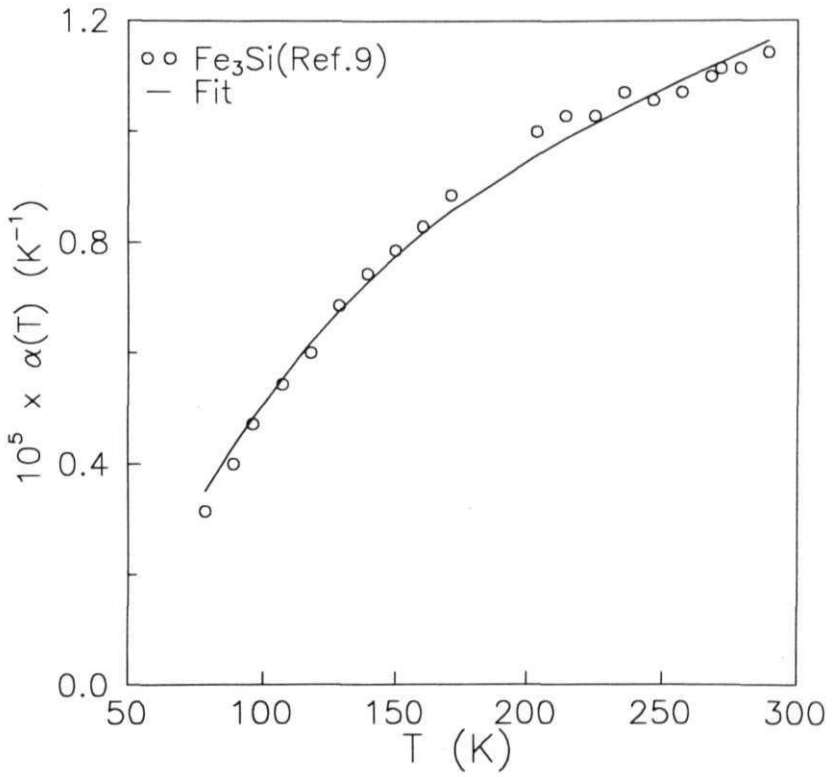Fig.5.3 : $\alpha(T)$ data of Fe_3Si alloy taken from ref.9. The solid line shows the fit to the data.

Thus the maximum number of holes per cell possible in **the** d-band, N_{0d} is 6. The net magnetic moment is $5\mu_B$, which is the value of n_{0d}. Hence at zero temperature the relative magnetization is given by, $\zeta_0 = \frac{n_{0d}}{N_{0d}} = 0.83$. Using this value of Co, the thermal expansion coefficient $\alpha(T)$ data obtained from ref.9 are fitted to the theoretical expression obtained from the tempeature derivative of eqn.(3.2) with A, m, $\gamma'_{mag}, \Theta_D, \Theta_E, p, g', g''', l'$ as parameters. But the fit returned the value of p to be 3. Hence in the final fit we have not used the Einstein terms in the expression for the vibrational part of the thermal expansion. The parameters obtained from the best fit are given in Table.5.1. The value of Θ_D obtained from the fit is 430 $\pm$ 12 K. The value of m returned by the fit is 0.254 which shows the energy band is not purely parabolic.

In the case of Fe, in the absence of any exchange interaction. 3.5 electrons per atom occupy each d-subband of width 4.05 eV. In the case of Fe_3Si one can think of a cell of four Fe atoms, one of which is replaced by a Si atom. And then in a cell of Fe_3Si, there are 12 electrons in each d-subband at 0 K in the absence of interactions. For a cell of four Fe atoms there are 4 x 3.5 electrons per cell in each of the d-subbands and they are related to the width w of the occupied bands as (following eqn.(3.89))

$$\frac{12}{4 \times 3.5} = \frac{w^{1.254}/1.254}{(4.05)^{1.489}/1.489} \; . \tag{5.1}$$

where 0.489 is the value of m and 4.05 eV is the value of occupied d-band width for Iron. The eqn.(5.1) gives the value of $w = 4.059$ eV. In the case of Fe_3Si, the width w' of the d-band in the absence of interaction (which includes the width occupied by the electrons and the width occupied by the holes) is given by,

$$w' = 4.059 \times \left(\frac{15}{12}\right)^{\frac{1}{1.254}} = 4.849eV \; . \tag{5.2}$$

Sample	Fe$_3$Si	Fe$_{1.8}$Mn$_{1.2}$Si		Fe$_{1.5}$Mn$_{1.5}$Si		Fe$_{1.2}$Mn$_{1.8}$Si
	T<T$_C$	T<T$_C$	T>T$_C$	T<T$_C$	T>T$_C$	80K<T<300K
g'(eV^{-1})	0.148 ±0.004	0.250 ±0.006	0.170 ±0.008	0.213 ±0.006	0.195 ±0.007	0.194 0.010
g"(eV^{-1}) ×10^{-3}	3.776 ±0.04	25.490 ±0.60	3.649 ±0.08	3.077 ±0.06	3.904 ±0.07	3.461 ±0.10
f'(eV^{-1}) ×10^{-4}	4.367 ±0.04	4.119 ±0.06	4.319 ±0.08	3.713 ±0.06	3.268 ±0.07	4.066 ±0.10
Θ_D(K)	430.0 ±1.20	439.4 ±0.60	439.4 ±0.60	441.1 ±0.60	441.1 ±0.60	444.8 ±1.00
ζ_0	0.830	0.253	0	0.177	0	0
A(K^{-2}) ×10^{-9}	0.320 ±0.04	1.922 ±0.60	-	2.131 ±0.60	-	-
m	0.254 ±0.004	0.292 ±0.006	-	0.446 ±0.006	-	-
γ'_{em}(K^{-2}) ×10^{-9}	1.170 ±0.04	7.646 ±0.60	9.270 ±0.80	8.454 ±0.60	9.168 ±0.70	9.836 ±1.00
γ'_{mag}(K$^{-5/2}$) ×10^{-11}	7.380 ±0.04	6.939 ±0.06	-	5.032 ±0.06	-	-

Table-5.1 : Debye temperatures, anharmonicity parameters, electron-magnetic and magnon terms obtained from the fit of the thermal expansion data in both the ferromagnetic and paramagnetic of Fe$_{3-x}$Mn$_x$Si (0 < x <1.8) alloys are given The values of Co obtained from the band structure analysis of these alloys are also given.

Thus, the value of the band width ϵ_{0d} occupied by 3 holes per cell each in every d-sub-band is,

$$\epsilon_{0d} = (u' - u') = (4.849 - 4.059)eV = 0.79eV . \qquad (5.3)$$

Using this value of ϵ_{0d} - 0.79 eV, the fitted value of $m = 0.254$ and $N_{0d} = 6$, the linear contribution to specific heat can be calculated using eqn.(3.66) which comes out to be 20.41 $mJ/molK^{-2}$.This matches well with the experimental value of 19.5 $mJ/molK^{-2}$[9]. As we fitted the experimental data only in the range of 80 - 300 K, the linear contribution to thermal expansion from the fit came out to be $\gamma'_{em} = 1.170$ x 10^{-9} K^{-2} which is positive, unlike obtained from the very low temperature experiment [9]. From the fitted value of $A = 3.20$ x 10^{-10} K^{-2} and using the eqn.(3.76), the electron-magnetic Grüneisen parameter value is calculated out to be, $\Gamma_G^{em} = 0.853$. The values of the bulk modulus and the molar volume used are 1.82 x 10^{11} Nm^{-2}[9] and 27.23 cc [9] respectively.

Even though Miles et.al. [9] could not observe any spin wave contribution to thermal expansion, the fit using our model returned a magnon contribution to thermal expansion (γ'_{mag}) of the order of 7.380 x $10^{-11}K^{-5/2}$ which is very small. Assuming just above $T_C = 830$ K, a complete spin disorder where the magnetic entropy will become equal to $S(Tc) = 3Rln2 = 17.3$ $J/molK$ for a spin half system, the magnon Griineisen constant is calculated to be $\Gamma_G^{mag} = 1.011$ using the eqn.(3.87).

5.1.3   Results and Discussion for $Fe_{3-x}Mn_xSi$ alloys

After getting a good agreement in the electron-magnetic contribution to specific heat and the Debye temperature for Fe_3Si we have next used the same analysis for ternary alloy samples. As seen in the Fig.5.2 the $\alpha(T)$ data show an anomaly around

the T_C values for x — 1.2 and $x = 1.5$ alloys, whereas the frartional length change data show only a slope change (Figs.5.1a and 5.1b). The data in the temperature range 80-300K could not be fitted with a single set of parameter values for both the $x = 1.2$ and $x = 1.5$ samples. They were fitted with two different set of parameter values separably for $T < T_C$ and $T > T_C$. Only the Debye temperature is kept same for the fit below T_C, as obtained from the fit above Tc-

As seen from the plots for $x = 1.2$ alloy a good fit with a r.m.s. deviation of 0.5% could be obtained from 190 K upto the room temperature by taking the term $\gamma'_{em}/2 = A \left| (1 + \zeta_0)^{\frac{n_i}{m+1}} + (1 - \zeta_0)^{\frac{m}{m+1}} \right|$ as a single parameter as Co is zero in the paramagnetic region and also by taking the magnon contribution $\gamma'_{mag} = 0$. Before proceeding to fit the thermal expansion data below Tc one needs to know the value of ζ_0. Following Switendick [18], we take that for one Mn atom substitution, one electron per unit cell is removed. Hence for $Fe_{1.8}Mn_{1.2}Si$ the total number of electrons in the d-band are 22.8 per cell. Therefore the total number of holes per cell is. $N_{0d} = (30.0 - 22.8)$ — 7.2. The net magnetic moment of the above sample is 1.82 μ_B [21]. So the relative magnetization Co = 0.253. The data for $T < Tc$ could be fitted to eqn.(3.2) upto 172 K with a r.m.s. deviation less than 0.8 %. Here a different set of parameter values are except the value of Θ_D which is kept constant to the value obtained from the fit in the paramagnetic region.

Similarly for $x = 1.5$ sample the fractional length change data in the paramagnetic region ($160K < T < 300K$; $T_C = 157$ K) are fitted to the eqn.(3.2) by taking the term γ'_{em} as a single parameter and keeping the term $\gamma'_{mac} = 0$. The percentage r.m.s. deviation is also about 0.6% in this case. For fits below T_C one notes that there are 22.5 electrons per cell in the d-band of $Fe_{1.5}Mn_{1.5}Si$. Thus N_{0d} is found out to be 7.5 and ζ_0 calculated out to be 0.177 by using the value of n_{0d} to be 1.33

as obtained from the measured net magnetic moment [21] In the ferromagnetic region the *AL/L* data are fitted to the eqn.(3.2) below *Tc* using this calculated value of ζ_0. In the same spirit of $Fe_{1.8}Mn_{1.2}Si$ alloy sample a different set of parameter values are obtained, with only the Debye temperature being kept fixed to the value obtained from the fit of the paramagnetic region.

In the case of $Fe_{1.2}Mn_{1.8}Si$, the fractional length change data did not show any transition as it is non-magnetic in our experimental range, it could be fitted with only one set of parameter values.

(*i*) Analysis of Vibrational Contribution

The values of the parameters obtained from the best fits in both the ferromagnetic and paramagnetic regions for all the samples are given in Table-5.1. The values of Θ_D obtained from the fits are 430 K, 439.4 K. 441.0 K and 444.8 K for $x = 0$, 1.2, 1.5 and 1.8 respectively showing an increase of Debye temperature with Mn concentration. For $x = 1.2$ and 1.5 alloys the anharmonic parameter g' came out to be more in the ferromegnetic region than in the paramagnetic region. The other two anharmonic parameters g'' and $/'$ do not show any appreciable change with Mn addition.

The vibrational specific heat C_{ph} is calculated using the eqn.(3.18) for all the $Fe_{3-x}Mn_xSi$ alloys using the paramter values obtained from fits. The vibrational entropies are calculated using the relation $S_{ph} = \int_0^{\cdot} (C_{ph}/T)dT$. The temperature variation of S_{ph} of the alloys for x - 0, 1.2, 1.5 and 1.8 are plotted in Fig.5.4. The plot shows that the vibratoioal entropy reduces with Mn addition which comes from the increase in Θ_D. We do not see any observable difference in the vibrational entropy in between the ferromagnetic and paramagnetic regions of the $x = 1.2$ and 1.5
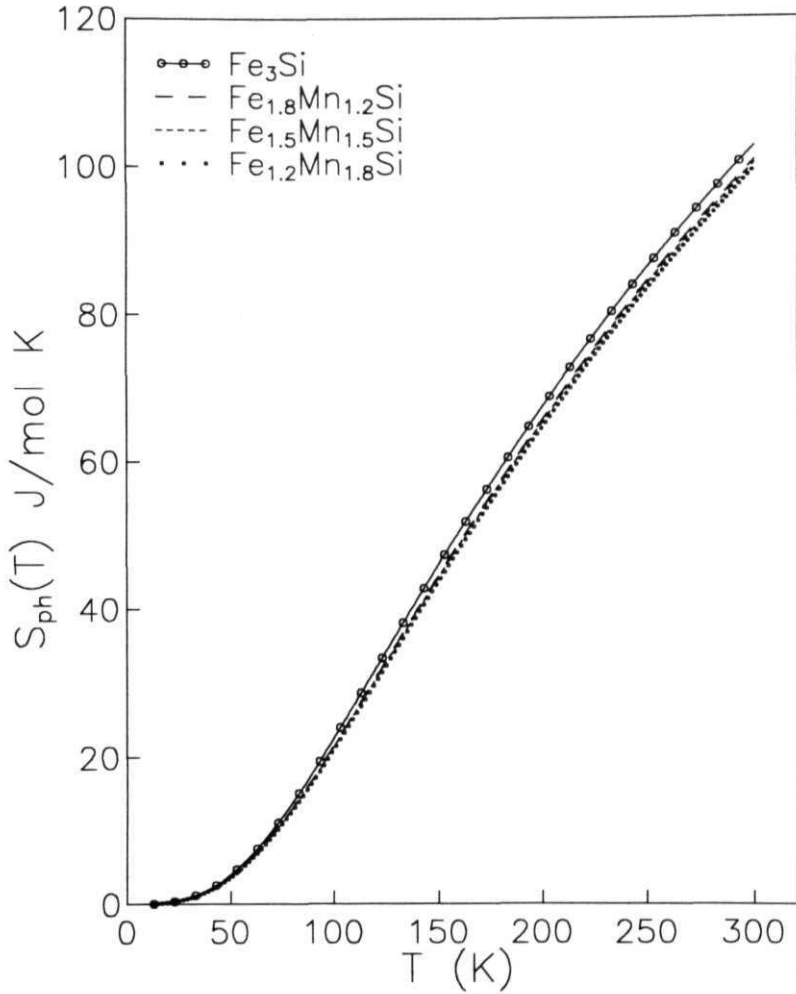
**Fig.5.4** : Temperature variation of vibrational specific heat of $Fe_{3-x}Mn_x Si$ alloys.

alloys. From the vibrational part of the thermal expansion and the vibrational specific heat the vibrational Gruneisen constants (Γ_G^{pn}) are calculated using eqn.(3.20) and are given in Table-5.2.

(it) Analysis of Magnetic Contribution

The values of 77l, obtained from the fits show an increase from the value 0.254 in the case of Fe_3Si to 0.292 for $Fe_{1.8}Mn_{1.2}Si$ sample and 0.446 for $Fe_{1.5}Mn_{1.5}Si$ alloy. The linear electronic term in the paramagnetic region of $x = 1.2$ and 1.5 and for $Fe_{1.2}Mn_{1.8}Si$ alloy does not differ much from each other (see Table-5.1). Using the values of ζ_0 and the fitted values of A and m the linear terms γ'_{em} in the ferromagnetic region for all the samples are calculated and they show an increase with Mn concentration. In fig.5.5a the electron-magnetic cotributions to the thermal expansion coefficient α_{em} are plotted which show an increase with Mn substitution in $Fe_{3-x}Mn_xSi$ alloys. This may be because. with Mn substitution the itinerant ferromagnetic character of Fe_3Si decreases. This is understandable from the point of view of the increase in the Mn-Mn antiferromagnetic interactions which competes with the ferromagnetic order. Another important observation is that the magnon contribution to thermal expansion decreases with the addition of Mn (see fig.5.5b).

For $Fe_{1.8}Mn_{1.2}Si$ as the total number of electrons in the d-band is 22.8, in the absence of interactions the number of electrons in each upspin and downspin d-subbands are 11.4 for every unit cell. The band width w occupied by this many number of electrons can be calculated using the fitted m = 0.292.

$$\frac{11.4}{12} = \frac{w^{1.292}/1.292}{(4.059)^{1.254}/1.254} . \qquad (5.4)$$
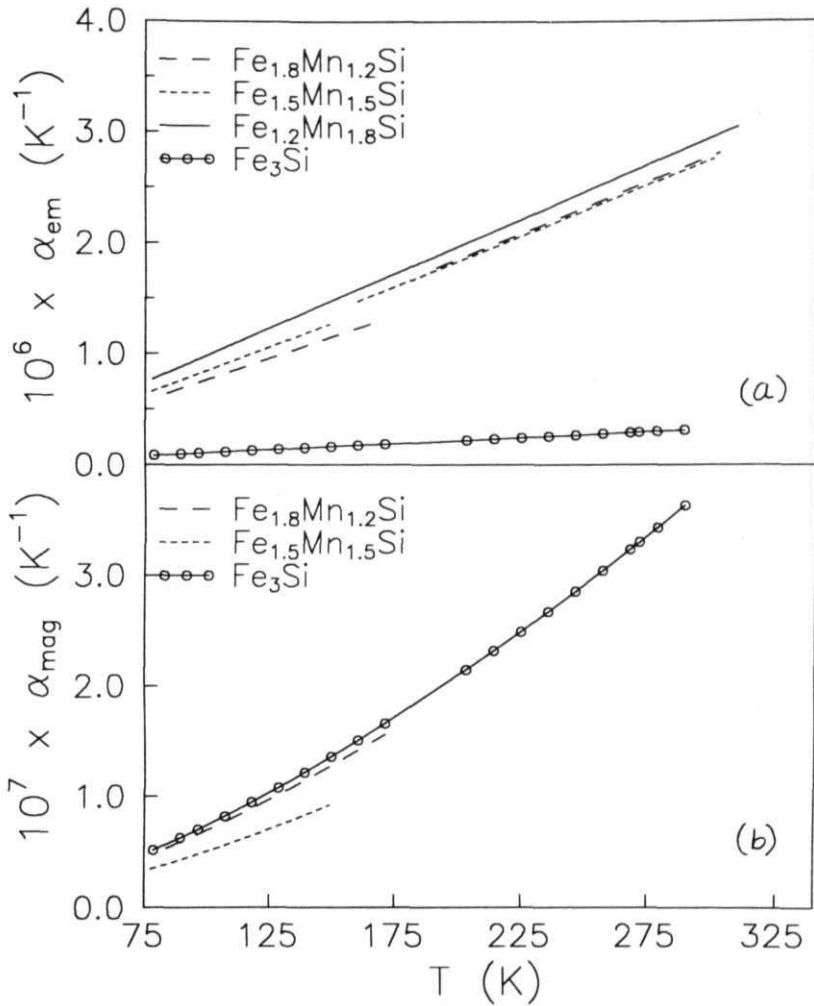
Fig.5.5 : (a) Temperature variation of electron-magnetic contribution to thermal expansion coefficient (α_{em}) of $Fe_{3-x}Mn_xSi$ $(x = 0,\ 1.2,\ 1.5,\ 1.8)$ alloys. (b) Temperature variation of magiiori contribution to thermal expansion coeffificent (α_{mag}) of $Fe_{3-x}Mn_xSi$ $(x = 0,\ 1.2,\ 1.5)$ alloys.

Where 4.059 eV is the band width occupied by 12 electrons per cell in Fe_3Si alloy with $m = 0.254$ and it gave the value of w to be 3.831 eV. From this value of w the d-band with (u') of this alloy including the unoccupied part is calculated to be

$$u' = 3.831 \times \left(\frac{15}{11.4}\right)^{\frac{1}{1.292}} eV = 4.738eV$$

Thus the unoccupied d-band width, i.e., the width of the band occupied by 3.6 holes per cell in each d-subbands is, $\epsilon_{0d} = u' - w - 0.907$ eV. Using this value of ϵ_{0d}, N_{0d} = 7.2, B_T = 2.28 x $10^{11} Nm^{-2}$ [30] and V = 27.475 cc (molar volume) and the fitted values of m and A the electron magnetic Griineisen constant (Γ_G^{em}) is calculated to be 6.0 using eqn.(3.76) and the value of the electron magnetic coefficient of the specific heat γ_{em} came out to be 23.94 $mJ/molK^2$ form eqn.(3.73). The fit gave the value of $\gamma'_{mag} = 6.939$ x $10^{-11} K^{-5/2}$. From the T_C = 188 K and taking the magnon entropy at T_C to be of 17.3 $J/molK$ Γ_G^{mag} comes out to be 0.129 from eqn.(3.87).

For $Fe_{1.5}Mn_{1.5}Si$ alloy there are 22.5 electrons per cell in the d-band. Hence the number of holes participating in the itinerant ferromagnetism is, N_{0c} = 7.5. Thus in the absence of interaction at absolute zero there will be 11.25 electrons per cell each in the upspin and downspin d-subbands. The band width w occupied by these 11.25 electrons is found out to be 3.557 eV using the fitted $m = 0.446$ for this alloy. Then the value of the band width w' is calculated to be 4.340 eV. From these values of w and w', the value of ϵ_{0d} comes out to be 0.783 eV. Using the value of $\zeta_0 = 0.177$ for this alloy, B_T = 1.433 x $10^{11} Nm^{-2}$ [30], V = 28.18 cc (molar volume) and the fitted values of m and A the values of Γ_G^{em} and γ_{em} are calculated to be 3.17 and 32.36 $mJ/molK^2$ respectively. The best fit returned the value of the magnon contribution to thermal expansion, γ'_{mag} = 5.032 x $10^{-11} K^{-5/2}$. From the

Sample	γ_{em} (mJ/mol K^2)	Γ_G^{em}	Γ_G^{mag}	Γ_G^{ph} T<T$_C$	Γ_G^{ph} T>T$_C$
Fe$_3$Si	20.41 (19.5)	0.853	1.010	1.425	-
Fe$_{1.8}$Mn$_{1.2}$Si	23.94	6.002	0.129	3.040	2.070
Fe$_{1.5}$Mn$_{1.5}$Si	32.36	3.170	0.046	1.680	1.520
Fe$_{1.2}$Mn$_{1.8}$Si	-	-	-	-	2.280

Table-5.2 : Calculated linear contribution to specific heat γ_{em} with the electron-magnetic Gruneisen parameter (Γ_G^{em}), magnon Gruneisen parameter (Γ_G^{mag}) and vibrational Gruneisen parameter (Γ_G^{ph}) of Fe$_{3-x}$Mn$_x$Si alloys The value of γ_{em} inside the brakets is taken from ref.9.
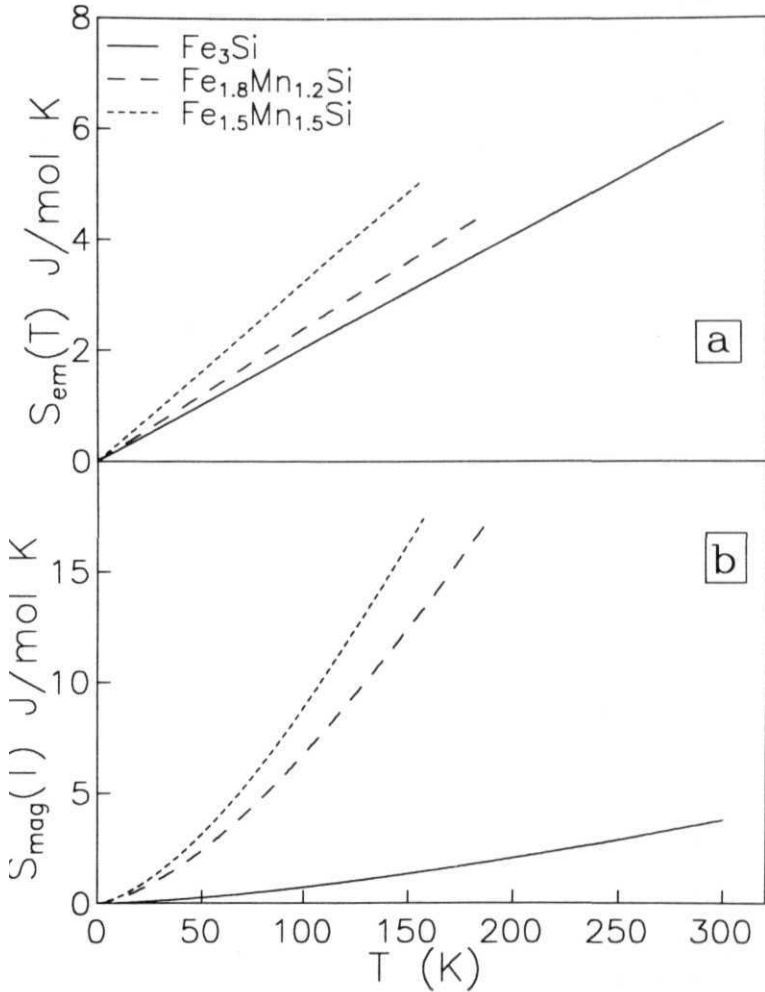
Fig.5.6 : (a) Electron-magnetic and (b) magnon contributions to entropy with temperature for $Fe_{3-x}Mn_xSi$ (x = 0, 1.2, 1.5) alloys.

value of $T_C = 157$ K, Γ_C^{mag} is calculated to be 0.046. The values of Γ_C^{em} and Γ_C^{mag} are summarized in Table-5.2.

The electron-magnetic and magnon contributions to entropy are calculated using eqns.(3.70) and (3.81) respectively. Fig.5.6a shows the electron-magnetic contribution to the entropy for $x = 0$, 1.2 and 1.5 alloys. From the plot one can see that S_{em} increases with MB addition which is may be due to the decrease of the itinerant character. Similarly from fig.5.6b where the magnon contribution to entropy S_{mag} is plotted for different x, one can see that the magnon **entropy** increases with the increase in Mn.

5.2 $Fe_{3-x}Mn_x Al$ Alloys

The ternary alloys $Fe_{3-x}Mn_x Al$ are of great technological interest because of their possible applications as stainless steel. The behaviour of their basic magnetic and structural properties with the substitution of Mn for Fe are quite interesting and are addressed using experiments such as neutron diffraction, magnetization, NMR and Mossbauer spectroscopy. Fe-Mn-Al alloys show a remarkable decrease of average magnetic moment with increasing Mn content [23]. In a follow up work [24] on disordered $Fe_{3-x}Mn_x Al$ upto 13.9 at% alloys using magnetization measurements and magnetic diffuse neutron scattering experiments showed that both Fe and Mn atoms have a localized moment (2.2 μ_B) which decreases with increase in Mn concentration. Further work on the system after inducing atomic order with annealing were carried out and the magnetic behaviour was observed [25]. Recently the effect of chemical ordering on magnetic properties of $Fe_{3-x}Mn_x Al$ both in ordered and disordered states were studied using Mossbauer spectroscopy [26]. In the Chapter-4

the crystal structure of Fe_3Al has been **discussed extensively. In** the ordered state, the distribution of Mn showed a preference for B and D sublattices which have predominantly Fe neighbours on A, C sites, but the A, C sites were also found to be occupied with half to one third concentration. The observed Mn moment with increasing Mn content, may be due to increasing number of antiparallel **moments** to the resultant magnetic moment.

However there have been no work reported to date on the thermal properties like specific heat, entropy and **thermal** expansion studies on $Fe_{3-x}Mn_xAl$ alloy system. In this work we study the behaviour of magnetic and lattice contributions to thermal expansion, specific heat and entropy for a wide concentration range 0 < x < 1.2.

5.2.1   Sample preparation and Expansion measurements

Alloys **of composition** $Fe_{3-x}Mn_xAl$ in the concentrations of x = 0.3, 0.9 and 1.2 were prepared taking requisites quantities of JMC Puratronic grade I iron powder, m3N7 purity manganese chips and m3N5 purity Al shots. They were mixed well and then made into pellets before melting them in an arc furnace with a water cooled **copper** hearth. Melting was done repeatedly to ensure homogeneity. Then the alloy ingots were homogenized at 1000° C for 48 hours sealing them in quartz tubes under a pressure of 10^{-4} torr and were quenched in brine solution. Small rectangular pieces of approximate dimensions 2 x 2 x $2mm^3$ were cut from the ingots and were annealed at 400° C for a week to get ordered samples. From the density measurements the molar volumes were found out to be 29.875 cc. 29.609 cc and 30.557 **cc** for x = 0.3, 0.9 and 1.2 alloys. The thermal expansion measurements were performed on these samples following the thermal expansion procedure described in Chapter-2.

5.2.2   **Results and** Discussion

Magnetization measurements show that for $Fe_{3-x}Mn_xAl$ alloys with $x = 0.3$, 0.9 compositions, the Curie temperatures are above room temperature. The alloy with $x = 1.2$ shows the onset of transition at about 150 K and the width of transition is as large as 30 K [13]. The observed fractional length change data are shown in **Figs.5.7a** to 5.7c. The $Fe_{1.8}Mn_{1.2}Al$ alloy shows a slope change around the T_c in $\Delta L/L$ data (**Fig.5.7c**) and a broad anomaly in $\alpha(T)$ data (**Fig.5.8**). **In Chapter-**4 the structure and different contributions **to** thermal **expansion** for Fe_3Al has been discussed. Therefore here we will confine ourselves only on **the** effect of Mn substitution in Fe_3Al.

As all **the** samples are ferromagnetic, band structure calculations are needed for the determination of ζ_0. In Chapter-4 we have seen that there are a total of 18.646 electrons per cell for Fe_3Al in its d-band. The value of m from the fir came out to be 0.364 for Fe_3Al. Following the same reasoning as **in** the $Fe_{3-x}Mn_xSi$ alloys described in subsection 5.1.3, we assume that by substituting one Mn atom for one Fe atom, one electron per unit cell is removed. Therefore for $Fe_{2.7}Mn_{0.3}Al$ alloy total number of electrons in the d-band will be 18.346 and hence N_{0c} will be 11.654. The net magnetic moment for this alloy is 2.85 [25] which is the value of n_{0d}. Therefore ζ_0 is calculated to be 0.245. Similarly for $x = 0.9$ alloy there are 17.746 electrons per cell in the d-band. Hence the value of N_{0d} is 12.254 holes per cell in the d-band in the absence of any interaction. For $x = 1.2$ alloy there are 17.446 electrons per cell in the absence of any interaction in the d-band which gives N_{0d} to be 12.554. As there are no available value of net magnetic moments for the exact compositions $x = 0.9$ and 1.2 alloys, they are taken from the interpolation of
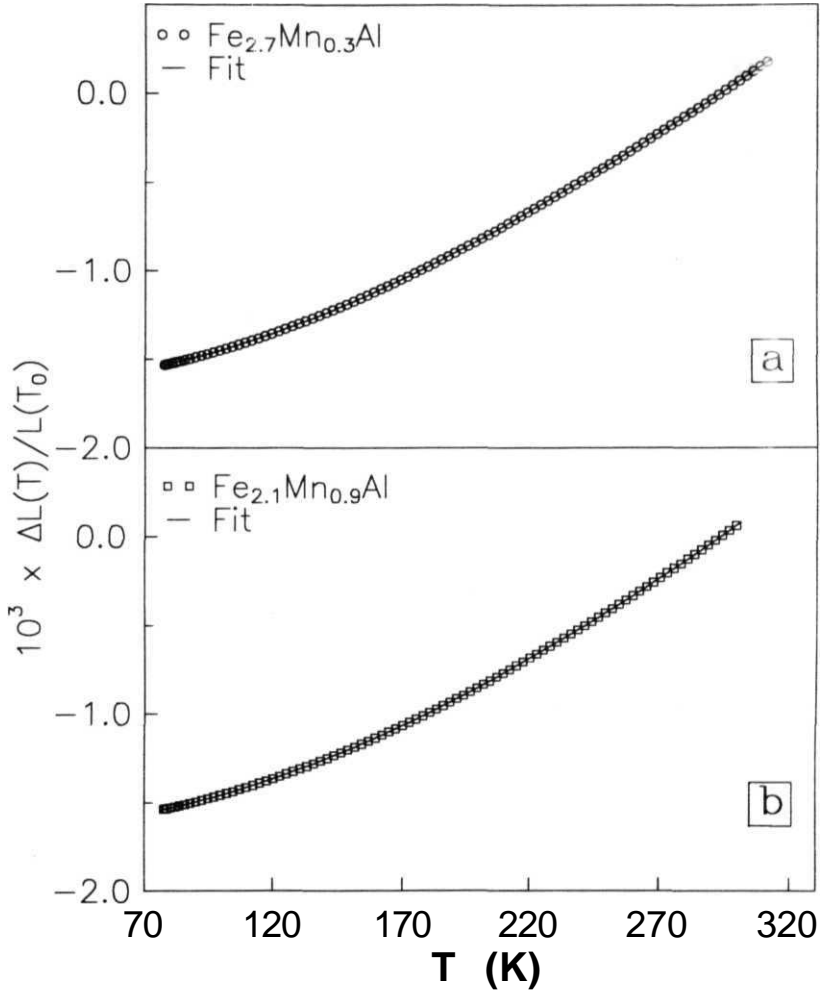
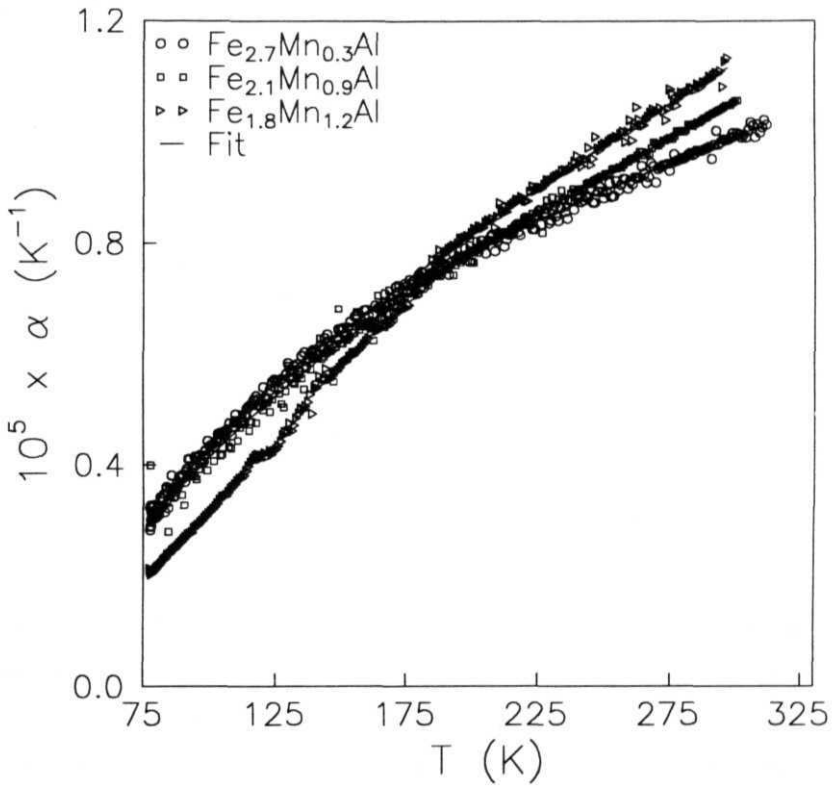**Fig.5.7** : Fractional length change data of (a) $Fe_{2.7}Mn_{0.3}Al$ and (b) $Fe_{2.1}Mn_{09}$ 4/ alloys. The solid lines give the fits of the experimental data points.
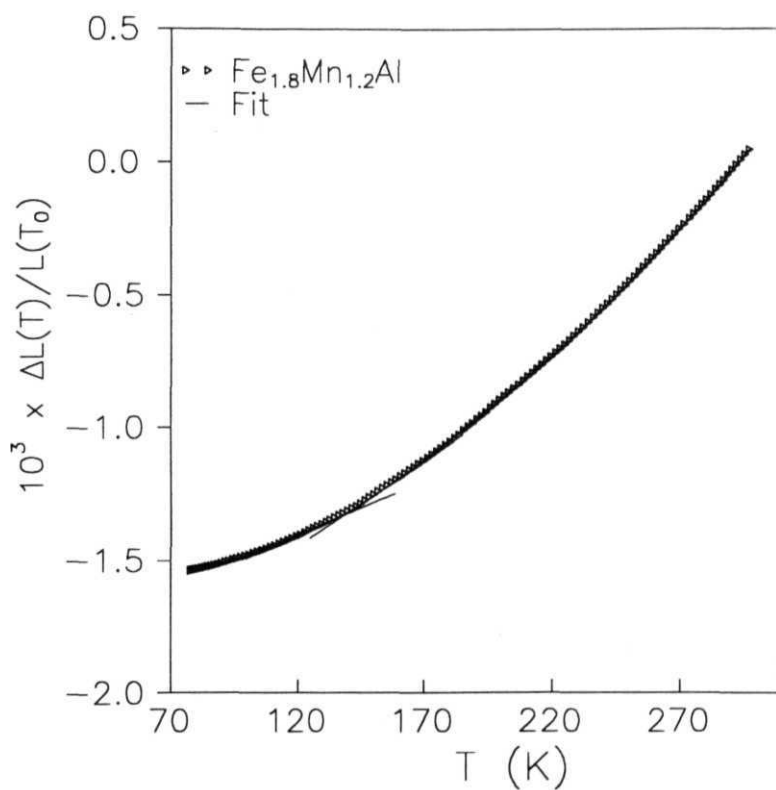
Fig.5.7c : Fractional length change data of $Fe_{1.8}Mn_{1.2}Al$ alloy. The solid lines represent the fits above and below T_C separately.

Fig.5.8 : Temperature variation of linear thermal expansion coefficients of $Fe_{3-x}Mn_xAl$ alloys.

the magnetic moment values given in literature [25]. Thus the values of n_{0_d} have come out to be 0.93 and 0.54 for $Fe_{2.1}Mn_{0.9}Al$ and $Fe_{1.8}Mn_{1.2}Al$ alloys respectively. Hence for $Fe_{2.1}Mn_{0.9}Al$ alloy ζ_0 = 0.93/12.254 = 0.076 and for $Fe_{1.8}Mn_{1.2}Al$ alloy ζ_0 = 0.54/12.554 = 0.043.

Using the calculated values of Co the fractional length change data were fitted to our model. Figs.5.7a and 5.7b show the fitted $\Delta L/L$ data of $Fe_{2.7}Mn_{0.3}Al$ and $Fe_{2.1}Mn_{0.9}Al$ samples. The percentage r.m.s. deviation of the fits are about 0.5%. But for $Fe_{1.8}Mn_{1.2}Al$ sample data in the entire temperature range could not be fitted to one set of parameter values. The data could be fitted separately for the temperature ranges $80K < T < 120K$ and $150K < T < 300K$. The data below T_C are fitted by keeping the value of Debye temperature fixed to the value that is obtained from the fit in the paramagnetic region.

All the parameter values obtained from the fits are given in Table-5.3. The Θ_D values obtained from the fits are 418.2 K, 427.3 K and 473.3 K for x = 0.3, 0.9 and 1.2 alloys respectively and like in the case of $Fe_{3-x}Mn_xSi$ series, here also the value of Θ_D increases with the Mn concentration. Though in the case of Fe_3Al the lattice vibrational part yielded an optic mode, in these alloys fits have returned the value of p to be 3. The value of the parameter g shows a decrease with the addition of Mn in the ferromagnetic region. In the case of $Fe_{1.8}Mn_{1.2}Al$ alloy the cubic anharmonicity parameter g' is found out be more in the ferromagnetic region than in the paramagnetic region. The value of the quartic anharmonicity parameter has increased by atleast one order of magnitude in the ferromagnetic region than in the paramagnetic region which may be due to a softening of the lattice during the magnetic transition.

The values of m obtained from the fits remained more or less constant (0.396

Sample	$Fe_{2.7}Mn_{0.3}Al$	$Fe_{2.1}Mn_{0.9}Al$	$Fe_{1.8}Mn_{1.2}Al$	
	$T<T_C$	$T<T_C$	$T<T_C$	$T>T_C$
$g'(eV^{-1})\times10^{-2}$	9.832±0.08	6.612±0.09	6.660±0.07	6.009±0.08
$g''(eV^{-1})\times10^{-3}$	3.674±0.08	17.01±0.90	5.502±0.07	1.550±0.08
$f'(eV^{-1})\times10^{-4}$	33.95±0.80	21.53±0.90	6.636±0.07	0.286±0.008
$\Theta_D(K)$	418.2±0.8	427.3±0.9	473.3±0.7	473.3±0.7
ζ_0	0.245	0.076	0.043	0
$A(K^{-2})\times10^{-9}$	2.914±0.08	5.109±0.09	5.909±0.07	-
m	0.396±0.008	0.383±0.009	0.379±0.007	-
$\gamma'_{em}(K^{-2})\times10^{-8}$	1.158±0.08	2.042±0.9	2.364±0.07	2.584±0.08
$\gamma'_{mag}(K^{-5/2})\times10^{-10}$	1.105±0.08	0.972±0.09	0.538±0.07	-

Table-5.3 : The Debye temperatures, lattice anharmonicity paramters, electron-magnetic and the magnon terms obtained from the fit of the thermal expansion data of $Fe_{3-x}Mn_xAl$ ($0.3 < x \leq 1.2$) samples.

for $Fe_{2.7}Mn_{0.3}Al$, 0.383 for $Fe_{2.1}Mn_{0.9}Al$ and 0.379 for $Fe_{1.8}Mn_{1.2}Al$ alloys). **The** electron-magnetic term of the thermal **expansion** increases with increase **in Mn** concentration and approaches **the** value obtained in the paramagnetic region **of** the $Fe_{1.8}Mn_{1.2}Al$ alloy. In **Fig.**5.9a the electron-magnetic contribution α_{em} is plotted for different x to see the effect of Mn addition on Fe_3Al. One can see that α_{em} increases with Mn concentration, which may be due to the decrease in the value of ζ_0, indicating a decrease in the itinerant character. Also from **Fig.**5.9b it is seen that the magnon contribution **to** thermal expansion coefficient (α_{mag}) decreases with increase in Mn concentration.

5.2.3 Calculations of **Magnetic Gruneisen Constants**

For $Fe_{2.7}Mn_{0.3}Al$ alloy, there are a total of 18.346 electrons per cell in the d-band. Hence in the absence of interactions there will be 9.173 electrons per cell in each of the upspin and downspin d-subbands. The width of the each occupied d-subbands of Fe_3Al is 3.205 eV, it contains 9.325 electrons per cell and $m = 0.364$. The width of the occupied part of the band of $Fe_{2.7}Mn_{0.3}Al$ alloy from the fitted m value 0.396 is calculated as

$$\frac{9.173}{9.325} = \frac{w^{1.396}/1.396}{(3.205)^{1.364}/1.364} \ . \tag{5.5}$$

which gives a value of $w = 3.136$ eV. From this, the width w' including the un-occupied portion of the d-band in the absence of any interaction is calculated to **be**

$$w' = 3.136 \times \left(\frac{15}{9.173}\right)^{\frac{1}{1.396}} eV = 4.460 \ eV \ . \tag{5.6}$$
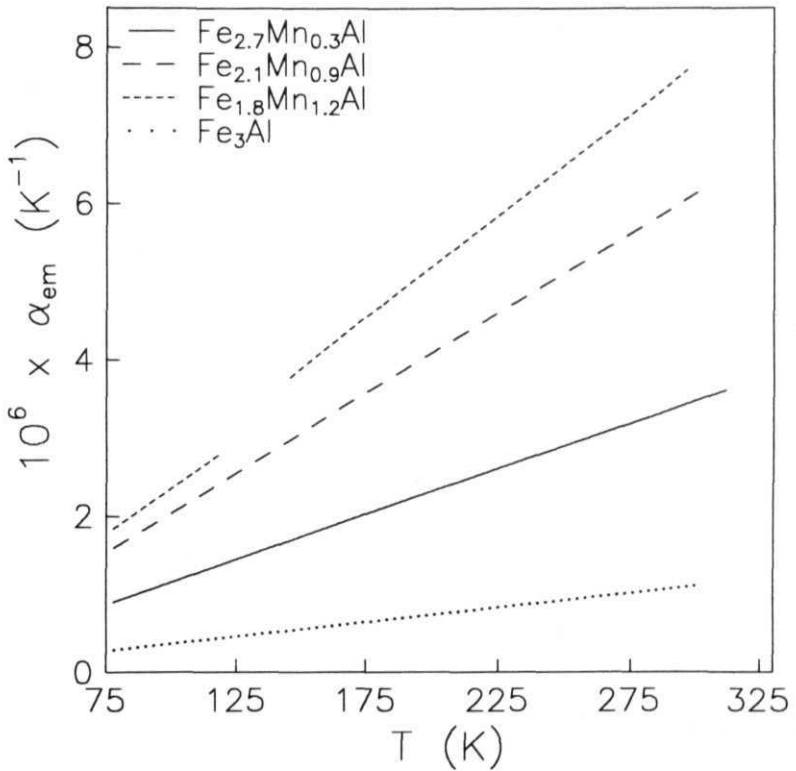
Fig.5.9a : Electron-magnetic contribution α_{em} with temperature for $Fe_{3-x}Mn_xAl$ ($x = 0$, 0.3, 0.9 and 1.2) alloys.
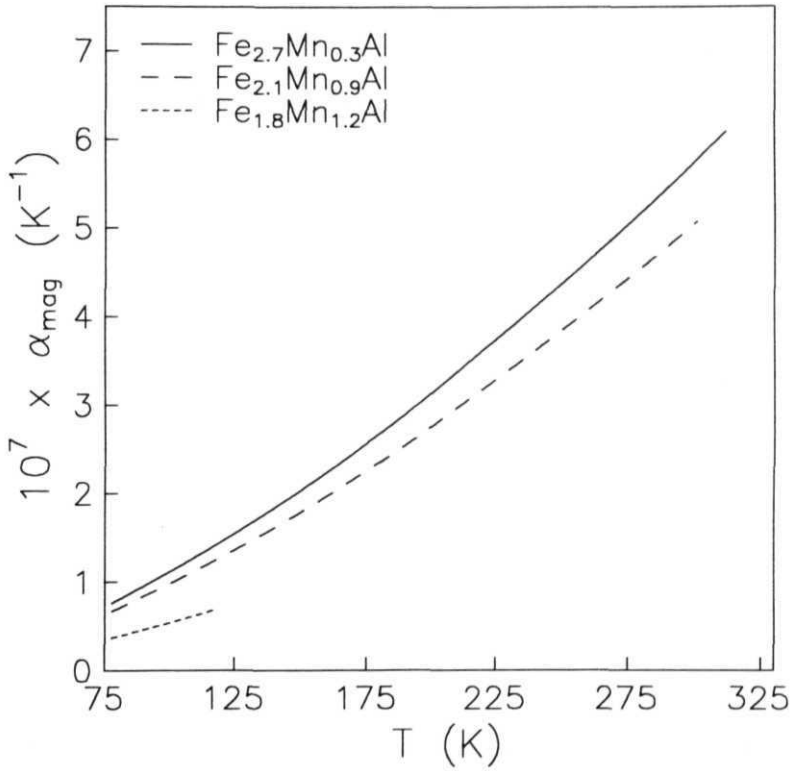
Fig.5.9b : Temperature variation of magnon contribution, α_{mag} for $Fe_{3-x}Mn_xAl$ (x = 0.3, 0.9 and 1.2) alloys.

The width ϵ_{0d} occupied by $N_{0d} = 11.654$ **holes** per cell in the absence of interactions is thus found out to be,

$$\epsilon_{0d} = w' - w = (4.460 - \mathbf{3.136})\text{eV} = 1.324 eV \tag{5.7}$$

Using the value of $\epsilon_{0d} = 1.324$ eV, $N_{0d} = 11.654$, $B_T = 1361$ x 10^{11} $\overset{Nm^{-2}}{\wedge}$ (taking a weighted average of the values of bulk moduli of the constituent atoms) , the molar volume $V = 29.875$ cc and fitted values of m and A, the linear coefficient of the specific heat γ_{em} is calculated to be 28.632 $mJ/molK$ from eqn.(36). Using eqn.(3.76) the electron magnetic Griineisen parameter is calculated to be, $\Gamma_G^{em} = 4.48$. The fit returned the value of **the magnon** contribution to thermal expansion, $\gamma'_{mag} = 1.105$ x $10^{-10} K^{-5/2}$. The magnon Griineisen parameter is calculated to be, $\eta = 0.479$, using eqn.(3.87) and $T_C = 440$ K for **the** Curie **temperature of** this alloy.

For $Fe_{2.1}Mn_{0.9}Al$ alloy there are a total of 17.746 d-band electrons, and in the absence of interactions each upspin and downspin d-subbands will contain 8.873 electrons per cell. They will occupy a width w, where

$$\frac{8.873}{9.325} = \frac{w^{1.383}/1.383}{(3.205)^{1.364}/1.364} . \tag{5.8}$$

This gives $w = 3.073$ **eV.** The width w' is given by

$$w' = 3.073 \times \left(\frac{15}{8.873} \right)^{\frac{1}{1.383}} eV = 4.492 \ eV \tag{5.9}$$

Using these values of w and w', ϵ_{0d} is found out to be,

$$\epsilon_{0d} = (4.492 - 3.073)eV = 1.419 eV . \tag{5.10}$$

The above values, with $A = 5.110 \times 10^{-9} K^{-2}$ (sec Table-5.3) give the value of γ_{em} to be $28.02 \ mJ/molK^2$ and $\Gamma_G^{em} = 7.76$ using $B_T = 1.1\% > 10^{11} Nm^{-2}$ (taking a weighted average of the bulk moduli of the constituent atoms) and the molar volume $V — 29.609 \ cc$. The magnon Grüneisen parameter is calculated to be $\eta = \Gamma_G^{em} = 0.218$ from the fitted value of γ'_{mag} and $T_C = 310$ K for this alloy.

In the ferromagnetic $Fe_{1.8}Mn_{1.2}Al$ alloy the total number of electrons in the d-band is 17.446 and in the absence of interaction each d-subband contains 8.723 electrons per cell and the value of u for this alloy can be calculated from

$$\frac{8.723}{9.325} = \frac{u^{1.379}/1.379}{(3.205)^{1.364}/1.364} . \tag{5.11}$$

This gives $w = 3.039$ eV. The width u' is calculated as

$$u' = 3.039 \times \left(\frac{15}{8.723}\right)^{\frac{1}{1.383}} eV = 4.502 \ eV$$

Using these values of u and u',

$$\epsilon_{0d} = (4.502 - 3.039)eV = 1.463eV.$$

Using the values of $B_T = 1.117 \times 10^{11} \ Nm^{-2}$, $V = 30.557 \ cc$ (molar volume) and the fitted values of m and A the values of the coefficient of electron-magnetic specific heat and Γ_G^{em} are calculated to 27.74 $mJ/molK^2$ and 8.73 respectively. The magnon contribution to the thermal expansion came out to be $\gamma'_{mag} = 5.380 \times 10^{-11} \ K^{-5/2}$ and taking the $T_C = 129$ K the value of $\eta = \Gamma_G^{mag}$ is found out to be 0.031. The values of Γ_G^{em} and Γ_G^{mag} are summarized in Table-5.4 for $Fe_{3-x}Mn_xAl$ alloys.

Sample	γ (mJ/mol K^2)	Γ_G^{cm}		Γ_G^{ph} T<T$_C$	Γ_G^{ph} T>T$_C$
Fe$_{2.7}$Mn$_{0.3}$Al	2803	4.477	0.479	0.778	-
Fe2.1Mno.9Al	28.02	7757	0.218	0456	-
Fe$_{1.8}$Mn$_{1.2}$Al	27.95	8 73	0.031	0.442	0 398

Table-5.4 : Calculated linear contribution to specific heat γ_{cm} with the electron-magnetic Gruneisen parameter (Γ_G^{cm}), magnon Gruneisen parameter (Γ_G^{mag}) and vibrational Gruneisen parameter (Γ_G^{ph}) of Fe$_{3-x}$Mn$_x$Al alloys

5.2.4 Calculation of Vibrational, Electron-Magnetic and Magnon Contributions to Entropy

From the fitted parameter values the lattice and magnetic contributions **to** the entropy are calculated and plotted in Figs.5.10 and 5.11. The vibrational contribution to the entropy is estimated from the vibrational contribution to the specific-heat which is first calculated from the fitted parameter values using eqn.(3.18). Fig.5.10 shows the variation of S_{ph} with temperature for different x. Even the values of S_{ph} decreases with Mn concentration the difference is not much among Fe_3Al, $Fe_{2.7}Mn_{0.3}Al$ and $Fe_{2.1}Mn_{0.9}Al$ alloys. But for the $Fe_{1.8}Mn_{1.2}Al$ alloy it has reduced by quite a large amount. In between the ferromagnetic and the **paramagnetic** regions of $Fe_{1.8}Mn_{1.2}Al$ alloy there is no observable change in the vibrational contribution to entropy as the major part comes from Θ_D which is same for both the regions. The values of the vibrational Gruneisen constants for different x are calculated from the vibrational contributions to thermal expansion and specific heat and are given in Table-5.4.

The electron-magnetic contributions to the entropy S_{em} are calculated using the eqn.(3.70) and are plotted in Fig.5.11a for different x. As shown in the plot there is a slight increase in the values of S_{em} with Mn concentration, but the increase is not much. In Fig.5.11b we have plotted the magnon contributions to the entropy, calculated using the eqn.(3.81) for different x. The value of S_{mag} shows a increase with the addition of Mn.
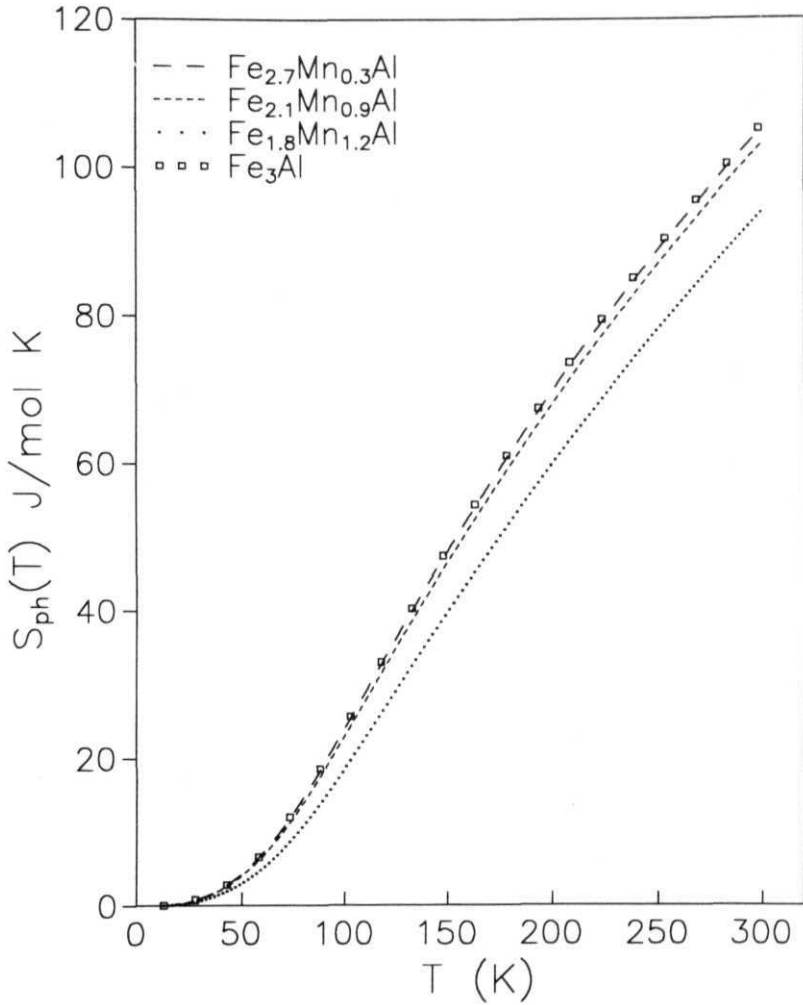
Fig.5.10 : Vibrational entropy with temperature for $Fe_{3-x}Mn_xAl$ Alloys.
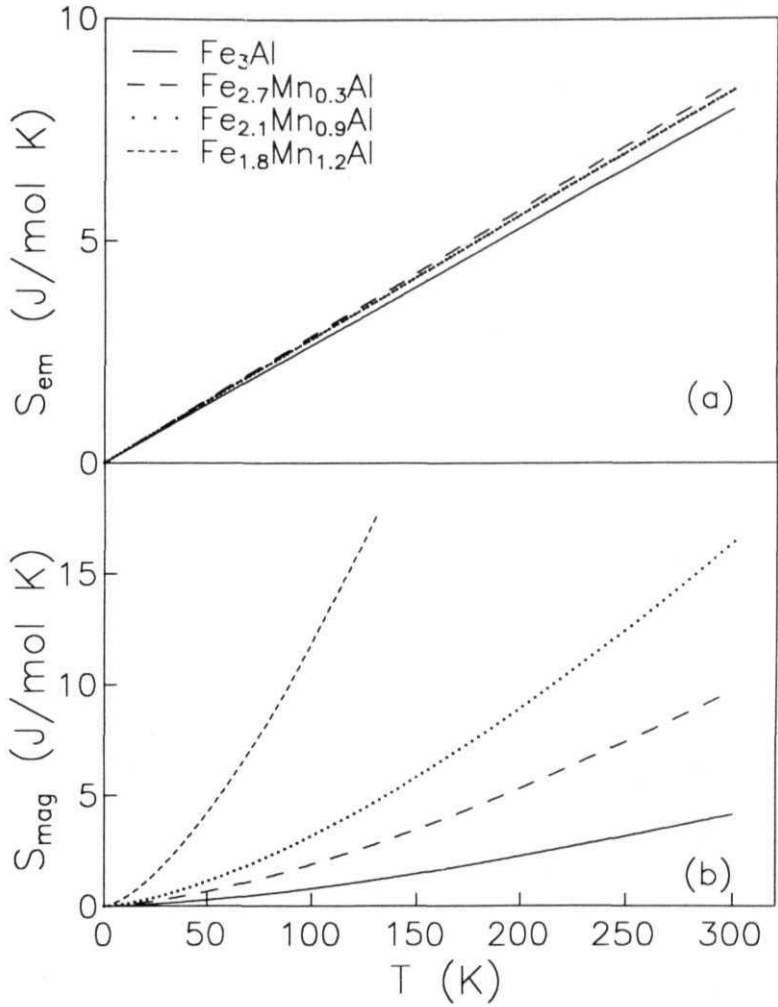
Fig.5.11 : (a) Electron-magnetic and (b) magnon contributions to entropy of $Fe_{3-x}Mn_xAl$ alloys.

5.3 Conclusion

We have taken two binary alloy systems Fe_3Si and Fe_3Al and have substituted Mn in them for a wide concentration range to study the behaviour of thermal expansion. For $x = 1.2$, 1.5 in $Fe_{3-x}Mn_xSi$ alloy and $x — 1.2$ in $Fe_{3-x}Mn_xAl$ alloy the thermal expansion coefficient data have shown clear transitions at T_c with a slope change in the data of $\Delta L/L$. The analysis gives an increase in the Debye temperature values with Mn addition in both the systems. The electron-magnetic contributions to the thermal expansion coefficient α_{em} and the entropy S_{em} increase with Mn addition showing a decrease in the itinerant character. The magnon contribution to the thermal expaasion coefficient α_{mag} however show a decrease with Mn concentration.

References

[1] **J.T.T.** Kumaran and C. Bansal, Solid State Commun. 69, 779, (1989); 74, 1125 (1990).

[2] A. Chkravarti, R. Ranganathan, A.K. Raychaudhuri, **J.T.T.** Kumaran and C. Bansal, Solid State Cornmun. 77, 17 (1991).

[3] N. Niculescu and J.I. Budnik, Solid State Commun. 24, 631 (1977).

[4] E.J.D. Garba and R. Jacobs, J. Phys. F : Met. Phys. 16. 1485 (1986).

[5] S. Yoon and J.G. Booth. Phys. Lett. **A48.** 381 (1974).

[6] A. Paoletti and L. Passari, Nuovo Cem. 32. 1450 (1964).

[7] J. Moss and P.J. Brown. J. Phys. F 2, 358 (1972).

[8] K.P. Gupta, C.H. Cheng and P.A. Beck, J. Phys. Chern. Solids 25, 1147 (1964).

[9] J.R. Miles, T.F. Smith and T.R. Finlayson, Phil. Mag. 65. 1215 (1992).

[10] T.F. Smith, G.K. **Bristow,** C.V. Boughton and P.R.W. Hudson, J. Phys. F **10,** 2867 (1980).

[11] J.R. Miles, T.F. Smith and T.R. Finlayson, Aast. J. Phys. **41,** 781 (1988).

[12] T.V.S.M. Mohan Babu, C. Bansal and S.N. Kaul. J. Mag. Mag. Mater. **140-144,** 127 (1995).

[13] T.V.S.M. Mohan Babu, Ph.D. Thesis (1995), University of Hyderabad.

[14] A.G.H. Anderson and E.R. Jette, Amer. Soc. Met. 24. 275 (1936).

[15] P.V. Blackenhagen and C. Lin, Physics of Transition Metals, Institute of Physics Conference Sereies, No.55 (Bristol : Inst. of Phys.), p.-371.

[16] F. Tao, Q.W. Yan, Z.G. Shen, P.V. Blakenhagen, H. Lin and C. Lin, Acta Phys. Sinicia 6, 570 (1987).

[17] M. Szymanski, M. Jankowski, A. Dobrzynski, A. Wisniewski and S. Bednarski, J. Phys. C 3, 4005 (1991).

[18] A.C. Switendick. Solid State Commun. 19, **511** (1976).

[19] E.J.D. Garba and R.L. Jacobs, J. Phys. H 16, 1485 (1986).

[20] A.R. Williams, V.L. Moruzzi, CD. Gellat, J. Kubler and K. Schwarz, J. Appl. Phys. **53,** 2109 (1982).

[21] S. Yoon and J.G. Booth, J. Phys. F 7, 1079 (1977).

[22] M. Tuszynski, **W. Zarck** and E.S. Popiel, Hyperfine Interact., **59,** 369 (1990).

[23] A.S. Ilyushin and W.E. Wallace, J. Solid State Chem. 17, 385 (1976).

[24] E. Wieser and S. Mager, Phys. Stat. Sol. (a) 40, 497 (1977).

[25] S. Mager. A. Wieser, T. Zemick. O. Schneeweiss. P.N. Stetsenko and V.V. Surikov, Phys. Stat. Sol. (a) *52,* 249 (1979).

[26] T.V.S.M. Mohan Babu and C. Bansal, Phys. Stat. Sol. (b) **193,** (1996).

[27] S.J. Pickart and R. Nathans, Phys. Rev. **123,** 1163 (1961).

[28] S. Ishida. J. Ishida, S. Asano and J. **Yamashita, J.** Phys. Soc. Japan 41, 1570 (1976).

[29] H. Okamoro and P.A. Beck, Monatsch. Chem. **103**, 907 (1972).

[30] L.F. Lutskaya, Sov. Phys. Solid State 27. 404 (1985).

CHAPTER 6

DETERMINATION OF CONFIGURATIONAL ENTROPY AND STABILITY LIMIT OF A BULK METALLIC GLASS FROM THERMAL EXPANSION MEASUREMENTS

6.1   Introduction

Our understanding of the glass state is still far form complete inspite of the fact that glass making was discovered long ago [1]. A very large number of materials can now be produced in the glassy or amorphous state and the techniques of making them are equally varied e.g., rapid quenching of melt [2-4], vapour deposition on cold substrate [5], electro-deposition [6], electron beam irradiation [7,8]. solid state amorphisation by hydrogen dissolution or thermal interdiffusion of two elemental polycrystalline metals [9,10], high energy mechanical ball milling [11-15], etc. Glasses differ structurally from the crystalline solids in the absence of long range lattice order as shown by X-ray diffraction [16]. Other new and **technologically** important physical properties of glassy materials make them very useful for applications [17].

The conventional root to making a glassy solid by undercooling of melt has been more widely used for a long time and better understood as compared to the other recent methods of solid state amorphisation. Ordinarily a liquid will solidify by the process of nucleation and growth of crystals into a crystalline solid if cooled below the melting temperature and left for sufficient time. The nucleation rate increases with increase in undercooling temperature. However if the liquid is cooled rapidly it can continue to remain in the undercooled state and a configurational freezing of the atomic arrangement of the liquid state takes place at a temperature T_g (which is termed as the Glass transition temperature). because there is not enough time for atomic rearrangements to lead to a crystalline atomic configuration [1,16]. The glass transition temperature however depends a little in the cooling rate but is nevertheless taken to be a well defined transition temperature [1].

Fig.6.1 shows a schematic illustration of the change in thermodynamic variables such as volume (V), entropy (S) or enthalpy (H) across a liquid Co crystal or supercooled liquid to glass transformation [16]. The glass transition is accompanied by a change in slope of these thermodynamic variables and differential quantities such as thermal expansion coefficient (a) and specific heat (C) therefore show a discontinuity at T_g suggesting a second order like behaviour. Without going into less definitive and contentious issues such as whether the glass transition is a truly second order transition because of the kinetic dependence of T_g, or whether the glass state is truly equilibrium thermodynamic state, the glass and the supercooled liquid states are treated on the same footing and a quantitative understanding of the thermodynamic quantities such as free energy and **entropy** difference between supercooled liquid and crystalline states has been made [16]. However very little is said about the thermodynamic functions of the actual glass state itself which is fundamentally different from **the** supercooled liquid phase at least in one aspect viz - the translational degrees of freedom which exist in the liquid phase get. frozen in the glass phase.

6.1.1 **Bulk** Metallic Glass

Metallic alloys require very high quenching rates, of the order of 10^6 K/sec or so, to form glasses. These metallic glasses are very important technologically, as they show high fracture strength, excellent soft magnetic behaviour and good corrosion resistance [18]. But the high quenching rate of the melt for the glass formation, has restricted the physical dimensions of these glasses **to** thin ribbons. During past several years a lot of effort has gone into finding systems from which glasses can can be made in bulk form with ease. Recently it has been possible to obtain metallic
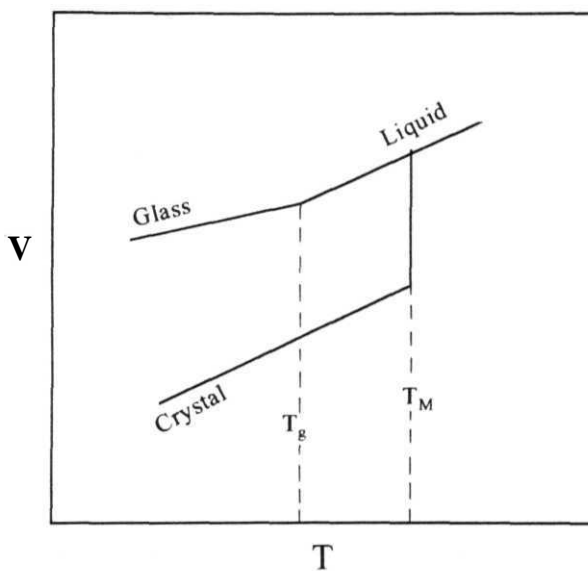
Fig.6.1 : A schematic illustration of the change in volume across a liquid to crystal and supercooled liquid to glass state. A change in slope is seen at the glass transition temperature between the liquid and the glass state and a jump at T_M between the liquid and the crystal.

glasses in some alloy systems such as Zr - Ni - Cu - Al [19], La - Al - Ni [20], $Mg - Cn -$ [21] and $Zr - Ni - Tl - Cu$ [22] Be at low cooling rates. These glasses therefore can be fabricated in bulk dimensions and can also be processed for technological applications as the temperature interval ΔT_x between the glass transition temperature (T_g) and **the** crystallization temperature (T_x) is quite large in these materials. To understand the glass forming ability and their phase stability against crystallization it is essential to have estimates of various thermodynamic parameters. In this work a simple method is used to estimate the configurational **entropy** of glass by calculating its total entropy from thermodynamic considerations and subtracting from it the **vibrational** and electronic entropies obtained from thermal expansion measurements. Gibb's free energy difference between the glassy and **the** crystalline states has been calculated, which gives a measure of the thermal stability of the glass state. Here, a bulk metallic glass of composition $Zr_{65}Ni_{10}Cu_5Al_{7.5}$ is used which has a high AT, value (= 112 K) to calculate **the** vibrational, electronic and configurational entropies **in** the glassy as well as crystalline states.

6.2   Sample preparation

The samples were prepared by arc melting requisite quantities of Hafnium free Zr (99.5% purity) and high purity Cu, Ni and Al in an Edmund **Bühler** D-7400 arc melting furnace under a Ti gettered argon atmosphere. There was negligible weight loss after melting. The alloy ingot was cut into small pieces and transferred to a Vycor glass tube of 7 mm inner diameter constricted to 4 mm diameter at one end. After induction melting the melt was injected into copper moulds by application of slight gas pressure from the other end of the Vycor tube. Rectangular blocks of

dimensions 22.5 x 5 x 3 mm^3 **were** cast **by** this procedure. The surface of **the** moulded sample was polished to remove the crystallized **phase** which formed **in** contact with the copper mould. The bulk sample obtained was amorphous as confirmed by the X-ray diffraction pattern recorded with Inel position sensitive detector using $Co\ K_\alpha$ radiation (A = 0.1790 nm) (see Fig.G.2).

Fig.6.3 shows **the** Differential Scanning **Calorimetry** (DSC) measurements on the sample. The DSC measurement has been done **with** a heating rate of 10 C per minute. The glass **transition** temperature T_g came out **to** be 624 K (see the inset (a) of **Fig**.6.3) which compares well with the value of T_G = 623 K for the sample of same composition given in literature [19]. The crystallization temperature came out to be T_X = 736 K (inset (b) of Fig.6.3).

6.3   Thermal Expansion Measurements

A sample of cuboid shape and dimensions 3 x 2.5 • 1.2 mm^3 was cut from the main block for thermal expansion measurements. The sample was cut carefully to have parallel faces. The faces were polished to have a smooth surface. The thermal expansion measurements were carried out using the three terminal capacitance dilatometer as described in Chapter 2. The sample temperature was scanned at the rate of 2 mK/sec and the capacitance values were recorded at intervals of 4 sec. An average of fifty readings was taken to get the **observations** at 0.4 K intervals. The glass sample was then crystallized by heat treating it at 873 K for a period of 24 hrs and thermal expansion measurements were carried out on the crystallized sample.

Fig.6.4 shows the fractional length change $\Delta L(T)/L(T_0)$ data as a function of
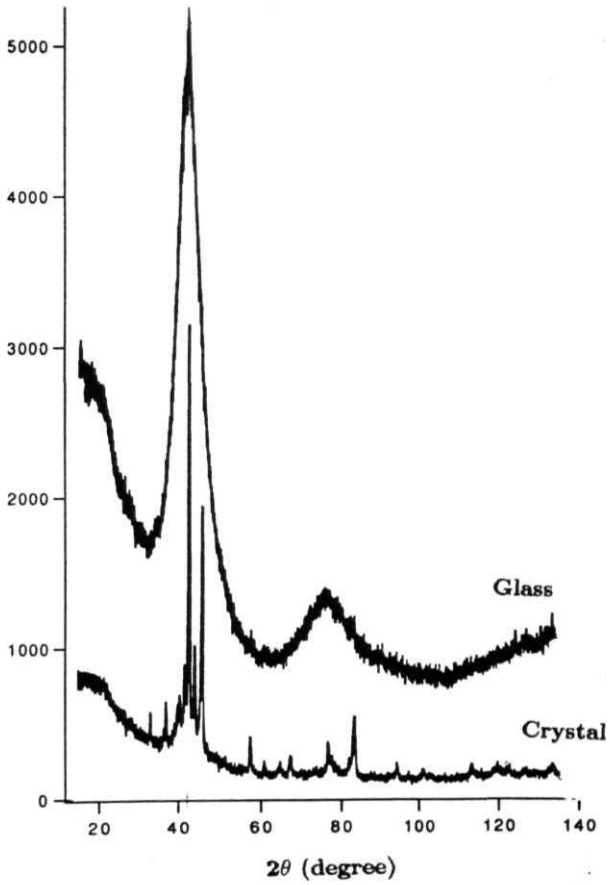
Fig.6.2 : The X-ray diffraction patterns of $Zr_{65}Ni_{10}Cu_{17.5}Al_{7.5}$ bulk metallic glass (G) and of its crystalline state (X) recorded with Inel position sensitive detector using Co K_α radiation.

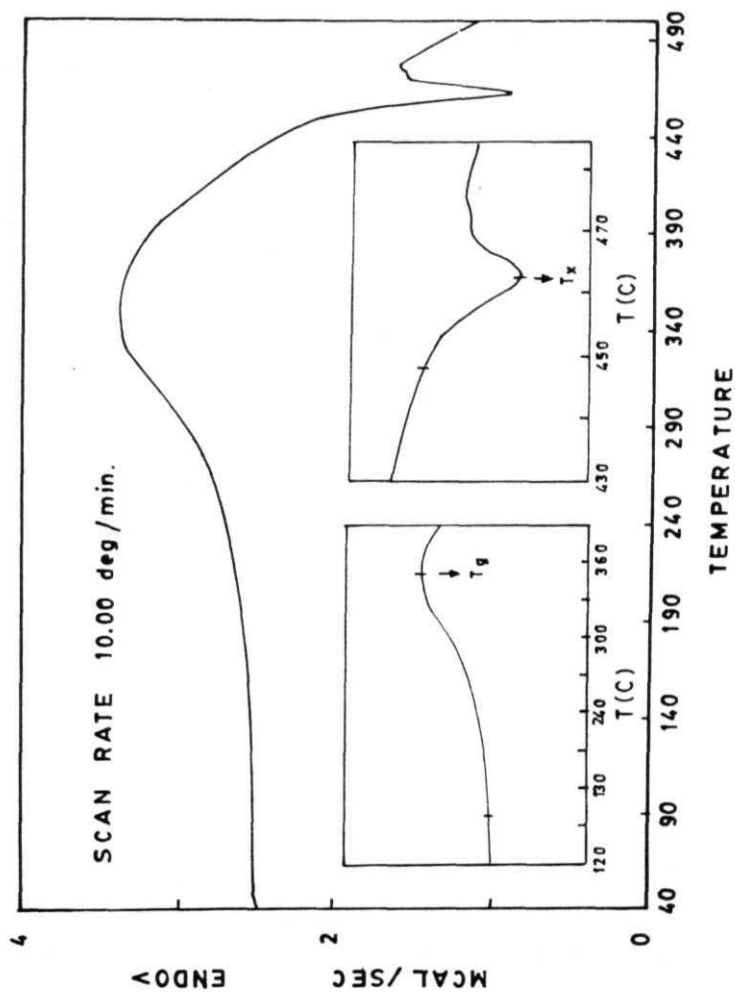**Fig.6.3 :** Differential Scanning Calorimetry measurements with a heating rate of 10 degree celcius per minute on $Zr_{65}Ni_{10}Cu_{17.5}Al_{7.5}$ bulk metallic glass. Insets (a) and (b) show the values of T_g and T_X respectively.

temperature in both glassy and crystalline phases. In the figure every fifth data point is plotted for better clarity. Fig.6.5 shows the variation of thermal expansion co-efficient $\left(\alpha(T) = \frac{\Delta l}{\Delta T} \frac{1}{L(T_0)}\right)$ as a function of temperature as obtained directly from the measured fractional length change data by numerical three point differentiation. As expected the thermal expansion of glass shows less change with temperature than that of the crystal.

6.4 Data Analysis

The fractional length change data is analyzed using the anharmonic model described in Chapter 3. The $\Delta L(T)/L(T_0)$ data is fitted to the expression

$$\frac{\Delta L(T)}{L(T_0)} = \frac{\langle x \rangle_T - \langle x \rangle_{T_0}}{a(T_0)} \tag{6.1}$$

where $\langle x \rangle_T$ is the average lattice displacement at temperature T which is given by the expressions (3.4). (3.14) and (3.24) and reproduced here for continuity,

$$\langle x \rangle_T = a(T_0)\frac{\gamma_{el}}{2}T^2 + \frac{3g}{4c^2}\left\{\varepsilon - \left(\frac{15g^2}{16c^3} - \frac{8f}{c^2}\right)\varepsilon^2 - \frac{35}{16}\left(\frac{15}{4}\frac{g^2 f}{c^5} + \frac{3f^2}{c^4}\right)\varepsilon^3\right\} \tag{6.2}$$

$$\varepsilon = \left\{\left(\frac{3}{p}\right)3k_B T\left(\frac{T}{\Theta_D}\right)^3 \int_{D}^{\Theta_D} \frac{z^3 dz}{e^z - 1} + \left(\frac{p-3}{p}\right)\frac{k_B \Theta_E}{e^{\Theta_E/T} - 1}\right\}$$

γ_{el} gives a measure of the electronic contribution to the lattice displacement. Θ_D and Θ_E are respectively the Debye and Einstein temperatures and p is the average number of phonon branches actually excited over the entire range of temperature.

The fitting of the experimental data was done using $\gamma_{el}, g' = g/c^2$ and $g'' = g^2/c^3$. $f - f/c^2, \Theta_D, p$ and Θ_E as parameters. The solid lines in figs.6.4 and 6.5 show
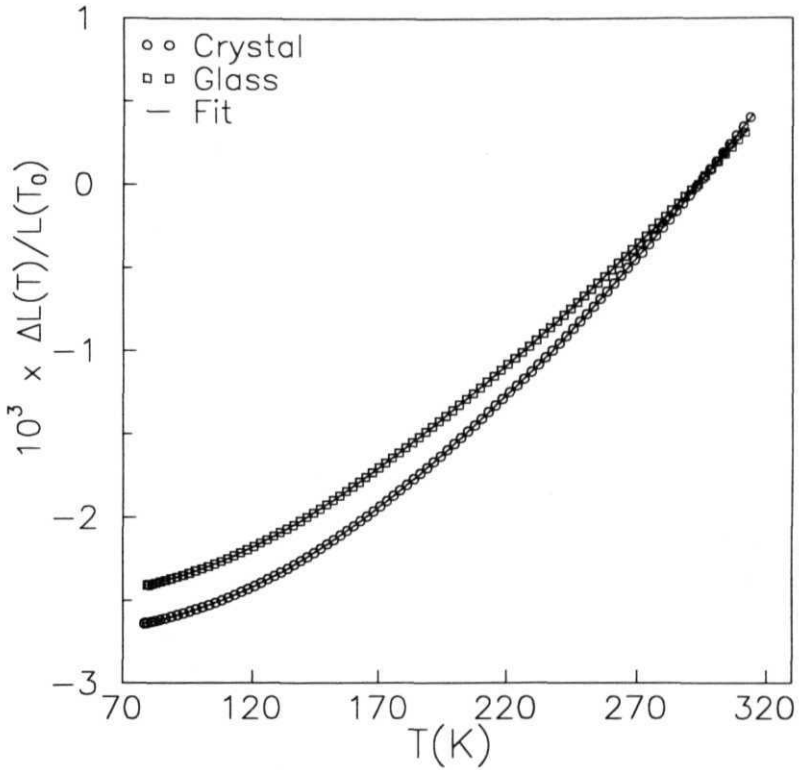
Fig.6.4 : Fractional length change data as a function of temperature for the crystalline and the glassy $Zr_{65}Ni_{10}Cu_{17.5}Al_{7.5}$ alloy. The solid line represents the fits to the data using eqns.(6.1) and (6.2)
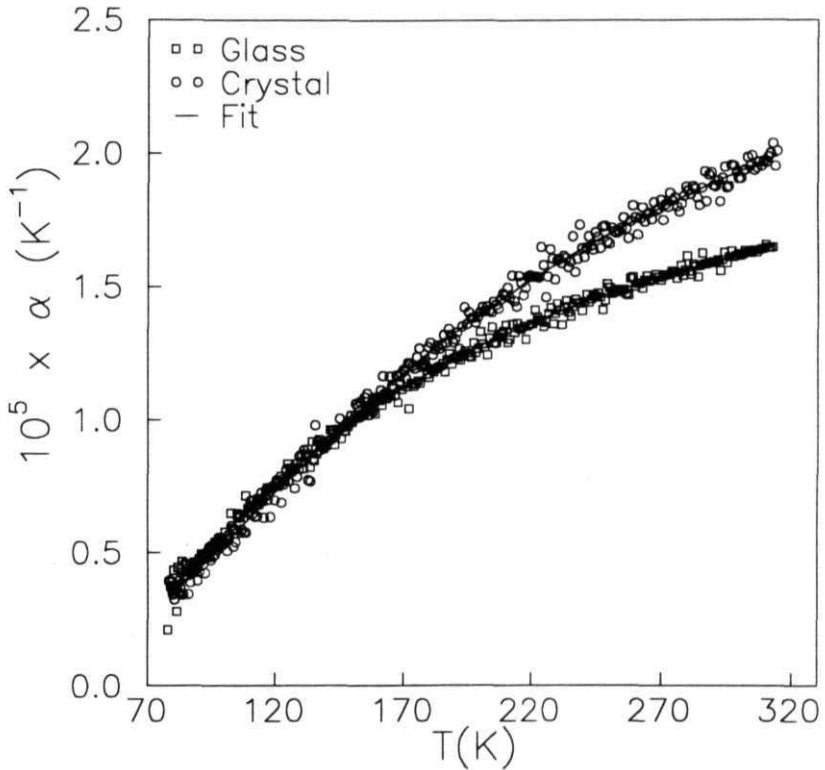
Fig.6.5 : Measured thermal expansion coefficient (a) data as a function of temperature for the crystalline and the glassy $Zr_{65}Ni_{10}Cu_{17.5}Al_{7.5}$ alloy. The solid line shows the analytic derivative of eqn.(6.1).

the fits. The fits in both **the** glass and crystalline phases are excellent with a r.m.s. deviation is of about 0.2%. Table-6.1 shows the values of the fitted parameters.

The anharmonicity parameters g'' and $/'$ have increased by quite large amount in the glass phase as compared to the crystal phase. The large increase in the quartic anharmonicity parameter $/'$ shows softening of lattice in the glass and suggests that the lattice potential becomes more shallow as compared to the crystal phase. The glass phase does not show any optic mode whereas the crystal phase gives an average of 7.5 optic modes with an Einstein temperature of 494.7 K which is lower than the Debye temperature 582.0 K. The value of electronic parameter γ in **the** crystal phase is twice that of **the** glass phase.

A check on the consistency of the parameters obtained for the fits to thermal expansion data can be made by calculating the total specific heat (vibrational+electronic) and comparing with experimental results on specific heats of the system. This consistency is shown in the next section.

6.5   Calculation of Specific Heat

As described in the chapter 3, the vibrational specific heat C_{ph} is calculated using the relation [23] (see also eqn.(3.18))

$$C_{ph} = 3N\varepsilon' - 6N \left(\frac{15}{8} \frac{g^2}{c^3} - \frac{3}{4} \frac{f}{c^2} \right) \varepsilon \times \varepsilon' \tag{6.3}$$

where,

$$\varepsilon' = \left\{ \left(\frac{3}{p} \right) 3k_B \left(\frac{T}{\Theta_D} \right)^3 \int_0^{\frac{\Theta_D}{T}} \frac{z^4 e^z}{(e^z - 1)^2} dz + \left(\frac{p-3}{p} \right) k_B \left(\frac{\Theta_E}{T} \right)^2 \frac{e^{\frac{\Theta_E}{T}}}{(e^{\frac{\Theta_E}{T}} - 1)^2} \right\} \tag{6.4}$$

Sample	Glass	Crystal
Θ_D (K)	562.3+08	582.6+07
g' (eV)	0239+0 008	0 251±0.007
g″ (eV^{-1})	(165.531±0.8)×10^{-3}	(2.972±0.06)×10^{-3}
f (eV^1)	(207.833±0.8)×10^{-4}	(3.488±0.06)×10^{-4}
γ_{el} (K^{-2})	(4 686±0.06)×10^{-9}	(8.987±0.07)×10^{-9}
p	3.	10.5±0.03
Θ_f (K)	-	**494.7±0.3**

Table-6.1 : The characteristic Debye and Einstein temperatures and the anharmonicity parameters obtained from the fit of the fractional length change data in both the glassy and crystalline states

and N is the Avogadro number. Fig.6.6 shows C_{ph} for **both** the glass and the crystal phases, calculated using the fitted parameters p, Θ_D, Θ_E, g'' and $/'$. As expected C_{ph} for the glassy phase is more than the crystalline phase.

The electronic specific heat is calculated using the relation [24],

$$C_{el} = \frac{3B_T V \gamma_{el}}{\Gamma_G^{el}} T \tag{6.5}$$

Where B_T is the isothermal bulk modulus. V is the molar volume, and Γ_G^{el} is **the** electronic **Grüneisen** parameter. The experimental values of the Young's modulus of $Zr_{65}Ni_{10}Cu_{12.5}Al_5$ alloy in the glassy and the crystalline phases are measured to be 72 GPa and 117 GPa [25] respectively. By taking a weighted average of the Poisson's ratio for this material, which come out to be 0.36, the bulk modulii are calculated. The bulk modulii B_T are estimated to be 85.7 GPa and 139.3 GPa **in** glassy and crystalline phases respectively. The molar volume of the above alloy in the glassy phase is measured to be 11.79 cc whereas it is 12.07 cc for the crystalline phase. Using the above mentioned experimental values of B_T and V and taking the electronic Grüneisen parameter as 2/3 which is the free electron value, the C_{el} is calculated for both the states. The total specific heat $(C_{el} + C_{ph})$ calculated using the parameters obtained from **our** thermal expansion data compares very well (within 6%) with the experimental specific heat as a reported by Zhang et. al. [19] in the temperature range 400 K to 620 K (see Fig.6.7). This gives confidence in our method of calculating the vibrational and electronic entropies. Next we find the total entropy difference between glass and crystalline states from thermodynamic consideration and subtract from it the vibrational and electronic entropy to get the configurational entropy.
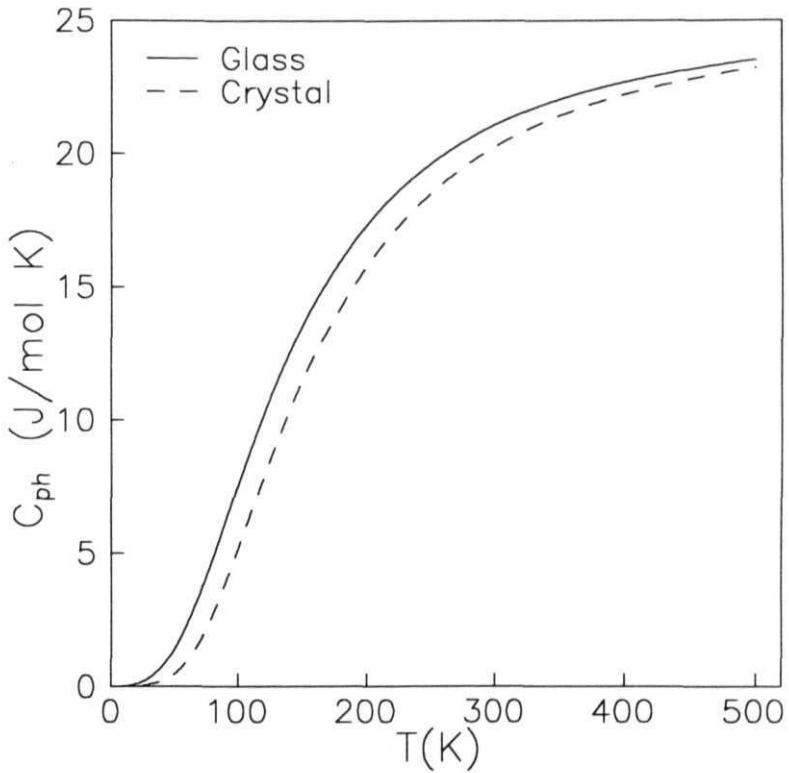
Fig.6.6 : Vibrational contribution to specific heat calculated using the fitted parameter values for the crystalline and the glassy $Zr_{65}Ni_{10}Cu_{17.5}Al_{7.5}$ alloy.
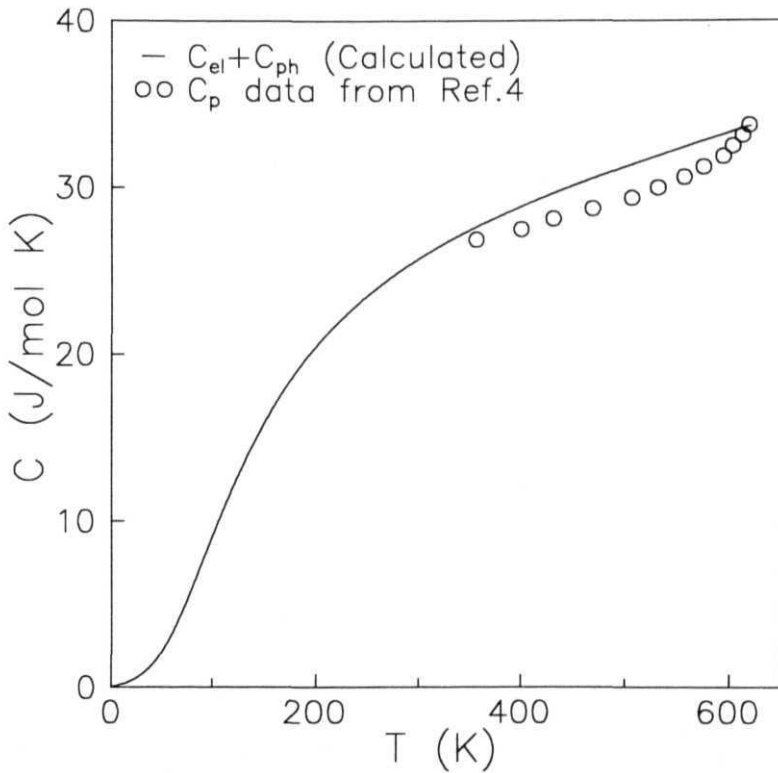
Fig.6.7 : Total specific heat (C = C_{el} + C_{ph}) of the glass calculated using the parameters obtained from our thermal expansion data fitting compared with the specific heat data of Zhang et.al. taken from ref.19.

6.6   Estimation of Thermodynamic Parameters

6.6.1   Supercooled Liquid State

From Fig.6.8 the entropy difference between the supercooled liquid and the crystal at a temperature $T < T_M$ is given by

$$\Delta S^{LX}(T) = \Delta S_M + \int_{T_M}^{T} \frac{\Delta C_P^{LX}}{T} dT \qquad (6.6)$$

Where $\Delta S^{LX}(T)$ is the entropy difference between the supercooled liquid and crystal at any temperature T, ΔS_M is the entropy of fusion at the melting temperature T_M and ΔC_P^{LX} is the specific heat difference between the supercooled liquid and the crystal.

The enthalpy difference between the supercooled liquid and the crystal (ΔH) can be calculated as follows.

$$
\begin{aligned}
\Delta H^{LX} &= \int_{T,X}^{T,L} dQ = \int_{T}^{T_M} C_p^X dT + \int_{T_M,X}^{T_M,L} dQ + \int_{T_M}^{T} C_p^L dT \\
&= -\int_{T_M}^{T} C_p^X dT + T_M \Delta S_M + \int_{T_M}^{T} C_p^L dT \\
&= T_M \Delta S_M + \int_{T_M}^{T} \Delta C_p^{LX} dT \qquad (6.7)
\end{aligned}
$$

The Gibbs free energy difference. ΔG^{LX} being the driving force for crystallization. which measures the ability for glass formation is calculated as,

$$\Delta G^{LX}(T) = T_M \Delta S_M + \int_{T_M}^{T} \Delta C_P^{LX} dT - T\Delta S_M - T\int_{T_M}^{T} \frac{\Delta C_P^{LX}}{T} dT \qquad (6.6)$$

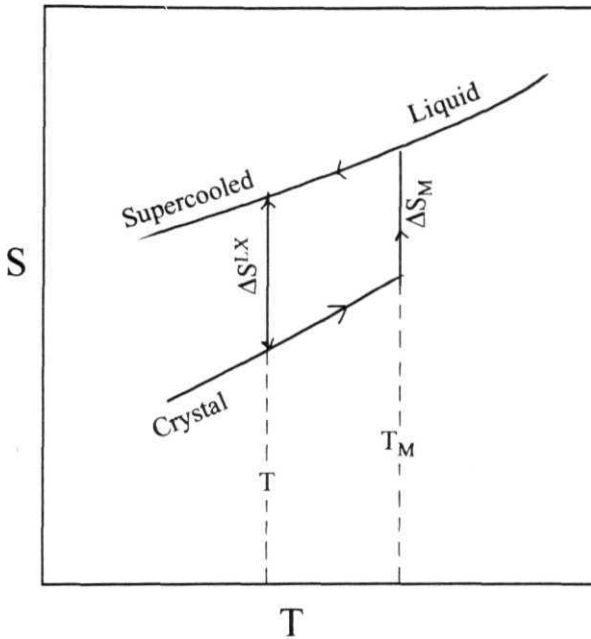The entropy of fusion ΔS_M can be calculated as [26],

Fig.6.8 : A schematic illustration for the calculation of the entropy difference (ΔS^{LX}) between the supercooled liquid and cystal states. Arrow heads indicating the path to be followed

$$\int_0^{T_M} C_P^L dT - \int_0^{T_M} C_P^X dT = T_M \Delta S_M \qquad (6.9)$$

or,

$$\int_0^{T_M} \Delta C_p^{LX} dT = T_M \Delta S_M \qquad (6.10)$$

Now if one assumes ΔC_P^{LX} is constant upto a **temperature** which is not much below T_M then, eqn.(6.10) can be written as.

$$T_M \; \Delta C_P^{LX} \; = T_M \Delta S_M \qquad \textbf{(6.11)}$$

or,

$$\Delta C_P^{LX} \; = \Delta S_M \qquad \textbf{(6.12)}$$

By substituting the value for ΔC_P^{LX} in the expressions for $\Delta S^{LX}(T) \Delta H^{LX}(T)$ and $\Delta G^{LX}(T)$ the eqns.(6.6),(6.7) and (6.8) can be approximated as,

$$\Delta S^{LX}(T) \;=\; \Delta S_M - \Delta S_M ln\left(\frac{T_M}{T}\right) \quad . \qquad \textbf{(6.13)}$$

$$\Delta H^{LX}(T) \;=\; T \Delta S_M \quad . \qquad (6.14)$$

$$\Delta G^{LX}(T) \;=\; T \Delta S_M ln\left(\frac{T_M}{T}\right) \quad . \qquad (6.15)$$

6.6.2 Glass State

To reach the glass state one goes to temperature $T < T_g$ as shown in **Fig.6**.9 The entropy difference between glass and crystal, $\Delta S^{GX}(T)$ at a temperature $T < T_g$
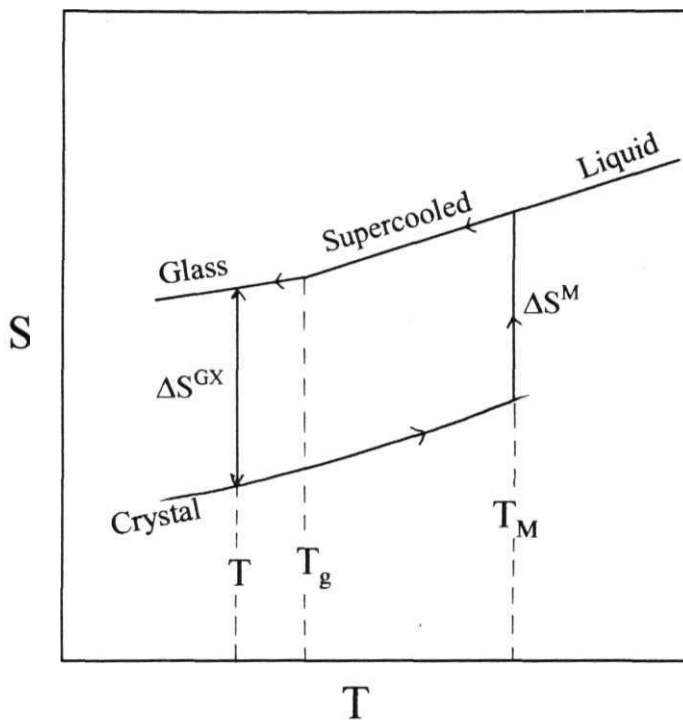
Fig.6.9 : A schematic illustration of entropy in the supercooled liquid, glass and the crystal states of the same material. The arrow heads indicate the path to be followed for the calculation of $\Delta S^{GX}(T)$.

can be calculated as,

$$\Delta S^{GX}(T) = \int\limits_{T,X}^{T,G} dS = \int\limits_{T,X}^{T_M} \frac{C_P^X}{T} dT + \int\limits_{T_M,X}^{T_M,L} dS + \int\limits_{T_M}^{T_g} \frac{C_P^L}{T} dT + \int\limits_{T_g}^{T,G} \frac{C_P^G}{T} dT$$

$$= \int\limits_{T}^{T_g} \frac{C_P^X}{T} dT + \int\limits_{T_g}^{T_M} \frac{C_P^X}{T} dT + \Delta S_M + \int\limits_{T_M}^{T_g} \frac{C_P^L}{T} dT + \int\limits_{T_g}^{T} \frac{C_P^G}{T} dT$$

$$= \Delta S_M + \left(\int\limits_{T_g}^{T} \frac{C_P^G}{T} dT - \int\limits_{T_g}^{T} \frac{C_P^X}{T} dT \right) + \left(\int\limits_{T_M}^{T_g} \frac{C_P^L}{T} dT - \int\limits_{T_M}^{T_g} \frac{C_P^X}{T} dT \right)$$

$$= \Delta S_M + \int\limits_{T_g}^{T} \frac{C_P^G - C_P^X}{T} dT + \int\limits_{T_M}^{T_g} \frac{\Delta C_P^{LX}}{T} dT \tag{6.16}$$

If we take a temperature near T_g, when Cp can be approximated as. $Cp = Cp - \Delta C_P^{LG}$, where ΔC_P^{LG} is the specific heat jump at T_g when **the** supercooled liquid freezes into a glass. Then by rewriting the equation (6.16) as.

$$\Delta S^{GX}(T) = \Delta S_M + \int\limits_{T_M}^{T_g} \frac{\Delta C_P^{LX}}{T} dT + \int\limits_{T_g}^{T} \frac{C_P^L - \Delta C_P^{LG} - C_P^X}{T} dT$$

$$= \Delta S_M + \int\limits_{T_M}^{T_g} \frac{\Delta C_P^{LX}}{T} dT + \int\limits_{T_g}^{T} \frac{\Delta C_P^{LX}}{T} dT - \int\limits_{T_g}^{T} \frac{\Delta C_P^{LG}}{T} dT \tag{6.17}$$

Now substituting for $\Delta C_P^{LX} = \Delta S_M$ and taking ΔC_P^{LG} as the jump at T_g and assuming that T is not much below T_g,

$$\Delta S^{GX}(T) = \Delta S_M - \Delta C_P^{LX} \ln\left(\frac{T_M}{T}\right) + \Delta C_P^{LG} \ln\left(\frac{T_g}{T}\right) \tag{6.18}$$

Similarly the enthalpy difference between the glass and the crystal can be written' as,

$$\Delta H^{GX}(T) = T_M \Delta S_M - \Delta C_P^{LX}(T_M - T) + \Delta C_P^{LG}(T_g - T)$$

or

$$\Delta H^{GX}(T) \;=\; T\Delta S_M + (T_g - T)\Delta C_P^{LG} \tag{6.19}$$

So the Gibb's free energy difference (ΔG^{GX}) between the glass and the crystal which shows the stability of the glass can be estimated as,

$$\Delta G^{GX}(T) = \Delta H^{GX}(T) - T\Delta S^{GX}(T) \tag{6.20}$$

6.7 Estimation of Configurational Entropy of the Glass

The vibrational and the electronic entropies $(S_{ph}$ and $S_{el})$ of the glassy and the crystalline forms of the sample are calculated using the relation,

$$S_{ph} = \int_0^T \frac{C_{ph,el}}{T} dT \tag{6.21}$$

Assuming the crystal does not have any configurational entropy, the total entropy of the crystalline sample can be given by,

$$S^X = S_{ph}^X + S_{el}^X \tag{6.22}$$

The total entropy of the glassy alloy can be written as,

$$S^G = S_{ph}^G + S_{el}^G + S_{config}^G = S^X + \Delta S^{GX} \tag{6.23}$$

Where S_{config}^G is the configurational entropy of the glass and the expression for ΔS^{GX} is given by equation (6.18).

For the present Zr - Ni - Cu — Al sample the total crystalline entropy is calculated using the eqn.(6.22). Then for estimating total entropy of glass S^G, eqn.(6.23)

is used by taking the value of ΔS^{GX} which is estimated using eqn.(6.18). Similarly the total entropy for the supercooled liquid state is estimated by adding $\Delta S^{L\lambda}$ (calculated using eqn.(6.13)) to S^X. Fig.6.10 shows **the** temperature dependance of S^G, S^L and S^X. As expected the supercooled liquid freezes into glass at $T_g(=624$ K) where the entropy curve shows a slope change indicating a second-order phase transition-like behaviour. The Kauzman temperature [27] T_i^{LX} calculated from the insentropic condition $\Delta S^{LX} = 0$ is found to be T_M/e, where e is the base of the Naperian logarithm.

The vibrational entropy (S_{ph}^G) and the electronic entropy (S_{el}^G) are calculated from C_{ph}^G and C_{el}^G respectively. The vibrational and electronic specific heat is calculated from the fitted parameters obtained from the fit of the thermal expansion data of the bulk metallic glass. The configurational entropy $(S_{con,f}^G)$ of the glass then is estimated by subtracting $(S_{ph}^G + S_{el}^G)$ from S^G. The temperature dependance of S_{config}^G together with S_{ph}^G and S_{el}^G is given in the inset of fig.6.10. The magnitude of the configurational entropy of the bulk metallic glass in a small temperature range below T_G comes out to be 17 J/mol K. The configurational entropy of an ideal solid solution with n-components can be calculated as [28],

$$S_{config} = -R \sum_{i=1}^{n} X_i ln X_i \tag{6.24}$$

where X_i is the concentration of the ith component. The configurational entropy of the ideal solid solution of the composition $Zr_{65}Ni_{10}Cu_5Al_{7.5}$ is calculated as 8.45 J/mol K which is half of the estimated configurational entropy of the glass.

Another interesting result which comes out from this analysis is that one can define a new instability temperature T_i^{GX} from the isentropic condition, $\Delta S^{GX} = 0$ which gives the limiting temperature upto which a glass could be superheated
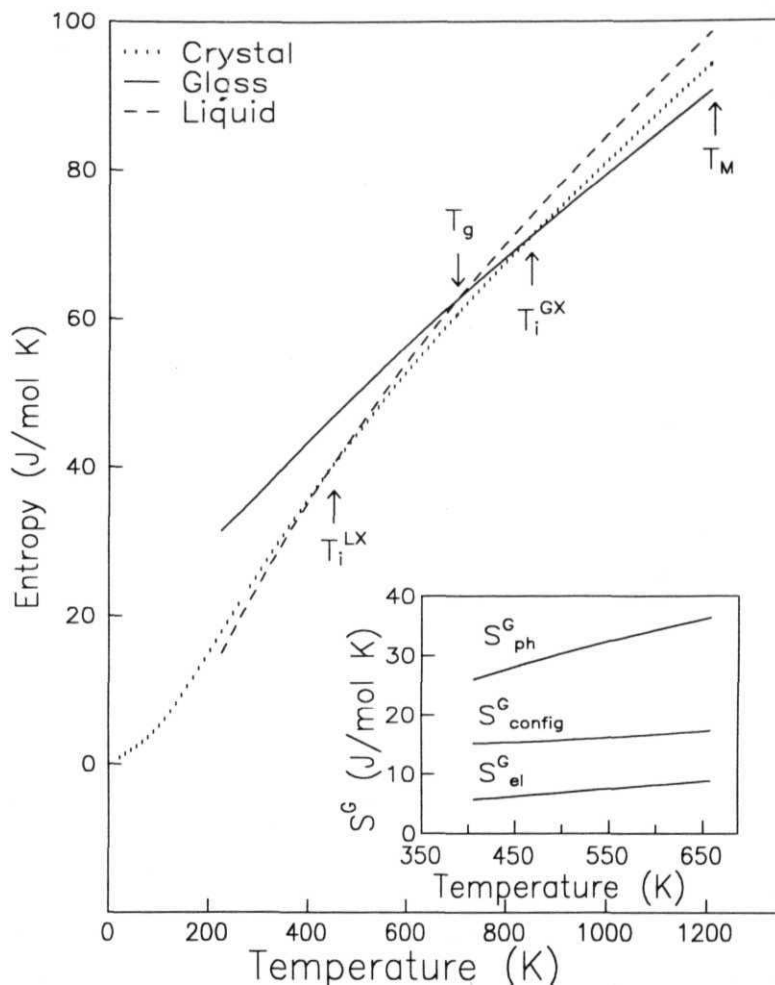
Fig.6.10 : Total entropy of the crystalline, glassy and the supercooled liquid phases of the bulk metallic glass $Zr_{65}Ni_{10}Cu_{17.5}Al_{7.5}$as a function of temperature. The curve for the glass phase between T_g and T_i^{GX} represents the superheated region. The electronic, vibrational and configurational entropy contributions of the glass are shown in the inset.

without being allowed to go into the liquid **phase.** For the bulk metallic glass used in this work, T_l^{gx} is found out to be 730 K (see Fig.6.10). A similar isentropic instability temperature for a superheated crystal was defined by Fecht and Johnson [29].

The enthalpy differences ΔH^{LX} and ΔH^{GX} are obtained using the eqns.(6.14) and (6.19). the Gibb's fee energy differences ΔG^{LX} and ΔG^{GX} are calculated using eqns(6.15) and (6.20) as a function of temperature and are plotted in Fig.6.11. One see's that ΔG^{LX} and ΔG^{GX} touch each other at T_g. At a undercooling of 100 K below T_M, ΔG^{LX}— 377.9 J/molwhich gives a very small driving force for crystallization indicating a good glass forming ability of these glasses. Similarly the excess Gibb's free energy ΔG^{GX} of the superheated glass relative to the corresponding crystalline form at a temperature 100 K above T_g is found to be 1.24 KJ/mol which gives a measure of the stability of the glassy phase.

6.8 Conclusion

The thermal expansion co-efficient around room temperature is found out to be less in the case of the bulk metallic glass $Zr_{65}Ni_{10}Cu_{15}Al_{7.5}$ than that in the corresponding crystalline phase. From the fit to **our** model the Debye temperatures are found out to be 562.3 K and 582.6 K for the glassy and crystalline states respectively. The glassy phase does not show any optic mode whereas the crystalline phase gives an Einstein temperature $\Theta_E = 494.7$ K with 10.5 as the average number of total excited modes (acoustic and optic). The total entropies S^X, S^L and S^G are calculated. The configurational entropy of the glass is found out to be 17 J/mol K just below T_g. A new isentropic temperature T_i^{Gx}— $730K$ is predicted upto which
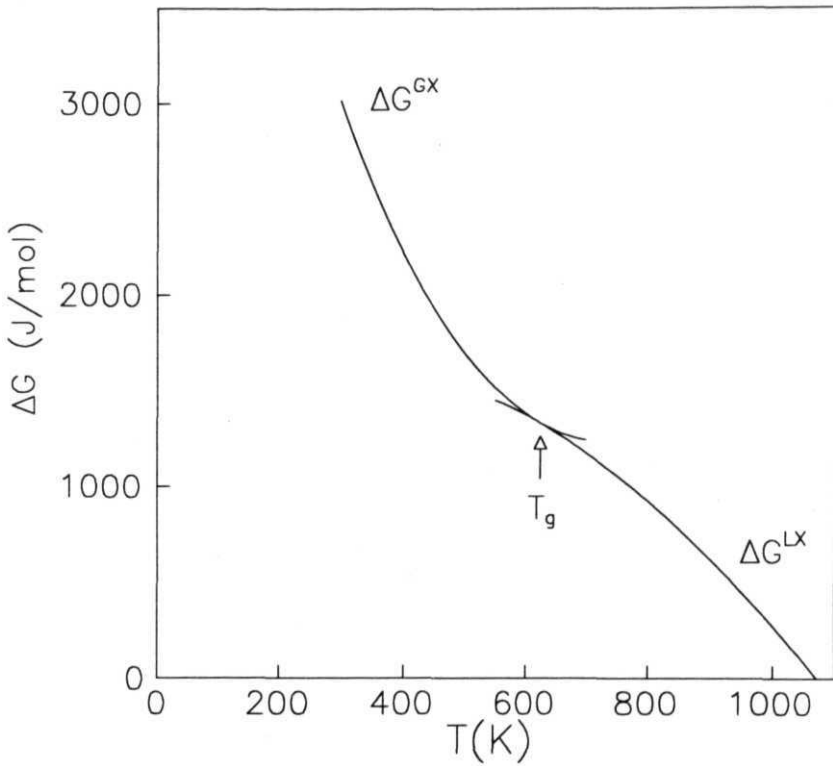
Fig.6.11 : Gibb's free energy differences ΔG^{LX} and ΔG^{GX} as a function of temperature calculated using eqns.(6.15) and (6.20) respectively.

this glass can be superheated. The Gibb's free energy difference between the glass and the crystal is estimated which gives a measure of the stability of **the** glassy state. The driving force ΔG^{LX} for crystallization is calculated to be very small indicating a good glass forming ability of these alloys.

The analysis employed in the present work is quite general and can be applied to other kinds of glasses. Furthermore, the knowledge of the parameters such as the configurational entropy and the Gibb's free energy differences obtained from such studies should also be useful from the point of view of testing various models for glasses.

References

[1] Y.T. Cheng and W.L. Johnson, Science **235,** 997 (1987).

[2] P. Duwez, **R.H. Wilens** and W. Klement, J. Appl. Phys. Lett. 31. 1136 (1960).

[3] P.L. Liu. R. Yen, N. Bloembergen and R.T. Hodgson, Appl. Phys. Lett 34. 864 (1979).

[4] R. Tsu, R.T. Hodgson. T.Y. Yen and J.E.E. Baglin, Phys. Rev. Lett. 42. 1256 (1979).

[5] J. Kramer, Ann. Phys. (Paris) **19,** 37 (1934); Z. Phys. **106,** 675 (1937).

[6] A. Brenner, D.E. Couch and E.K. Williams, J. Res. Natl. Bur. Stand. 44. 109 (1950).

[7] G.J.C Carpenter and E.K. Schulson, J. Nucl. Mater. 23. 180 (1978).

[8] G. Thomas, H. Mori, H. Fujita and R. Sinclair, Scr. Metall. **16,** 589 (1982).

[9] X.L. Yeh. K. Samwer and W.L. Johnson, Appl. Phys. Lett. 42, 242 (1983).

[10] R.B. Schwarz and W.L. Johnson, Phys. Rev. Lett. 51. 415 (1983).

[11] A.Y. Yermakov, Y. Yurchikov and V.A. Varikov, Phys. Met. Metallurg. (Engl. Transl.) **52,** 50 (1981).

[12] C.C. Koch, O.B. Kavin, C.G. Mc Kamey and J.O. Scarbrough, Appl. Phys. Lett. 43, 1017 (1983).

[13] R.B. Schwarz, R.R Petrich and C.K. Saw. J. Non-Cryst. Solids 76, 281 (1985).

[14] C. Politis and W.L. Johnson, J. Appl. Phys. 60, 1147 (1986).

[15] C. Politis, Physica 135B, 286 (1985).

[16] S.R. Elliot. Physics of Amorphous Materials. (Longman, London, 1984).

[17] R. Zallen, The Physics of Amorphous Solids. (John Wiley and Sons, New York, 1983).

[18] H.S. Chen. Rep. Prog. Physics 43, 23 (1983).

[19] T. Zhang, A. Inoue and T. Masumoto, Mater. Trans. JIM **32**, 1005 (1991).

[20] A. Inoue, T. Zhang and T. Masumoto, Mater. Trans. JIM 31, 425 (1990).

[21] A. Inoue, T. Nakamura, N. Nishiyama and T. Mashumoto, Mater. Trans. JIM 33, 937 (1992).

[22] A. Peker and W.L. Johnson. Appl. Phys. Lett. 63. 2342 (1993).

[23] G.D. Mukherjee, C. Bansal and Ashok Chatterjee. Phys. Rev. Lett. 76, 1876 (1996).

[24] T.H.K. Barron, J.G. Collins and G.K. White. Adv. Phys. **29**, 609 (1980).

[25] W.L. Johnson, private communication.

[26] C.V. Thompson and F. Spaepen, Acta. Metall. 27, 1855 (1979).

[27] W. Kauzmann, Chem. Rev. 43, 219 (1948).

[28] D.A. Porter and K.E. Easterling, Phase Transformations in Metals and Alloys.
      2nd edn. (Chapman and Hall, London, 1992).

[29] H.J. Fecht and W.L. Johnson, Nature 334, 50 (1988).

CHAPTER 7

EFFECT OF SUPERCONDUCTING TRANSITION ON
LATTICE ANHARMONICITY IN HIGH T_c
SUPERCONDUCTORS

7.1   Introduction

Since the discovery of superconductivity in mercury by Kamerling Onnes [1] a host of elements, alloys and compounds were found to exhibit superconductivity at low temperatures. But the limited srope of these conventional superconductors for **their** low transition temperature (T_C) initiated the search for compounds with higher T_C's. The discovery of superconductivity at about 35 K in the oxide compound La-Ba-Cu-0 [2] was followed by finding several other oxide systems. Y-Ba-Cu-0 [3,4], Bi-Sr-Ca-Cu-0 [5,6], Tl-Ba-Ca-Cu-O [7,8] and Hg-Ba-Ca-Cu-O [9,10] which have T_C's above the boiling point of liquid nitrogen. These came to be known as high-T_C superconductors. Ever since their discovery, the interesting properties of these materials and the mechanism of superconductivity in them has posed a challenge to the experimentalists as well as to the theoreticians. There have been many models which were proposed to explain various electronic, magnetic and thermal properties of superconductors. For the conventional superconductors the first satisfactory microscopic theory was given by Bardeen, Cooper and Schrieffer (BCS Theory) [11]. They showed that a conduction electron distorts the lattice due to Coulomb interaction and creates a virtual phonon. A second electron with the opposite spin of that of the former one, sees the lattice distortion by absorbing the virtual phonon. Both the electrons develope a weak attractive force through the exchange of the virtual phonon and they form a Cooper pair. These Cooper pairs which are formed due to this electron lattice electron interactions, condense into a state whose ground state energy is much less than the normal ground state energy and is separated from it by a band gap. Even though the BCS theory could explain most of the phenomenon observed in the conventional superconductors, it suggested an

upper limit of 40 K for the T_C of a superconductor. Hence the discovery of high-T_C cuprate superconductors showed the inadequacy of the BCS theory in these materials.

The mechanism responsible for inducing pairing in high-T_c cuprate superconductors continues to be elusive. One of the potential candidates is the electron-phonon interaction which according to one viewpoint [12 — 16] could be effectively large because of the imperfect screening of the coulomb interactions and can thus lead to high T_c. Another viewpoint [17 — 21] is based on the formation of bipolarons which can undergo Bose-Einstein condensation to give rise to superconductivity. There is yet another approach [22,23] which rests on the idea that the large effective coupling constant may have its genesis in the high lattice polarization caused by the lattice anharmonicity. The bipolaronic mechanism might also be intimately connected with this viewpoint.

Experimentally there have been a host of activities in recent years to explore the role of phonons in high T_c materials. A softening of the Raman mode at $335 cm^{-1}$ has been observed [24] at T_c in $YBa_2Cu_3O_{7-\epsilon}$. Ion channeling studies [25] on $YBa_2Cu_3O_{7-\epsilon}$ and $ErBa_2Cu_3O_{7-\epsilon}$ show a phonon anomaly due to the Cu-O atom vibrations. Pulsed neutron diffraction [26] on $Tl_2Ba_2CaCu_2O_8$ and inelastic neutron scattering measurements [27] on $YBa_2Cu_3O_7$ show local structural distortion at T_c in these materials. Polarized EXAFS results [28] show that the relative displacements of the axial oxygen in high T_c materials are not harmonic and change around T_c. $Cu-K$ edge polarized EXAFS data [29] for $YBa_2Cu_3O_7$ show an axial oxygen centered lattice instability at T_c suggesting a coupling between superconducting fluctuations and anharmonic phonons. Neutron resonance absorption spectroscopy [30] for Cu in $Bi_2Sr_2CaCu_2O_8$ indicates a rapid decrease in the kinetic energy slightly

above T_c and detailed neutron scattering measurements [31] for selected phonons **in** $Bi_2Sr_2CaCu_2O_8$ also show considerable anharmonic effects. In our opinion, thermal expansion results should offer more **direct** evidence of the anharmonic effects and therefore we have studied the temperature variation of the thermal expansion data of $YBa_2Cu_3O_{7-}$ (6 m 0.15) (Y-123) and $Bi_{1.6}Pb_{0.4}Sr_2Ca_2Cu_3O_y$ (Bi-2223) over a wide range of temperature both in the normal and superconducting phases. The data of $YBa_2Cu_3O_{7-}$ (δ = 0.15) superconductor have been taken from ref.33. In the case of $Bi_{1.6}Pb_{0.4}Sr_2Ca_2Cu_3O_y$ we have performed the thermal expansion measurements using our three terminal capacitance cell. For both the cases we have done the data analysis using our semiclassical model described in Chapter-3. We find that there is indeed an anomaly in the tliermal expansion behaviour of Y-123 and Bi-2223 superconductors which begins to show up at a temperature somewhat higher than T_c. In the case of Y-123 superconductor we try to attribute this **anomaly** to a lattice instability induced by polaron formation [32]. Bi-2223 superconductor shows an anomaly in the vibrational contribution to thermal expansion **at** the superconducting transition temperature and in the superconducting phase the thermal expansion shows the presence of the two dimensional (2D) Gaussian fluctuations near the transition temperature.
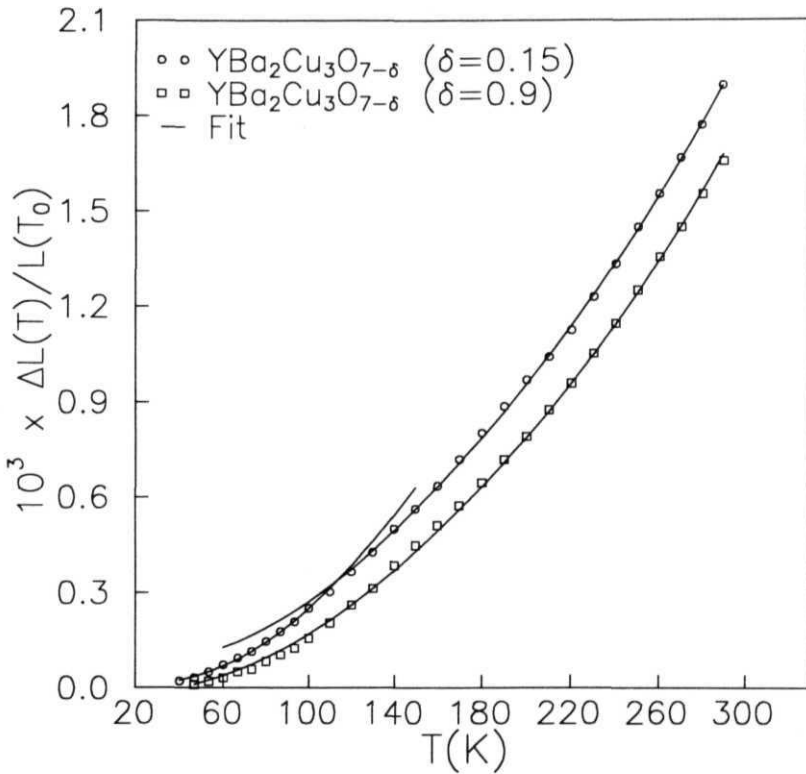
7.2 $YBa_2Cu_3O_{7-\delta}$ Superconductor

7.2.1   Data Fitting and Analysis

The fractional length change data taken from ref.33 are fitted to the eqn.(3.2) with the reference temperature being 20 K and the average lattice displacement $\langle x \rangle_T$ being given by eqn.(3.14) which we reproduce here for the sake of completeness :

where γ_{el} is the linear electronic contribution to the average lattice displacement and e is given by the **eqn.(3.15).** The parameters used were γ_{el}, g', g'', $/'$, Θ_D, p and Θ_E. The fit gives the best results for the average number of phonon modes $p = 3$. Therefore in the final fits we have used only the Debye terms and have removed the Einstein terms from the fitting function. For **superconducting** Y-123 we find, quite interestingly, that it is not possible to fit **the** fractional length change data with a single set of parameters. The r.m.s. deviation for the best fit in this case cames out to be as large as 40 %. However the data could be fitted separately for $T < T_p$ and $T > T_p$ where T_p is around 110 K as shown in the Fig.7.1. Clearly the fits are very good both below and above T_p. In fact the r.m.s. deviations in this case are 5 % below T_p and 2.5 % above T_p. The values of **the** parameters are given in Table.7.1. The value of Θ_D has been obtained from the fit below T_p and is kept fixed at the same value for the fitting above T_p, while other parameters **are** varied. The value of Θ_D obtained from our fit is 418.9 K and it compares quite impressively with the reported value of about 420 K [34.35] in literature. Interestingly enough, for nonsuperconducting $YBa_2Cu_3O_{7\ell}$ ($\delta = 0.9$) [33] the data could, however, be fitted to our model for the entire temperature range with a single set of parameters, the r.m.s. deviation being only 9 % in this case (see Fig.7.1).

To study the temperature dependence of the thermal expansion coefficient we differentiate eqn.(7.1) with respect to T and plot as a function of T. The plot is shown in fig.7.2 which clearly shows that the thermal expansion coefficient (a) has a finite discontinuity at T_p which is what is also expected from fig.7.1.

Fig.7.1 : The fractional length change data of superconducting $YBa_2Cu_3O_{7-\delta}$ $(S = 0.15)$ and non-superconducting $YBa_2Cu_3O_{7-\delta}$ $(6 = 0.9)$ with temperature. The solid lines show the fits to the data.
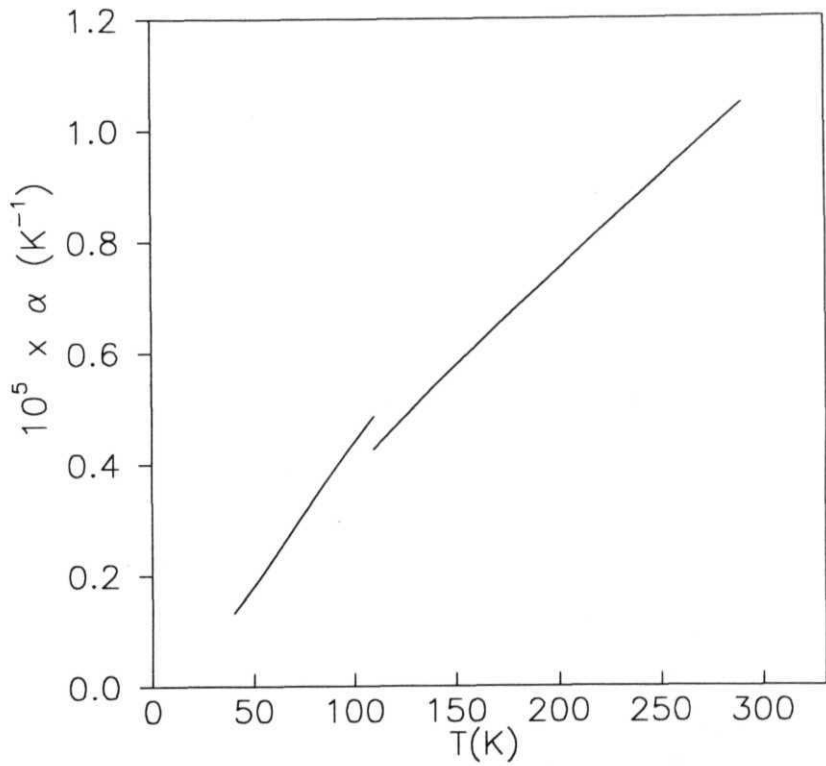
Fig.7.2 : The coefficient of linear thermal expansion of supercinducting $Y Ba_2 Cu_3 O_7$ $(6 = 0.15)$ with temperature.

Another feature we would like to mention is that **the** electronic contribution to the thermal expansion is linear in temperature in both normal and superconducting phases. This might have some correlation with the electronic specific heat behaviour of high T_c superconductors. But as the electronic Griineisen constant is not known for the **Y-123** superconducting sample the electronic specific heat could not be calculated.

7.2.2   Discussion

The cubic anharmonicity parameters g' and g'' are clearly larger below T_p than above T_p which implies an increase in the asymmetry of the lattice atom-atom potential below T_p. The quartic anharmonicity parameter $/'$ however shows the most dramatic increase in its value below T_p which indicates a softening of the lattice potential around T_p. The enhancement in the cubic and quartic anharmonicities leading to the asymmetry and softening of the lattice might originate in our opinion from the high lattice polarization present in the cuprates. This lattice polarization can give rise to a lattice instability favouring the possibility of polaron formation around T_p. This indirectly suggests the bipolaronic mechanism as a possible pairing mechanism in the high T_c superconductors. In a one - electron polaron problem the phonon dynamics is not affected by the polaron formation. But in a many electron system, the polaron formation will give rise to phonon - phonon interactions leading to **anharmonic** effects which will largely depend on the strength of the polaronic interactions. The polaronic interaction might be of Frohlich type or Holstein type depending on the material. If real anharmonic phonons are present in the system then one should also incorporate in the **polaron** formation **the** effect of electron - biphonon interaction which can be written in a mean field-like approximation [36]

Sample	YBa$_2$Cu$_3$O$_{7-\delta}$ ($\delta = 0.15$)		YBa$_2$Cu$_3$O$_{7-\delta}$ ($\delta = 0.9$)
	T< T$_p$	T > T$_p$	20 K < T < 300K
Θ_D (K)	418.9±0.8 [420.0]	418.9+08	425.0±1.0
g'(eV^{-1})	(5.32±.08)×10^{-2}	(2.51±.06)×10^{-2}	(2.26±.08)×10^{-2}
g''(eV^{-1})	(6.06±.06)×10^{-3}	(1.96±.06)×10^{-4}	(1.38±.08)×10^{-4}
f'(eV^{-1})	(9.98±.06)×10^{-4}	(1.35±.06)×10^{-5}	(1.21±.08)×10^{-5}
γ_{el}(K^{-2})	(1.37±.06)×10^{-8}	(1.54±.06)×10^{-8}	(1.49±.08)×10^{-8}

Table-7.1 : The Debye temperature, anharmonicity parameters and the coefficient of linear electronic term obtained form the fit of the thermal expansion data of superconducting (8=0.15) and non-superconducting (8=0 9) YBaCuO sample. The value of the Debye temperature inside square brackets is from literature **[34,35]**.

as

$$\mathcal{H} = \sum_{\vec{k}\vec{k}'\vec{q}\vec{q}'} B_{\vec{q}} B_{\vec{q}'} C^{\dagger}_{\vec{k}+\vec{q}'+\vec{q}} C_{\vec{k}} (a_{\vec{q}} a_{\vec{q}'} + a^{\dagger}_{-\vec{q}} a^{\dagger}_{-\vec{q}'}) \tag{7.2}$$

where $C^{\dagger}_{\vec{k}}(C_{\vec{k}})$ is the creation (annihilation) operator for the electron and $B_{\vec{q}}$ is the electron - phonon interaction matrix element. Bussman-Holder and Bishop have combined this interaction with the BCS hamiltonian to reproduce some of the interesting features of the high T_c superconductors. Morawitz $et.al.$ [37] have studied the effect of this non-linear electron phonon interaction on the normal state properties and the transition temperature of cuprates in the tight binding model. We would like to emphasize that the non-linear electron-phonon term will contribute a four-phonon interaction to the phonon dynamics in the lowest-order perturbation theory. This might be one of the probable reasons for the dramatic enhancement of the quartic anharmonicity below T_p.

We like to point out that we have used the thermal expansion data for poly-crystalline YBaCuO for which we do not distinguish among a, b and c axes and therefore the model we have used is an averaged isotropic model. Single crystals of high - T_c cuprates are however known to be highly anisotropic and for these materials one will naturally have to make separate analysis of each crystallographic direction. The parameters f, g etc. in that case are expected to come out different for the three directions exhibiting an anisotropy in the thermal expansion coeffi-cient. Nevertheless, the anomaly at $T > T_c$ observed for polycrystalline YBaCuO in its thermal expansion behaviour and its qualitative nature are expected to re-main even for the single crystals of YBaCuO. We try to attribute this anomaly to the polaron formation which can induce a lattice instability and mode softening.

If polarons and bipolarons do form in the high - T_c **cuprates** then these materials should show some polaronic: effects in their behaviour. Several advocates [17-21] of the polaronic mechanism have addressed themselves to this issue and it is well known that some of the normal state and superconductive properties of high - T_c cuprates can be explained using polaronic models. For **example,** if one calculates the transport properties of superconducting cuprates using the polarons and bipolarons as the charge carriers, one can very easily explain the linear - T resistivity behaviour exhibited by these materials [38,21]. Evidence of polaron formation in cuprates has also come, albeit indirectly, from photo-induced conductivity and photo-modulation experiment [39], optical conductivity data [40], $Cu-K$-edge EXAFS measurements [29], ion-channeling studies [25] and resonant neutron absorption spectroscopy [30]. Mustre de Leon *et al* [41] have recently performed an exact diagonalization of an electron-phonon model hamiltonian for the $O(4) - Cu(1) - O(4)$ cluster in the 123 compound and have shown that for strong electron-phonon coupling the motion of holes and ions become polaronic leading to a double well structure for the in-frared mode as observed in their EXAFS experiment. However these results and also our thermal expansion data analysis which do indicate the formation of po-larons in cuprates may or may not have any bearing on the mechanism of high T_c superconductivity.

7.3 $Ba_{1.6}Pb_{0.4}Sr_2Ca_2Cu_3O_y$ Superconductor

The $Ba_{1.6}Pb_{0.4}Sr_2Ca_2Cu_3O_y$ (Bi-2223) Superconductor was prepared and character-ized by Seshu Bai et.al. [42]. The susceptibility measurements gave the normal to superconducting transition temperature $T_C = (107 \pm 1)$K (see **Fig.7.3**). From the
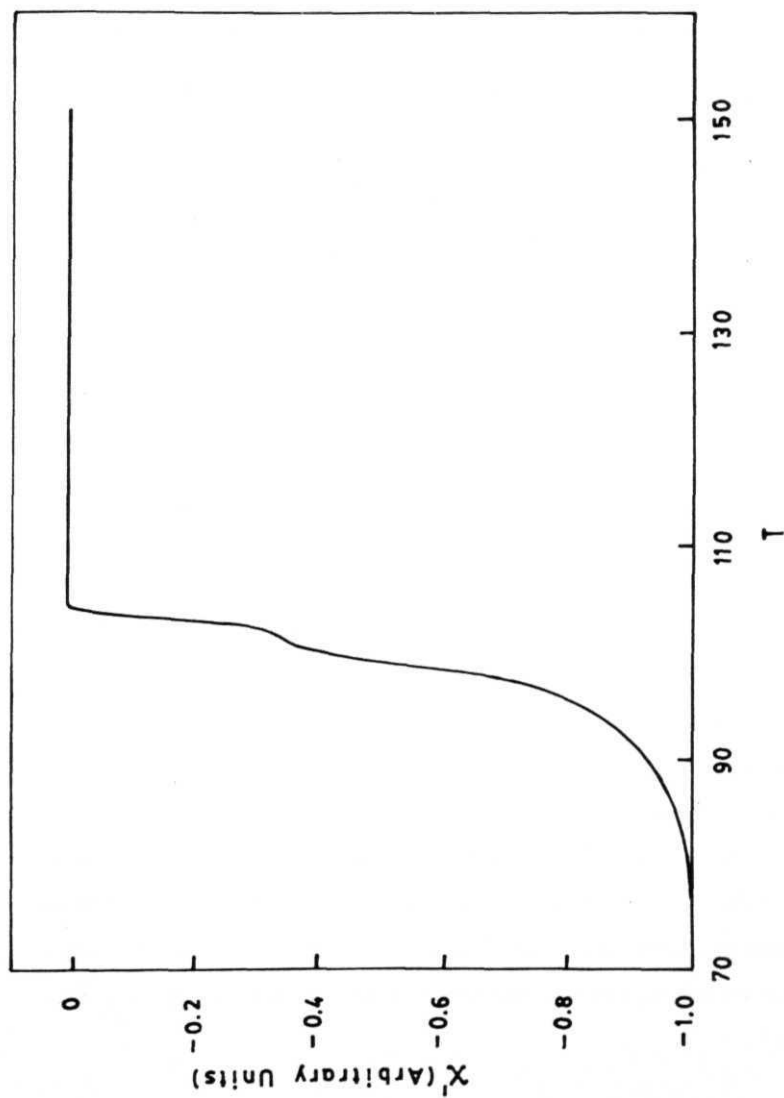
Fig.7.3 : Variation of ac susceptibility as a function of temperature of $Bi_{1.6}Pb_{0.4}Sr_2Ca_2Cu_3O_y$ superconductor.

original sample made by **Seshu** bai et.al. [42] we have cut a rectangular **piece of** dimensions $(2 \times 3 \times 3) mm^3$ and performed the **thermal** expansion measurements on it. **Fig.**7.4 shows the temperature dependence of the fractional length change $\Delta L(T)/L(T_0)$ (T_0 = 293.0 K) and the Fig.7.5 gives the $a(T)$ data obtained from the numerical three point differentiation of $\Delta L(T)/L(T_0)$ with respect to temperature. Even though the $\Delta L(T)/L(T_0)$ data does not show any observable change at T_c, the $\alpha(T)$ data gives a slope change.

7.3.1   Results and Discussion

As in Y-123 superconductor we have tried to fit the AL/L data of Bi-2223 super-conductor to the theoretical expression given by eqns.(3.2) and (7.1). separately in the temperature range above T_C (normal region) and below T_C (superconducting region). The AL/L data in the normal region (110K < T < 300K) is fitted to eqn.(3.2) with γ_{el}, g', g'', $/'$, Θ_D, p and Θ_E as parameters. The fit gives the best results for $p — 3$. Hence in the final fits we have used only the Debye terms. In-terestingly the AL/L data in the superconducting region (80K < T < 106K) could not be fitted to the eqn.(3.2) and (7.1). This may be because of our experimental temperature range in the superconducting phase is very near to T_C (108 K). In this temperature range strong fluctuations in the superconducting order parameter are expected due to the short coherence length of the superconductor. Experimentally the effects of fluctuations are also observed in the specific heat [43-47]. in the con-ductivity [48,49], in the dc-susceptibility [50] and on the resistivity [48,51.52] of the high temperature superconductors. Also it has been observed experimentally that the linear in temperature term in the low temperature specific heat data of Bi-2223
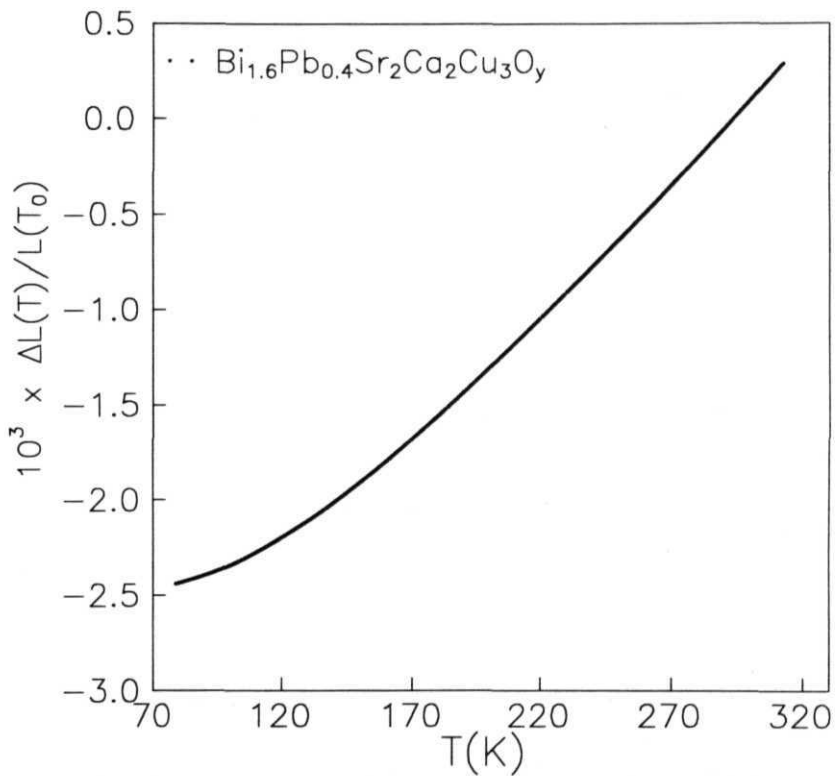
Fig.7.4 : Temperature variation of measured fractional length change data of $Bi_{1.6}Pb_4Sr_2Ca_2$ uperconductor.

superconductor is either absent or very small [53-55]. Therefore following the specific heat data analysis of Braun et.al. [56] near the superconducting transition temperature T_C we can write a theoretical expression for $\alpha(T)$ as,

$$\alpha(T) = \gamma_{BCS}e^{-1.5\frac{T_C}{T}} + \gamma_{GFL}\left|\frac{T-T_C}{T_C}\right|^{-1}$$
$$+ \frac{3g}{4c^2a(T_0)}\left[\varepsilon' - 2G \times \varepsilon \times \varepsilon' - 3F \times \varepsilon^2 \times \varepsilon'\right] \tag{7.3}$$

The first term comes from the mean field **contribution** by taking the BCS weak coupling limit to a where γ_{BCS} is a constant. The second term comes from the 2D Gaussian fluctuation contribution to a with γ_{GFL} being a constant. The third term comes from the analytical differentiation of eqn.(3.14) with respect to the temperature and $G = (15g^2/16c^3) - (8//c^2)$. $F = (35/16)[(15g^2f/4c^5) + (3f^2/c^4)]$. But as we could not write an analytical expression for AL/L from the theoretical expression of a given by the above eqn.(7.3). we decided to fit our experimental a data.

In the normal region the theoretical expression for a obtained by taking the differentiation of AL/L using for $\langle x \rangle_T$ the expression given in eqn.(7.1) with respect to temperature is,

$$\alpha(T) = \gamma_{el}T + \frac{3g}{4c^2a(T_0)}\left[\varepsilon' - 2G \times \varepsilon \times \varepsilon' - 3F \times \varepsilon^2 \times \varepsilon'\right] \tag{7.4}$$

We fit our experimental $\alpha(T)$ data in the temperature range above T_C with γ_{el}, g', g'', $/'$, Θ_D as parameters and the best fit reproduces the parameter values obtained from the previous fitting of the (AL/L) data. In **Fig.7.5** we show the fit of our data as a solid line against the experimental data points. Interestingly we find that

the data fits perfectly well upto T — 123.5 K and then starts deviating. Following the same analogy as in Y-123 superconductor case we term this temperature as Tp which is above T_C where the anomaly in the thermal expansion starts in the case of Bi-2223 superconductor. The r.m.s. deviation for the best fit in the temperature range $T > Tp$ came out to be 0.9%.

We have fitted the a data in the superconducting region to eqn.(7.3) taking $\gamma_{BCS}, \gamma_{GFL},\ 9,\ g'',\ /')\ \Theta_D$ as parameters. Fig.7.5 shows the fit as a solid line to the experimental data points and the fit is good upto about 105 K and the r.m.s. deviation is only 0.8%. This is in confirmity with the observations of Braun et.al. [56] in the analysis of specific heat data. They have also seen that the mean field and the 2D Gaussian fluctuation contributions are unable to fit the specific heat data inside a window of $(T_C \pm 5)K$. This has been attributed to the presence of the critical fluctuations which could be setting in inside this window. The data fitting of our experimental a in the superconducting region has been done by keeping the value of Θ_D fixed to the value obtained from the fit in the temperature region above T_C. The parameters obtained from the best fits in both the normal and the superconducting region are given in Table-7.2. The value of Θ_D obtained from our fit is 286.6 K which compares quite impressively with the reported value of about 280 K given in literature [53].

From Table-7.1 one can see that the behaviour of the anharmonicity parameters above and below T_C is similar to the behaviour seen in the case of Y-123 superconductor. The value of the cubic anharmonicity parameter g' is clearly larger below T_C than that of above T_C. There is a dramatic increase in the quartic anharmonicity parameter $/'$ below T_C, by almost three orders of magnitude in coming from normal to superconducting phase. This indicates softening of the lattice modes
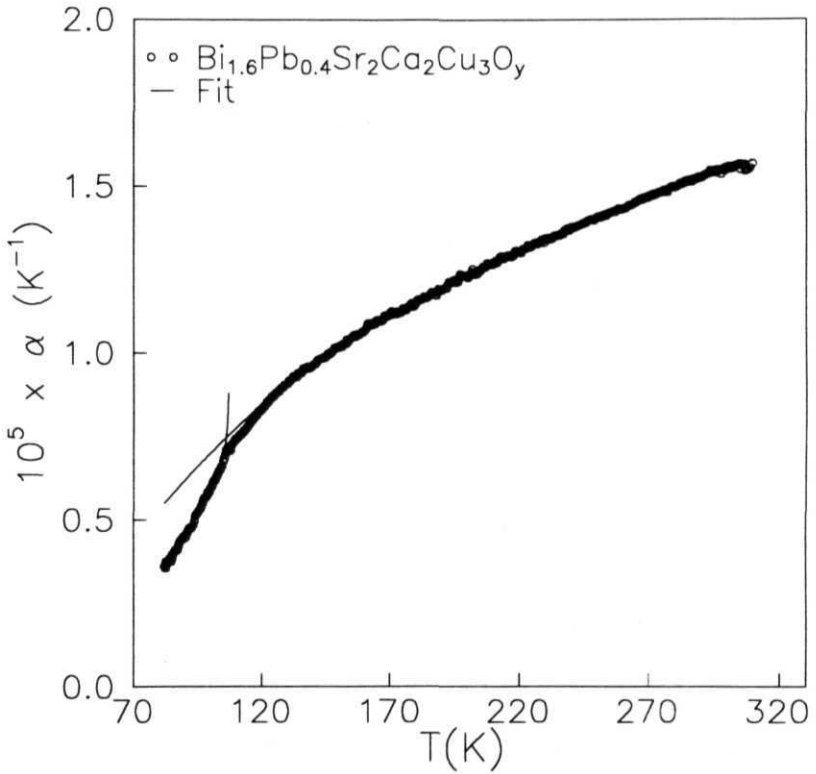
Fig.7.5 : The coefficient of linear thermal expansion data of $Bi_{1.6}Pb_{0.4}Sr_2Ca_2Cu_3O_y$ superconductor. The solid lines show the fits to eqn.(7.3) in the superconducting phase and to eqn.(7.4) in the normal phase.
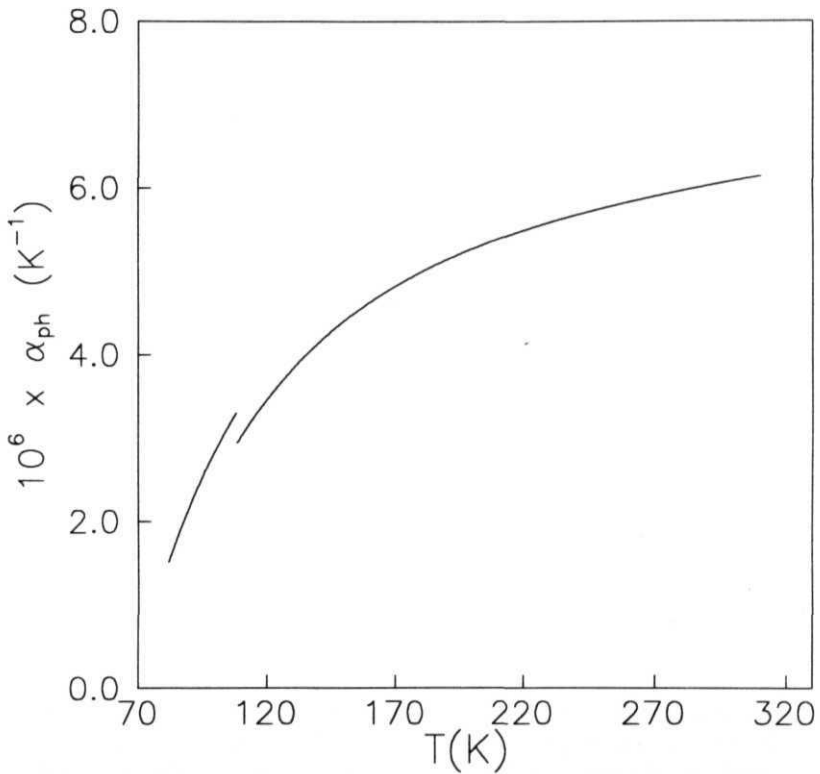
Fig.7.6 : Temperature variation of vibrational contribution (α_{ph}) to the thermal expansion coefficient data of $Bi_{1.6}Pb_{0.4}Sr_2Ca_2Cu_3O_y$ superconductor calculated using the parameters obtained from the fit.

Sample	$Bi_{1.6}Pb_{0.4}Sr_2Ca_2Cu_3O_y$	
	$T < T_C$	$T > Tc$
$\Theta_D (K)$	286 611.2 [~280.0]	286 6±1 2
g'(eV')	$(0.198\pm.07)\times10^{-2}$	$(0\ 192\pm.06)$
$g''(eV^{-1})$	$(7.223\pm.07)\times10^{-2}$	$(1.135\pm.06)\times10^{-5}$
$f'(eV^{-1})$	$(2.006\pm07)\times10^{-3}$	$(1.322\pm.06)\times10^{-6}$
$\gamma_{BCS}(K^{-1})$	$(1.364\pm.07)\times10^{-5}$	
$\gamma_{GFL}(K^{-1})$	$(2.110\pm.07)\times10^{-8}$	
$\gamma_{el}(K^{-2})$	-	$(3.187\pm.06)\times10^{-8}$

Table-7.2 : Debye temperature, anharmonicity parameters and the electronic terms obtained from the fit of the thermal expansion data of **the** $Bi_{1.6}Pb_{0.4}Sr_2Ca_2Cu_3O_y$ superconductor in the superconducting and **the** normal **states** The value of Θ_D given inside the square brackets is from literature **[53]**.

around T_C, which may be due to high lattice polarization present in the Bi-2223 superconductor. In Fig.7.6 we have plotted the vibrational contribution to the thermal expansion coefficient α_{ph}, calculated using **the anharmonic** parameters and Θ_D obtained from the fits, below and above T_C. There is indeed a jump in α_{ph} at T_C indicating the occurrence of lattice instability at T_C. This anomaly in α_{ph} is coming from only the **anharmonic** contributions to the lattice potential as Θ_D is same in both the superconducting and the normal phases.

7.4   Conclusion

The thermal expansion analysis in both Y-123 and Bi-2223 superconductors showed similar type of behaviour in the anharmonic terms in the lattice potential across the superconducting phase transition. The values of Debye temperatures obtained from the fits are 418.9 K and 286.6 K for Y-123 and Bi-2223 superconductors respectively. They agree impressively with the values given in the **literature** obtained from the specific heat measurements. In both the superconductors **the** cubic anharmonicity terms have increased below T_C implying an increase in the asymmetry of the lattice atom-atom potential in the superconducting phase. Also the quartic anharmonicity parameters have increased tremendously below T_C indicating the softening of the lattice potential and **favouring** a lattice instability around T_C . This agrees well **with** the other experimental findings using the Raman Spectroscopy [24]. ion-channelling [25], inelastic neutron scattering [27] etc. The vibrational contribution to α. showed an anomaly in both the superconductors around T_C.

References

[1] H. Kamerling Onnes, Leiden Commun. **1206,** 1226 (1911).

[2] J. Bednorz and K.A. **Muller,** Z. Phys. B Cond. Matter 64, 189 (1986).

[3] MX. Wu, J.R. Ashburn, C.J. Torang. P.H. Hor, R.I. Meng, L. Gao, Z.J. Huang, Y.Q. Wang and C.W. Chu, Phys. Rev. Lett. **58,** 908 (1987).

[4] A.F. Marshall, R.W. Barton, K. Char. A. Kapitulnik, B. Oh. R.H. Hammond and S.S. Laderman, Phys. Rev. B 37. 9353 (1988).

[5] C. Michel, H. Hervieu, M.M. Borel. A. Gardin, F. Deslandes, J, Provst and B. Raveau, Z. fur. Phys. Cond. Matter **68,** 421 (1987).

[6] H. Maeda, Y. Tanaka, M. Fukutomi and T. Asano, Jpn. J. Appl. Phys. 27, L209 (1988).

[7] Z.Z. Sheng and A.M. Herman, Nature **332,** 55 (1988).

[8] C.C. Torardi, M.A. Subramanian, J.C. Calabrese, J. Gopala Krishnan, K.J. Morrissey, T.R. Askew, R.B. Flippen. U. Chowdhry and A.M. Sleight. Science **240,** 631 (1988).

[9] S.N. Putillin, E.V. Antipov, O. Chenaissem and M. Marezio. Nature 362, 226 (1993).

[10] A. Schilling, M. Cantoni, J.D. Guo and H.R. Ott, Nature **353**. 56 (1993).

[11] J. Bardeen, L.N. Cooper and J.R. Scrieffer, Phys. Rev. B **108,** 1175 (1957).

[12] T Jarlborg, Helv. Phys. Acta 61, **421** (1988).

[13] R.E. Cohen, W.E. Pickett, H. Krakauer and D.A. Papaconstantopoulos. Phase Transitions **22**, 167 (1990).

[14] R.E. Cohen, W.E. Pickett and H. Krakauer, Phys. Rev. Lett. 64, 2575 (1990).

[15] CO. Rodriguez, A.I. Liechtenstein, I.I. Mazin, O.Jepsen, O.K. Andersen and M. Methfessol, Phys. Rev. B 42. 2692 (1990).

[16] R. Zeyher, Z. Phys. B 80, 187 (1990).

[17] D. Emin, Phys. Rev. Lett., 62. 1544 (1989).

[18] D. Emin and M.S. Hillery. Phys. Rev. B 39. 6575 (1989).

[19] J. Ranninger in Proceedings of the conference on "Lattice effects in high T_c superconductors", eds. Y. Bar-Yam, T. Egami, J. Mustre de Leon and A.R. Bishop (1992) p.389 and references theirin.

[20] B.K. Chakravarty, D. Feinberg. H. Zheng and M. Avignon, Solid State Commun. **64**, 1147 (1987).

[21] S. Sil and A. Chatterjee. Int. J. Mod. Phys. B 4, 1879 (1990); *ibid*, Mod. Phys. Lett. B. 6, 959 (1992).

[22] N.M. Plakida, V.L. Aksenov and S.L. Drechsler, Europhys. Lett. 4. 1309 (1987).

[23] J.R. Hardy and J.W. Hocken, Phys. Rev. Lett. 60, 2191 (1988).

[24] C. Thompsen, M. Cardona, B. Gegenheimer, R. Liu and A. Simon, Phys. Rev. B 37, 9860 (1988).

[25] R.P. Sharma, L.E. Rehn, P.M. Baldo and J.Z. Liu, Phys. Rev. Lett. 62. 2869 (1989); *ibid* Phys. Rev. B 40, 11396 (1989).

[26] B.H. Toby, T. Egarni, J.D. Jorgensen and M.A. Subramaniam, Phys. Rev. Lett. 64, 2414 (1990).

[27] M. Arai, K. Yamada, Y. Hidaka, S. Itoh, Z.A. Bowden, A.D. Taylor and Y. Endoh, Phys. Rev. Lett. 69, 359 (1992).

[28] S. Conradson, I. Raistrick and A.R. Bishop, Science **248.** 1394 (1990).

[29] J. Mustre-de Leon, S.D. Conradson, I. Batistic and A.R. Bishop, Phys. Rev. Lett. 65, 1675 (1990).

[30] H.A. Mook, M. Mostoller. J.A. Harvey. N.W. Hill. B.C. Chakoumakos and B.C. Sales, Phys. Rev. Lett. 65. 2712 (1990).

[31] H.A. Mook, B.C. Chakoumakos, M. Mostoller. AT. Boothroyd and D. Mck.Paul, Phys. Rev. Lett. 69, 2272 (1992).

[32] G.D. Mukherjee. A. Chatterjee and C. Bansal. Physica C **232,** 241 (1994).

[33] G. Oomi and K. Suenaga. J. Alloys and Compounds **181.** 219 (1992).

[34] S.J. Collocott, R. Driver. H.K. Welsh and C. Andrikidis. Physica C **152**. 401 (1988).

[35] C.A. Swenson, R.W. McCallum and K. No, Phys. Rev. B 40, 8861 (1989).

[36] A. Bussmann-Holder and A.R. Bishop, Phys. Rev. B **44,** 2853 **(1991).**

[37] H. Morawitz, V.Z. Kresin and S.L. Wolf in :Lattice Effects in High$-T_c$ Super-conductors eds.: Y. Bar-Yam, T. Egami, J. Mustre-de Leon and A.R. Bishop World Scientific (1992) p.372.

[38] D. Emin in Proceedings of the conference on "Lattice effects in high-T_c super-conductors", eds. Y. Bar-Yam, J. Egami, J. Mustre de Leon and A.R. Bishop (1992) p.377.

[39] CM. Foster, A.J. Heeger, Y.H. Kim and G. Stucky, Synthetic Materials 33. 171 (1989).

[40] D. Mihailovic, CM. Foster, K. Voss and A.J. Heeger, Phys. Rev. B **42**, 7189 (1990).

[41] J. Mustre-de Leon, **I. Batistic,** S.A. Trugman, A.R. Bishop and S.D. Conrad-son in : Lattice Effects in High$-T_c$ Superconductors, eds.: Y. Bar-Yam, T. Egami, J. Mustre-de Leon and A.R. Bishop World Scientific (1992) p.163.

[42] V. Seshu Bai, S. Ravi. T. Rajsekharan and R. Gopalan, J. Appl. Phys. 70, 4378 (1991).

[43] S.E. Inderhees. M.B. Salamon, N. Goldenfeld. J.P. Rice. B.G. Pazol, D.M. Ginzburg. J.Z. Liu and G.W. Crabtree, Phys. Rev. Lett. 60, 1178 (1988).

[44] K. Fossheim. O.M. Nes, T. Laegreid, C.N.W. Darlington, D.A. O'Connor and C.E. Gough, Int. J. Mod. Phyd. **B1**, 1171 (1988).

[45] D. Wohllenben, E. Braun, W. Schenelle, J. Harnischmacher, S. Ruppel and R. Domel, In : Proc. Int. Conf. of Superconductivity - ICSC, Jan. 10-14,

1990, Bangalore. India, eds: S.K. Joshi, C.N.R Rao and S.V. Subramanyam (World Scientific Publishing, Singapore, 1990). P.194

[46] W. Schnelle, E. Braun, H. Broicher, R. Domel. S. Ruppel, **W. Braunisch,** J. Harnischmacher and W. Wohllenben, **Physica** C168, 465 (1990).

[47] A. Junod, Physical properties of high temperature superconductors II, ed: D.M. Ginsberg (World Scientific, Singapore, 1990).

[48] W. Schnelle, E. Braun, H. Broicher, H. Weiss. H. Geus, S. Ruppel. M. Galffy, W. Braunisch, A. Waldorf, F. Seidler and D. Wohllenben, Physica **C161,** 123 (1989).

[49] J.J. Wnuk, **L.W.M.** Schreurs, P.J.T. Eggenkamp. P.J.E.M. van der Linden, Physica B 165/166. 1371 (1990).

[50] W.C. Lee, R.A. Klemm and D.C Johnson, Phys. Rev. Lett. 63, 1012 (1989).

[51] F. Vidal. J.A. Veira. **J.** Maza, **J.J. Ponte, F.** Gracia-Alvardo, **E.** Moran, J. Amador. C. Cascales, A. Castro M.T. Casais and I. Rasines, Physica C **156,** 807 (1988).

[52] M. Ausloos. P. Clippe and Ch. Laurent, Solid State Commun. 73, 137 (1990).

[53] S.J. Collocot and R. Driver, Physica C **167,** 598 (1990).

[54] K. Mori, M. Sasakawa. T. Igurshi, Y. Ishikawa, K. Sato, K. Noto and Y. Muto, Physica C **162-164,** 512 (1989).

[55] M.K. Yu, J.P. Franck, M.A.-K. Mohamed. W.A. Miner and J. Jung, Physica C **62-164,** 468 (1989).

[56] E. Braun, W. Schnelle. H. Broicher, J. Harnischmacher, D. Wohllenben. C Allgeier, W. Reith. J.S. Schilling, J. Bock, E. **Preisler** and G.J Vogt, Z. Phys. B - Condensed Matter, **84**, 333 (1991).

Summary

The important results of the work described in this thesis are summarized as follows :

1. A simple three terminal capacitance dilatometer is designed and constructed for thermal expansion measurements on small samples. The sample can be placed directly in between the two capacitor plates of the capacitance cell and a change in the length of the sample changes the capacitance of the cell which can be measured accurately. Using the known expansion data of copper the cell is standardized to give the expansion measurements of other materials. The fractional length changes can be measured using the new cell with an estimated error of 3.5 x 10"'.

2. For the analysis of thermal expansion data a new microscopic theoretical model is developed which is used to obtain vibrarional. electron-magnetic and magnon contributions to the coefficient of thermal expansion. Using the Einstein model for the optic modes and treating the acoustic modes in the frame work of Debye model, the theoretical expression for vibrational contribution to thermal expansion is obtained from an anharmonic lattice potential. The electron-magnetic and the magnon contributions to thermal expansion are obtained using the generalized Stoner-Wohlfarth model of itinerant electrons and Bloch's theory of magnons respectively. The model has been applied to analyze the thermal expansion behaviour of simple metals like Cu and Al, ferromagnetic transition metals such as Fe and Ni and alkali halides. It has been shown that the present model provides us with estimates of anharmonicity parameters of the lattice potential and also gives very accurate values of the characteristic Debye and Einstein temperatures. It has also been shown that our approach gives quite successfully the values of electron-magnetic, magnon and vibrational Griineisen parameters.

3. Thermal expansion measurements together with our theoretical model is used to study the changes in the vibrational properties of binary alloys due to chemical order-disorder transformations. From the analysis of the thermal expansion data, the vibrational entropy differences between the ordered and the disordered Fe_3Al and Ni_3Mn alloys are found to be substantially large fractions of the configurational entropy of mixing. This suggests that the lattice vibrations will play a **rather** important role in the order-disorder transformations of these binary alloys and contribute **significantly** to their phase stability. Our theoretical model together with the band structure data revealed from the thermal expansion data analysis of Ni_3Mn alloy that it contains both itinerant and localized moments and the effect of atomic disorder is to suppress the itinerant character of the alloy.

4. Thermal expansion measurements on chemically ordered $Fe_{3-x}Mn_xSi$ and $Fe_{3-x}Mn_xAl$ ternary alloys in a wide concentration range have shown clear transitions at T_C. The data analysis using our theoretical model gives an increase in the Debye temperatures with increase in Mn concentration in both the systems. The electron-magnetic contributions to thermal expansion coefficient and entropy are seen to be increasing with Mn addition showing a decrease in the itinerant character.

5. Thermal expansion measurements have been performed on a bulk metallic glass $Zr_{65}Ni_{10}Cu_{17.5}Al_{7.5}$ and its crystalline counterpart. It is seen that around room temperature the thermal expansion coefficient is less in the case of glass than that in its corresponding crystalline phase. A simple method is proposed for the calculation of the configurational entropy of a glass from thermodynamic considerations and thermal expansion measurements and for the present bulk metallic glass the value of the configurational entropy is estimated to be 17 J/mol K just below the glass

transition temperature. A new **isentropic temperature** is predicted **upto which** the glass can be superheated. Also the Gibb's free energy difference between the glass and the crystal is estimated which gives a measure of the stability of the glassy state.

6. Thermal expansion measurements and analysis in $YBa_2Cu_3O_{7\epsilon}$ and $Bi_{1.6}Pb_{0.4}$ $Sr_2Ca_2Cu_3O_y$ high-T_C superconductors have been done to study the effect of superconducting transition on lattice anharmonicity. In both the superconductors the values of the Debye temperatures obtained from our analysis match with the values given in literature. The cubic anharmonicity terms increased below T_C implying increase in the asymmetry of the lattice atom-atom potential in the superconducting phase. The quartic anharmonicity parameters have increased quite significantly below T_C indicating the softening of the lattice potential and favouring a lattice instability around T_C. Also the vibrational contribution to thermal expansion coefficient shows an anomaly in both the superconductors around T_C.